

NASA Technical Memorandum 86405

Operating Characteristics
of Multiple Critical
Venturi System and Secondary
Calibration Nozzles Used for
Weight-Flow Measurements in the
Langley 16-Foot Transonic Tunnel

(NASA-TM-86405) OPERATING CHARACTERISTICS
OF THE MULTIPLE CRITICAL VENTURI SYSTEM AND
SECONDARY CALIBRATION NOZZLES USED FOR
WEIGHT-FLOW MEASUREMENTS IN THE LANGLEY
16-FOOT TRANSONIC TUNNEL (NASA) 74 p

N86-10016

Unclas

G3/02 27465

Hubby L. Berry, Laurence D. Levin,
and Linda S. Baasport

NASA Technical Memorandum 86405

**Operating Characteristics
of the Multiple Critical
Venturi System and Secondary
Calibration Nozzles Used for
Weight-Flow Measurements in the
Langley 16-Foot Transonic Tunnel**

**Bobby L. Berrier, Laurence D. Leavitt,
and Linda S. Bangert**

*Langley Research Center
Hampton, Virginia*

NASA

National Aeronautics
and Space Administration

Scientific and Technical
Information Branch

1985

SUMMARY

An investigation has been conducted in the Langley 16-Foot Transonic Tunnel to determine and document the weight-flow measurement characteristics of a multiple critical venturi system and the nozzle discharge coefficient characteristics of a series of convergent calibration nozzles. The effects on model discharge coefficient of nozzle-throat area, model choke-plate open area, nozzle pressure ratio, jet total temperature, and number and combination of operating venturis were investigated. Tests were conducted at static conditions (tunnel wind off) at nozzle pressure ratios from 1.3 to 7.0. Results of this investigation indicate that the measurement uncertainty of the multiple critical venturi system is generally within 0.5 percent and that the discharge coefficients of the Langley 16-Foot Transonic Tunnel Stratford choke nozzles fall within the expected range of 0.9925 to 0.9975 if throat Reynolds number is slightly higher than 1×10^6 and if excessive total-pressure profile distortion is not present.

INTRODUCTION

Accurate measurement of air weight-flow rate being supplied to subscale wind tunnel models for jet exhaust simulation is critical to obtaining high-accuracy propulsion-model data. The demands for high-accuracy data from propulsion models increase proportionally with demands for aircraft with higher performance or lower fuel consumption or both. Weight-flow measurements are not only used to compute discharge coefficients but are also used to compute values of ideal isentropic gross thrust which are used in thrust ratios for determining nozzle efficiency.

With the introduction of a high-pressure air jet-simulation system in the Langley 16-Foot Transonic Tunnel, a turbine-type meter (refs. 1 and 2) was adopted for air weight-flow rate measurements. Because the calibration of electronic equipment associated with the turbine-meter frequency measurements "drifted" with time and also because turbine-meter calibration was a slight function of bearing wear, there was a gradual shift from use of a turbine-type meter to a calibration technique which uses sonic nozzles located at the exit of the model high-pressure plenum (refs. 3 to 5). Calibrations of these sonic nozzles against secondary standard nozzles with known performance were required to establish the relationship between upstream temperature and pressure measurements and weight-flow rate. Although this method for computing weight-flow rate proved to be very reliable and gave satisfactory results, calibrations before each model entry were required because the relationship between the upstream temperature and pressure measurements and the model air weight-flow rate was often a function of model design (e.g., upstream temperature and pressure measurement location, choke-plate open area, and nozzle-throat area). The secondary standard nozzles used in the Langley 16-Foot Transonic Tunnel for calibrating weight-flow rate measurements (and, as described in ref. 3, for obtaining balance tares resulting from airflow momentum and pressure) are Stratford choke (sonic) nozzles of the type described and analyzed in reference 6. In an effort to simplify and improve air weight-flow rate measurement, a multiple critical venturi system was installed in the high-pressure air supply system of the tunnel in late 1982. Design criteria, advantages, and operating characteristics of critical venturis can be found in references 7 and 8.

The objective of this paper is to determine and document the weight-flow measurement characteristics of the Langley 16-Foot Transonic Tunnel multiple critical venturi system and the nozzle discharge coefficient characteristics of a series of convergent calibration nozzles. The effects on model discharge coefficient of nozzle-throat area, model choke-plate open area, number and combination of operating venturis, nozzle pressure ratio, and jet total temperature are shown. This test was conducted at static conditions (tunnel wind off) and nozzle pressure ratio was varied from 1.3 to 7.0.

SYMBOLS

| | |
|------------------------------------|---|
| A_{choke} | total open area formed by holes in choke plate, in ² |
| A_{max} | maximum internal nozzle flow area, in ² |
| A_t | measured nozzle-throat area, in ² |
| A_x | measured throat area of individual venturi ($x = 1, 2, 4, 8, 16.1, \text{ or } 16.2$), in ² |
| C^* | critical-flow factor (see eq. (3a) and ref. 9) |
| C_d | measured discharge coefficient of Stratford choke nozzle, w_p/w_i |
| \bar{C}_d | average of Stratford-choke-nozzle discharge coefficients measured at choked flow conditions for a particular A_t and A_{choke} combination |
| $\bar{C}_{d,avg}$ | average of \bar{C}_d for a particular value of A_t (includes \bar{C}_d for all values of A_{choke} except screens) |
| $C_{d,x}$ | discharge coefficient of individual venturi ($x = 1, 2, 4, 8, 16.1, \text{ or } 16.2$) |
| D_{max} | maximum internal diameter of model tail pipe (see fig. 2(a)), in. |
| D_t | throat diameter of Stratford choke nozzle (see fig. 2(a)), in. |
| D_2 | diameter of Stratford choke nozzle at throat plane including nozzle base (see fig. 2(a)), in. |
| g | acceleration due to gravity, 32.174 ft/sec ² |
| K_0, K_1, \dots, K_{15} | constants used to determine critical flow factor (see eq. (3)) |
| $K_{R,1}, K_{R,2}, \dots, K_{R,5}$ | rake correction factors for individual internal jet total-pressure probes (see fig. 2(b)) |
| ΔK_R | total-pressure distortion parameter (maximum rake correction factor minus minimum rake correction factor times 100; percent deviation from no-distortion case ($K_{R,1}$ to $K_{R,5} = 1.0$)) |
| L_1 | length used for geometric definition of Stratford choke nozzle (see fig. 2(a)), in. |

L_2 distance throat circular arc profile extends upstream of throat
 (see fig. 2(a)), in.

l length of Stratford choke nozzles (see fig. 2(a)), in.

M throat Mach number

MCV multiple critical venturi code (sum of the venturi numbers that are being
 used)

NPR nozzle pressure ratio, $P_{t,j}/P_a$

$(NPR)_c$ nozzle pressure ratio required for choked flow (1.8928 for air)

p_a ambient pressure, psi

P_{rake} jet total pressure measured by individual rake probe at Stratford-choke-
 nozzle throat, psi

$(P_{rake})_{int}$ value of jet total pressure obtained by integrating rake-measured
 values at Stratford-choke-nozzle throat, psi

$P_{t,j}$ average jet total pressure obtained from internal probes in instrumentation
 section (see fig. 2(a)), psi; value may or may not be corrected to
 $(P_{rake})_{int}$ depending on values of rake correction factors
 $(K_{R,1}, K_{R,2}, \dots, K_{R,5})$ used

$P_{t,j,1}, P_{t,j,2}, \dots, P_{t,j,5}$ jet total pressure measured with individual internal
 probes (see fig. 2), psi

P_{V1} upstream pressure in multiple critical venturi system (see fig. 3(a)), psi

P_{V2} downstream pressure in multiple critical venturi system (see fig. 3(a)), psi

R gas constant, 53.36 ft-lbf/lb-°R

R_d throat Reynolds number for Stratford choke nozzle (eq. (9))

$R_{d,v}$ venturi-throat Reynolds number (eq. (4)), per inch

R_1, R_2 radii of curvature for geometric definition of Stratford choke nozzles
 (see fig. 2(a)), in.

r radius from nozzle centerline to probe centerline (see fig. 5), in.

r_t throat radius of Stratford choke nozzle (see fig. 5), in.

$T_{t,j}$ jet total temperature, °R

T_V upstream multiple critical venturi air temperature, °R

w_i ideal total weight-flow rate (see eq. (6)), lb/sec

$w_{i,x}$ ideal weight-flow rate for any individual critical venturi ($x = 1, 2, 4, 8, 16.1, \text{ or } 16.2$), lb/sec
 w_p measured total weight-flow rate, lb/sec
 X length used for geometric definition of Stratford choke nozzles (see fig. 2(a)), in.
 x venturi number (1, 2, 4, 8, 16.1, or 16.2)
 γ ratio of specific heats, 1.3997 for air
 μ absolute viscosity of air based on venturi-throat static conditions, lb/sec-in

Subscript:

nom nominal

APPARATUS AND METHODS

Test Facility

This investigation was conducted in the Langley 16-Foot Transonic Tunnel (ref. 10). All tests were made with the tunnel test section top in a raised position such that the model exhaust was vented to the atmosphere. Jet exhaust flow was simulated with high-pressure air supplied and maintained at a constant stagnation temperature by a heat exchanger in the system.

Single-Engine Propulsion-Simulation System

A sketch and a photograph of the single-engine nacelle model on which various Stratford choke nozzles were mounted are presented in figure 1 with a typical nozzle configuration attached. The body shell forward of station 26.50 was removed for this investigation.

An external high-pressure air system provided a continuous flow of clean, dry air at a controlled temperature of about 530°R. Air was brought through the support-system strut by six tubes and collected in a high-pressure (up to 900 psi) plenum located on top of the strut. The air was then routed aft and discharged perpendicularly into the integral centerbody—low-pressure-plenum—tail-pipe section through eight multiholed sonic nozzles equally spaced around the aft end of the high-pressure plenum. This design minimizes any forces imposed by the transfer of axial momentum as the air passes from the nonmetric high-pressure plenum to the metric tail pipe. Two opposing flexible metal bellows were used as seals and served to compensate for axial forces caused by pressurization. From the centerbody—low-pressure-plenum—tail-pipe section, the air was passed through a choke plate and an instrumentation section and then through the nozzle attached at model station 42.00. Details of the choke plate, which was a test variable, and of the instrumentation section are given in figure 2. Five choke plates with varying open areas (2.7 percent to 75.9 percent) were tested. Four of the choke plates were actually perforated disks with the upstream end of each hole countersunk. The choke plate with the largest open area

(75.9 percent) consisted of wire screen material supported by an open metal latticework.

Stratford Choke Nozzles

Since gas-flow measuring devices cannot generally be calibrated by direct weighing of the flow per unit of time, secondary standard nozzles are employed to calibrate weight-flow rate measurements (and, as described in ref. 3, to obtain balance tares resulting from airflow momentum and pressure). The secondary standard nozzles used at the Langley 16-Foot Transonic Tunnel are choke (sonic) nozzles of the type described in reference 6. Choke nozzle design guidelines from reference 6 are as follows:

1. Choked flow. This eliminates the need for difficult measurement of the static pressure in the throat. It also eliminates the effect of small variations in static pressure across the throat since the change in mass flow with changes in static pressure is equal to zero at a Mach number of unity.

2. Continuously curving wall profile through the throat. If the wall profile curves continuously through the throat, the flow in a choked nozzle can accelerate continuously and can develop only a very thin boundary layer. The reduction of discharge coefficient resulting from the boundary layer is thus very small.

3. $D_{\max}/D_t = 2$ to 3. This ratio is governed by practical circumstances but a ratio of two or three would seem reasonable.

4. $R_1/D_t = 2$. Although higher discharge coefficients could be obtained with lower values of this ratio, lower values of R_1/D_t also produce relatively large differences between discharge coefficient values for laminar and turbulent boundary layers. Thus, a moderate curvature for the throat is recommended to minimize this difference.

5. $L_2/D_t > 0.8$. Boundary-layer growth is roughly proportional to M^4 . For $R_1/D_t = 2$, this value has become very small at a distance upstream of the throat of $L_2/D_t = 0.8$ and discharge coefficient would be virtually independent of the shape of the nozzle profile upstream of this point, provided the surface were smooth and the flow attached.

6. $R_d > 10^6$. The uncertainty in discharge coefficient resulting from transition is decreased for throat Reynolds numbers above this value.

Seven sizes of Stratford choke nozzles were constructed with throat areas ranging from 0.999 in² to 11.352 in². Table I presents the geometry of these nozzles with the design guidelines from reference 6. As shown in table I, except for D_{\max}/D_t , which was limited by a fixed upstream duct area for all nozzles, the geometries of the seven secondary standard nozzles generally met the desired design criteria. Two exceptions are noted. Because of model restraints, L_2/D_t for the 8.501-in² and 11.352-in² throat area nozzles was less than the desired value. For the $A_t = 0.999$ in² nozzle, the throat Reynolds number did not meet or only marginally met the design criteria at low values of NPR because of the small throat diameter.

The $A_t = 1.933$ in² and $A_t = 5.711$ in² secondary standard nozzles (Stratford choke nozzles) were calibrated against several primary standard nozzles at the Colorado Engineering Experiment Station, Inc., in March of 1968. Primary standard

nozzles have known discharge coefficients which have been verified by laboratories such as the National Bureau of Standards. The range of discharge coefficients measured for these nozzles agreed well with that predicted theoretically in reference 6.

Multiple Critical Venturi System

Sketches and a photograph of the Langley 16-Foot Transonic Tunnel multiple critical venturi system are presented in figure 3. This system provides for high accuracy of flow measurement, an extremely wide range of weight flow, small pressure losses, and a very low level of noise in the airstream and pipe structures.

This flow-measurement system is designed to accommodate up to 44 lb/sec of air at a maximum pressure level of 1500 psi. As shown in figure 3(a), the system inlet flow is distributed uniformly into a common plenum by a radial inlet diffuser and a large perforated plate. The perforated plate also acts as a heat exchanger to eliminate small fluctuations in flow temperature. A pressure-tight bulkhead contains six critical-flow venturis. (See fig. 3(c).) The venturis vary in size in binary increments of throat area so that each successively larger venturi will pass twice the flow of the preceding one. The sizes of venturis in this system are multiples of 1, 2, 4, 8, and 16. values which also represent their nominal weight flow at 1600 psi. There are two venturis (numbered 16.1 and 16.2) of the largest size to provide maximum weight-flow capability within the smallest possible pressure vessel. Each venturi has its own individual screw-on cap. With all caps installed, no flow may pass through the system as each cap has an O-ring seal to prevent leakage. Any or all of the caps may be removed through the access port (see fig. 3(a)) to meet flow requirements. The binary sizes of the 6 venturis permit 47 increments of flow area to be used at any pressure level from 20 psi to 1500 psi. This provides a weight-flow range from 0.014 lb/sec at 20 psi to 44 lb/sec at 1500 psi, as shown in figure 4. Also shown in figure 4 are the pressure and weight-flow ranges covered during the current investigation.

Each individual venturi is designed to minimize losses and to reduce the noise which can be generated by a critical venturi. (See ref. 7.) Each venturi has an inlet radius of 3.64 times the throat radius, a 5° half-angle conical diffuser which enlarges to at least 5.80 times the throat area, and a perforated cylindrical diffuser with a perforated area equal to 8.00 times the venturi throat area. The 5° half-angle conical diffuser permits the venturi to maintain critical flow with pressure losses as low as 7 percent. The perforated cylindrical diffuser prevents the generation of noise and resonance in the airstream and pipe structures by shock systems which form in the conical diffuser at high pressure ratios.

The Langley 16-Foot Transonic Tunnel multiple critical venturi system was calibrated in the Boeing Airflow Calibration Facility over a pressure range from approximately 36 psi to 920 psi. Calibration results are shown in table II as tabulated discharge coefficients. The airflow standard used for this calibration was another multiple critical venturi system which was calibrated in 1977 by Colorado Engineering Experiment Station, Inc. (CEESI) with their 300 ft³ primary volumetric airflow standard. This calibration was certified by CEESI to have a measurement uncertainty within 0.07 percent over the air flow range from 0.1 lb/sec to 20.0 lb/sec. Transfer of this calibration to the Langley multiple critical venturi system was performed with an estimated precision of 0.03 percent over the entire calibration range. Since the certified calibration accuracy of the airflow standard used for calibration of the Langley system is within 0.07 percent, a calibration accuracy of 0.1 percent can

be validly assumed to apply to the Langley 16-Foot Transonic Tunnel multiple critical venturi system.

Instrumentation

Jet total pressure was measured at a fixed station in the model instrumentation section (see fig. 2) with a five-probe rake and a one-probe rake. Because of a plugged tube, the fourth probe from the bottom on the five-probe rake was not used for the current investigation. (See fig. 2(b).) Jet total pressure $p_{t,j}$ was obtained by averaging the five probe values measured. In addition, the jet total-pressure distribution at the nozzle throat was determined for each configuration tested with a 13-probe rake shown by the sketch of figure 5. This rake was mounted rigidly on each nozzle configuration to avoid relative movement between the rake and the nozzle throat resulting from model loads and vibration. The number of probes used with each nozzle varied with nozzle-throat diameter. Jet total pressures from the internal rakes and from the external 13-probe rake were measured with an electronic scanning pressure device.

The multiple critical venturi system (see fig. 3) described previously was used to measure the weight flow of the high-pressure air being supplied to the nozzles. Three pressure measurements upstream of the venturis (p_{v1}) and one pressure measurement downstream of the venturis (p_{v2}) were made with individual pressure transducers at the locations shown in figure 3(a). A temperature measurement upstream of the venturis (T_v) was made with a platinum resistance thermometer at the location shown in figure 3(a). The outstanding characteristics of this type of temperature measurement device can be found in reference 1.

Data Reduction

All data were recorded on magnetic tape. Fifty frames of data taken at a rate of 10 frames per second were averaged for each data point; average values were used in computations. Two nozzle-pressure-ratio-sweep runs were conducted on each configuration investigated, one with the 13-probe rake installed and one with it removed. Runs with the 13-probe rake installed were used only to provide total-pressure distributions at the nozzle throat and to determine rake correction factors, which are discussed later, for each internal total-pressure probe. Data obtained during the run with the rake removed were used to compute nozzle discharge coefficients.

The basic performance parameter used for the presentation of results is nozzle discharge coefficient C_d . Nozzle discharge coefficient is the ratio of measured weight flow w_p to ideal weight flow w_i . This parameter reflects the ability of a nozzle to pass weight flow and is reduced by any momentum and vena contracta losses (ref. 11). An excellent discussion of discharge coefficient losses in a venturi (which is a special purpose nozzle) is contained in reference 7. The two major sources of discharge coefficient losses given in this reference are

1. Development of a boundary layer along the nozzle walls because of the real-gas viscous effects
2. Variation of weight flow per unit area in the radial direction because of the centrifugal forces which exist in the gas as a result of flow through a contracting section

The values of measured weight flow used to determine nozzle discharge coefficients presented in this paper were determined from the multiple critical venturi system by use of equation (1).

$$w_p = w_{i,1}(C_{d,1}) + w_{i,2}(C_{d,2}) + \dots + w_{i,16.2}(C_{d,16.2}) \quad (1)$$

Since the product of ideal weight flow and discharge coefficient equals actual weight flow, each term in equation (1) represents the weight flow through a particular venturi shown in figure 3(c). For any venturi not used (capped off), the appropriate term or terms are dropped from equation (1). The venturis which are operating can be determined from the value of a unique multiple critical venturi code number MCV. Its value is the sum of the venturi numbers (see fig. 3(c)) that are being used. For example, MCV = 22 indicates that venturi number 2, venturi number 4, and venturi number 16.1 are being used (2 + 4 + 16 = 22). Venturi number 16.1 is always used when only one of the largest size venturis is required. The ideal weight-flow terms in equation (1) are defined as

$$w_{i,x} = \frac{P_{V1} A_x C^* \sqrt{g}}{\sqrt{RT_V}} \quad (2)$$

where x is the venturi number. Values for each venturi throat area A_x are given in figure 3(c). The critical-flow factor used in equation (2) is defined as

$$C^* = A + B(P_{V1}) + C(P_{V1})^2 + D(P_{V1})^3 \quad (3a)$$

where

$$A = K_0 + K_1(T_V - 460) + K_2(T_V - 460)^2 + K_3(T_V - 460)^3 \quad (3b)$$

$$B = K_4 + K_5(T_V - 460) + K_6(T_V - 460)^2 + K_7(T_V - 460)^3 \quad (3c)$$

$$C = K_8 + K_9(T_V - 460) + K_{10}(T_V - 460)^2 + K_{11}(T_V - 460)^3 \quad (3d)$$

$$D = K_{12} + K_{13}(T_V - 460) + K_{14}(T_V - 460)^2 + K_{15}(T_V - 460)^3 \quad (3e)$$

where constants K_0, K_1, \dots, K_{15} are provided in table III. Equation (3a) is limited to values of $P_{V1} = 0$ psia to 1500 psia and values of $T_V = 460^\circ R$ to $660^\circ R$. The venturi discharge coefficient terms $C_{d,x}$ in equation (1) are obtained from table II as a function of venturi throat Reynolds number per inch, which is defined as

$$R_{d,v} = \frac{P_{V1} C^* \sqrt{g}}{\mu \sqrt{RT_V}} \quad (4)$$

The viscosity term μ in equation (4) is obtained from the following approximation of Sutherland's formula:

$$\mu = (2.6812 \times 10^{-8}) \frac{2.27(0.8333T_v)^{1.5}}{0.8333T_v + 198.6} \quad (5)$$

Ideal weight flow through each nozzle tested was determined from equations (6) depending on the value of nozzle pressure ratio NPR. If $\text{NPR} < (\text{NPR})_c$:

$$w_i = P_{t,j} A_t \left(\frac{1}{\text{NPR}} \right)^{1/\gamma} \sqrt{\frac{2\gamma}{(\gamma - 1)RT_{t,j}} \left[1 - \left(\frac{1}{\text{NPR}} \right)^{(\gamma-1)/\gamma} \right]} \quad (6a)$$

If $\text{NPR} > (\text{NPR})_c$:

$$w_i = P_{t,j} A_t \sqrt{\frac{\gamma}{RT_{t,j}} \left(\frac{2}{\gamma + 1} \right)^{(\gamma+1)/(\gamma-1)}} \quad (6b)$$

Nozzle discharge coefficients presented in this paper were then determined from measured nozzle weight-flow (eq. (1)) and nozzle ideal weight-flow (eq. (6)) values.

As discussed in the "Instrumentation" section, a 13-probe rake was used to measure jet total-pressure profiles at the throat of each configuration tested. Values of average (for internal probes 1 to 5; see fig. 2(b)) jet total pressure $p_{t,j}$, individual internal-probe total pressures, $p_{t,j,1}$ to $p_{t,j,5}$, radial position of each probe used on the 13-probe rake r/r_t , and individual throat jet total pressures (measured with 13-probe rake) p_{rake} are provided in table IV for each configuration and NPR tested. Typical exhaust total-pressure profiles measured at the nozzle throat are shown in figure 6 for several configurations. The values of wall static pressure shown in figure 6 were assumed to be equal to $0.5283p_{t,j}$ (for $M = 1.0$). The total-pressure profiles measured at the throat of each configuration were used to determine rake correction factors $K_{R,1}, K_{R,2}, \dots, K_{R,5}$ for each individual internal total-pressure probe. The area under each total-pressure profile at the throat (typical examples shown in fig. 6) was obtained by using a compensating polar planimeter to provide an integrated value of jet total pressure at the throat $(p_{\text{rake}})_{\text{int}}$ for each $p_{t,j}$ set by the internal total-pressure probes. The integrated values of jet total pressure at the throat $(p_{\text{rake}})_{\text{int}}$ were then plotted against jet total pressure measured with each internal rake probe $p_{t,j,1}, p_{t,j,2}, \dots, p_{t,j,5}$. A typical plot of this variation is presented in figure 7 for internal probe number 1 (see fig. 2(b)) on the configuration with $A_t = 0.999 \text{ in}^2$ and $A_{\text{choke}} = 3.853 \text{ in}^2$. The resulting slope of the line representing this variation is equal to the rake correction factor for the particular probe and configuration plotted. For the example given in figure 7, the result is the value of $K_{R,1}$ for the configuration with $A_t = 0.999 \text{ in}^2$ and $A_{\text{choke}} = 3.853 \text{ in}^2$. Values of rake correction factors obtained in this manner for all internal jet total-pressure probes in all configurations tested are provided in the table of figure 2(b). Two passes through the data reduction code were then conducted using equations (7) and (8) to compute average jet total pressure and nozzle pressure ratio, respectively.

$$p_{t,j} = \frac{\sum_{i=1}^5 (p_{t,j,i})(K_{R,i})}{5} \quad (7)$$

$$\text{NPR} = \frac{p_{t,j}}{p_a} \quad (8)$$

The first data reduction pass used rake correction factors equal to 1.0 (uncorrected internal total-pressure probe data). The second data reduction pass used the rake correction factors determined with the procedure discussed above and provided in the table of figure 2(b). The resulting values of $p_{t,j}$ and NPR were used to determine nozzle ideal weight-flow rate w_i and nozzle discharge coefficient C_d for each data reduction pass. Of course, when the rake correction factors determined from measured total-pressure profiles at the throat are used, the jet total pressures measured with the internal rakes are corrected to the integrated rake values and most, if not all, of the effects of boundary-layer growth and streamline curvature are removed from the data. The resulting values of discharge coefficient should then be near unity.

As mentioned in the "Instrumentation" section, three measurements of the upstream venturi pressure p_{v1} were recorded simultaneously for each data point. Except for the case when a study of discharge coefficient sensitivity to small errors in measured p_{v1} was conducted, the value of p_{v1} used in equations (2), (3a), and (4) was the average of the three separate measurements.

Throat Reynolds number of the Stratford choke nozzles is defined as

$$R_d = (0.3192 \times 10^6) \left(\frac{D_t}{12} \right) (p_{t,j}) \quad (9)$$

The constant used in equation (9) represents Reynolds number per foot at a total pressure of 1 psia and was obtained from chart 25 of reference 12 for $M = 1.0$ and $T_{t,j} = 530^\circ\text{R}$.

RESULTS AND DISCUSSION

Validation of Multiple Critical Venturi System

An initial study was conducted to determine the sensitivity of the multiple critical venturi system operation (determination of nozzle weight flow and discharge coefficient) to individual venturi measurements (p_{v1} and T_v). As described in the "Instrumentation" section, three separate measurements of p_{v1} were made. Two separate passes through the data reduction code were made for the $A_t = 3.992 \text{ in}^2$ configuration, one for a single measurement of p_{v1} in equations (2), (3a), and (4) of the "Data Reduction" section and one for the average of the three p_{v1} measurements. Resulting discharge coefficients from these two data reduction passes are presented in figure 8 as a function of NPR. Although the differences between these two data sets are small, close examination indicates a slightly smaller data spread when the

averaged venturi pressure is used, particularly at $NPR < 2.0$. The relative effect of a small error in T_v or in p_{v1} on measured weight-flow rate is shown in the following table for $MCV = 22$ (venturi number 2, venturi number 4, and venturi number 16.1 operating).

| T_v , °R | p_{v1} , psi | w_p , lb/sec | Error, percent |
|------------|----------------|----------------|----------------|
| 560 | 200 | 2.7068 | Baseline |
| 561 | 200 | 2.7043 | .09 |
| 560 | 210 | 2.8428 | 5.02 |
| 560 | 1000 | 13.7788 | Baseline |
| 561 | 1000 | 13.7643 | .11 |
| 560 | 1010 | 13.9195 | 1.02 |

Two baseline venturi operating conditions were assumed for the calculations presented in the above table, one at low-weight-flow conditions ($p_{v1} = 200$ psi) and one at high-weight-flow conditions ($p_{v1} = 1000$ psi). A venturi operating temperature of $560^\circ R$ was assumed at both baseline flow conditions. Weight-flow values at both conditions were computed with an assumed temperature measurement uncertainty of 1° and then with an assumed pressure measurement uncertainty of 1 percent of gage full-scale reading (for example, 10 psi for a 1000-psi gage reading). As illustrated by the data in this table, a 1° uncertainty in measurement of T_v would have very little effect on computed weight flow. However, as shown in the table, a 1-percent uncertainty in the measurement of p_{v1} would have a significant effect on the computed value of weight flow. The uncertainty in w_p was particularly large at low-weight-flow operating conditions since a large gage size is required to cover the full operating range of the multiple critical venturi system. For this reason, measured weight flows (and thus discharge coefficients) presented in the remainder of this paper were computed with an average value of p_{v1} from the three separate measurements. This procedure will help eliminate data scatter, particularly at low values of NPR . It also points out the importance of correctly sizing the pressure transducers used to measure the upstream venturi pressure.

As mentioned in the "Stratford Choke Nozzles" section, the Langley 16-Foot Transonic Tunnel Stratford choke nozzles with $A_t = 1.933$ in² and $A_t = 5.711$ in² have been previously calibrated against primary standard nozzles at the Colorado Engineering Experiment Station, Inc. (CEESI). Correct operation of the Langley 16-Foot Transonic Tunnel multiple critical venturi system was validated by comparing discharge coefficients of these two nozzles obtained from the venturi system with those obtained during the CEESI calibration (unpublished data). This comparison is presented in figure 9. The data points on figure 9 identified with flags were obtained at unchoked nozzle conditions ($NPR < (NPR)_c$). Thus, the exhaust velocity at the nozzle throat for these data points was not sonic and the equation for Reynolds number (eq. (9)) given in the "Data Reduction" section is not valid ($M \neq 1.0$). Reynolds numbers for these data points were computed with the appropriate constants from chart 25 of reference 13. As shown in figure 9, excellent agreement generally exists between the multiple critical venturi discharge coefficients and the CEESI calibration data, particularly for the $A_t = 5.711$ in² nozzle. Venturi-derived discharge coefficients generally agree within 0.5 percent with the calibration data at $NPR > 1.5$ for the $A_t = 1.933$ in² nozzle and at $NPR > 1.75$ for the $A_t = 5.711$ in² nozzle. The loss

of data agreement at very low NPR (less than 1.75) may be a result of inaccuracies in the $p_{t,j}$ measurement. The data shown in figure 9 indicate that the Langley 16-Foot Transonic Tunnel multiple critical venturi system provides an accurate (within 0.005) measurement of nozzle discharge coefficients, particularly at $NPR > 1.75$. Substitution of a lower range pressure transducer for p_{v1} measurement during low-NPR operation should measurably improve the accuracy of discharge coefficients for $NPR < 1.75$.

Stratford-Choke-Nozzle Discharge Coefficients

Stratford-choke-nozzle discharge coefficients measured with the multiple critical venturi system are presented in figures 10 and 11 as a function of NPR for every combination of nozzle-throat area and choke-plate open area tested. Discharge coefficients shown in figure 10 were computed with jet total pressure $p_{t,j}$ corrected to the integrated value of total pressure at the throat by use of the rake correction factors discussed in the "Data Reduction" section. Discharge coefficients shown in figure 11 were computed with jet total pressure as measured with the internal rakes ($K_{R,1}$ to $K_{R,5} = 1.0$). Also presented in figures 10 and 11 are the average discharge coefficients for choked flow conditions \bar{C}_d (average of all C_d for $NPR > 1.89$) for each nozzle--choke-plate combination.

When jet total pressure is corrected to the integrated value at the throat (see fig. 10), discharge coefficients at $NPR > 2.0$ are approximately equal to unity. With only two exceptions ($A_t = 0.999 \text{ in}^2$, $A_{\text{choke}} = 1.750 \text{ in}^2$ and $A_t = 5.711 \text{ in}^2$, $A_{\text{choke}} = 3.853 \text{ in}^2$), values of average discharge coefficient \bar{C}_d are within 0.005 of unity (demonstrated accuracy of multiple critical venturi system; see fig. 9). This result was expected since correcting internal jet total pressure to the value at the throat (assuming no total-pressure losses between the internal instrumentation location and the nozzle throat) would eliminate most of the loss sources described in reference 7. Two of the most notable total-pressure losses which would be eliminated are the boundary-layer growth along the nozzle walls and the distortion of the total-pressure profile resulting from upstream piping effects. The rake correction factors affect jet total pressure $p_{t,j}$ (see eq. (7)), nozzle pressure ratio NPR (see eq. (8)), and ideal weight-flow rate w_i (see eq. (6)) only; measured weight-flow rate w_p (see eqs. (1) to (5)) is not affected by the rake correction factors. Thus, the discharge coefficients shown in figures 10 and 11 are based on the same measured values of weight-flow rate.

Figure 11 presents Stratford-choke-nozzle discharge coefficients computed from uncorrected internal jet total pressures. Discharge coefficients shown in this figure include total-pressure losses from the internal total-pressure instrumentation location to the nozzle throat. Average nozzle discharge coefficients \bar{C}_d shown in figure 11 are always less than unity and range in value from 0.978 to 0.996, depending on the configuration. Computed discharge coefficients given in reference 6 for nozzles conforming to the design guidelines from which the Langley 16-Foot Transonic Tunnel Stratford choke nozzles were designed ranged from 0.9925 to 0.9975. The values of \bar{C}_d measured during the present test which fall below the range of computed discharge coefficients given in reference 6 ($\bar{C}_d < 0.9925$) probably result from nonconformance to prescribed design guidelines for some of the current test nozzles. These effects are discussed later along with the effects of nozzle-throat area and choke-plate open area on measured discharge coefficient.

As shown in figures 10 and 11, nozzle discharge coefficient is nearly independent of NPR once choke flow conditions are reached at the nozzle throat ($NPR > 1.89$).

However, several of the nozzles with smaller throat areas ($A_t < 3.002 \text{ in}^2$) did show a slight increasing trend of C_d with NPR. Since the small-throat-area nozzles have throat Reynolds numbers of approximately 1×10^6 at low NPR (see table I), this variation in C_d with NPR may be a result of transition (and movement thereof) from a laminar to a turbulent wall boundary layer.

The effect of MCV (number and combination of venturis operating) on measured discharge coefficient is shown in the (d) and (f) parts of figures 10 and 11. If the multiple critical venturi system operates as designed, the number and combination of venturis operating should have no effect on measured discharge coefficient. As shown in these figures, the data agreement for all MCV values tested is excellent, and it can be concluded that the number and combination of venturis operating does not have an effect on measured discharge coefficient.

To investigate the effect of venturi temperature (and thus jet total temperature), the $A_t = 5.711 \text{ in}^2$ configuration with $A_{\text{choke}} = 3.853 \text{ in}^2$ was tested at $(T_{t,j})_{\text{nom}} = 530^\circ\text{R}$ and 550°R . Again, if the multiple critical venturi system is operating properly, venturi temperature should have no effect on measured discharge coefficient. These data are shown in figures 10(e) and 11(e), and excellent agreement of discharge coefficients for the two different venturi temperatures is exhibited; measured discharge coefficient is independent of venturi temperature.

Figure 12 presents a summary plot showing the effect of Stratford-choke-nozzle-throat area A_t on average nozzle discharge coefficient \bar{C}_d for all choke-plate open areas A_{choke} tested. Average discharge coefficients are those values listed on figures 10 and 11 and do not include unchoked (NPR < 1.89) nozzle data. The data points identified with flags in figure 12 were obtained on a configuration with A_{choke} greater than A_t . This condition would indicate that the flow through the choke plate is not choked and that the choke plate is serving as a flow straightening device only. Whether or not the choke-plate flow is choked or unchoked should have no effect on discharge coefficient. As shown in figure 12, average discharge coefficients tend to peak for nozzle throat areas between 2.0 in^2 and 6.0 in^2 . A more descriptive conclusion is that for the Stratford choke nozzles of the current test, average discharge coefficient decreases for nozzle-throat areas less than 2.0 in^2 or greater than 6.0 in^2 . As mentioned previously, the range of experimental average discharge coefficients (0.978 to 0.996 for uncorrected internal total pressures) from the current investigation exceeds the range of computed discharge coefficients (0.9925 to 0.9975) given in reference 6. From figure 12, the average discharge coefficients for nozzles of the current test with $1.933 \text{ in}^2 < A_t < 5.711 \text{ in}^2$ generally fall within the computed discharge coefficient range of reference 6. It is hypothesized that discharge coefficients for the Stratford choke nozzles with $A_t = 0.999 \text{ in}^2$, 8.501 in^2 , and 11.352 in^2 are reduced because of nonconformance to the design criteria of reference 6. Comparison of the current Stratford-choke-nozzle geometries with the design guidelines of reference 6 is shown in table I. Table I indicates that although Stratford recommends that nozzle operation be limited to nozzle-throat Reynolds numbers greater than 1×10^6 , the $A_t = 0.999 \text{ in}^2$ nozzle of the current test does not reach this value until an NPR between 2.0 and 3.0 is reached. Thus, the $A_t = 0.999 \text{ in}^2$ nozzle is operating near the extreme end of this design guideline. Another factor which could affect discharge coefficient values of small-throat-area nozzles is that the nozzle wall boundary-layer thickness constitutes a large percentage of the throat area. However, if wall boundary-layer thickness were a problem, it should be eliminated by correcting the internal total pressure to the integrated value of total pressure at the throat. As indicated by the right side of figure 12 (corrected $p_{t,j}$), this is not the case, and the decrease in discharge

coefficient for the lower values of A_t appears to be caused by some other factor (probably operating at a Reynolds number which is too low, as discussed earlier).

As shown in table I, the recommended value of L_2/D_t was not obtained with the $A_t = 8.501 \text{ in}^2$ and 11.352 in^2 nozzles of the current test. The reason for this deviation from prescribed guidelines is that the maximum internal tail-pipe-model diameter D_{max} was fixed at a constant value. Both of these nozzles show substantial decreases in discharge coefficient (for $K_{R,1}$ to $K_{R,5} = 1.0$) to values below the lower bound of computed discharge coefficients from reference 6. One factor which could affect discharge coefficient for the large-throat-area nozzles is upstream convergence. Since D_{max} of the current model was fixed, the amount of convergence leading into the throat decreases with increasing throat area. For the nozzles with larger throat areas, particularly for the $A_t = 11.352 \text{ in}^2$ nozzle, throat convergence was small. Results from reference 13 indicate that flow distortion (distortion of total-pressure profile at the throat) increases significantly with decreasing nozzle contraction ratio A_{max}/A_t . The effect of nozzle contraction ratio (hence, of throat area) and of choke-plate open area on a total-pressure distortion parameter ΔK_R derived from the rake correction factors is presented in figure 13. The total-pressure distortion parameter shown in figure 13 is an indicator of distortion at the internal total-pressure instrumentation location. As shown in figure 13, ΔK_R increases rapidly as contraction ratio is decreased (by increasing A_t) to values less than 3.5. The $A_t = 8.501 \text{ in}^2$ and 11.352 in^2 nozzles have contraction ratios of 2.37 and 1.77, respectively. Figure 13 also indicates that total-pressure distortion is reduced by increasing choke-plate open area.

The amount of flow distortion in the large-throat-area nozzles discussed above could have a significant effect on the measurement of $p_{t,j}$ and, thus, on discharge coefficient. Correcting internal rake total-pressure measurements to the integrated value of jet total pressure at the nozzle throat should eliminate flow distortion effects on discharge coefficient. As shown in the right side of figure 12, applying the rake correction factors to the discharge coefficient computation either eliminates or greatly reduces the decrease in \bar{C}_d exhibited by the $A_t = 8.501 \text{ in}^2$ and $A_t = 11.352 \text{ in}^2$ nozzles when uncorrected total-pressure measurements are used to compute \bar{C}_d (left side of fig. 12). This result indicates that most of the decrease in \bar{C}_d measured for the large-throat-area nozzles is caused by flow distortion in the total-pressure profiles.

The effect of choke-plate (flow straightener) open area A_{choke} on average discharge coefficient is presented in figure 14. Choke-plate open area should have no effect on nozzle discharge coefficient unless a large amount of flow distortion is introduced by the choke plate itself. From the results shown in figure 13, the choke plates with the smallest open areas produce the largest amounts of flow distortion, particularly for large-throat-area nozzles. As shown in figure 14, choke-plate open area generally has little effect on average discharge coefficient except for the two nozzles with the largest throat areas tested. The variation in \bar{C}_d with A_{choke} for $K_{R,1}$ to $K_{R,5} = 1.0$ is less than 1.5 percent for all nozzles tested and is generally less than 0.5 percent for nozzles with $A_t < 8.501 \text{ in}^2$. Total-pressure profile distortion is obviously affecting the discharge coefficient data spread for the two nozzles with the largest throat areas. Correcting measured total pressures with the rake correction factors (right side of fig. 14) reduces the variation of \bar{C}_d with A_{choke} from 0.9 to 1.5 percent to 0.6 to 0.8 percent for these two nozzles. The only consistent trend shown in figure 14 is that the $A_{\text{choke}} = 15.286 \text{ in}^2$ choke plate

always provides the highest value of average discharge coefficient when $K_{R,1}$ to $K_{R,5} = 1.0$. The variation in \bar{C}_d with A_{choke} for all other choke plates tested is generally less than 0.3 percent.

A summary plot of the discharge coefficients for the Langley 16-Foot Transonic Tunnel Stratford choke nozzles is presented in figure 15. The discharge coefficient parameter $\bar{C}_{d,avg}$ shown in this figure is the average of all average discharge coefficients \bar{C}_d obtained at each nozzle-throat area (see figs. 12 and 14), with one exception. Since most nozzle test procedures typically dictate a choke-plate flow straightener (as opposed to screens) and since the screen configurations

($A_{choke} = 15.286 \text{ in}^2$) consistently produced higher discharge coefficients than the other choke-plate configurations, data for the screen configurations are omitted from $\bar{C}_{d,avg}$. In addition, since discharge coefficients obtained for unchoked flow conditions ($NPR < 1.89$) were omitted from the computation of average discharge coefficient \bar{C}_d , these data are also not included in $\bar{C}_{d,avg}$. Thus the data of figure 15 are for choked flow Stratford choke nozzles with choke-plate flow straighteners only. Discharge coefficients for unchoked flow conditions can be obtained from figures 10 and 11. Discharge coefficients for Stratford choke nozzles with screens as flow straighteners can be obtained from figures 12 and 14.

When internal total-pressure rakes are corrected to the integrated value of total pressure at the throat, $\bar{C}_{d,avg}$ is generally within 0.5 percent of unity (fig. 15). When internal total-pressure rakes are not corrected (typical), measured discharge coefficients for $1.933 \text{ in}^2 < A_t < 5.711 \text{ in}^2$ generally fall within the computed range of discharge coefficient given in reference 6 for these types of nozzles. Measured discharge coefficient for the $A_t = 0.999 \text{ in}^2$ nozzle falls below the computed value (ref. 6), probably because nozzle-throat Reynolds number falls below the limit recommended in reference 6. Discharge coefficients for the $A_t = 8.501 \text{ in}^2$ and 11.352 in^2 nozzles fall below the computed value because of total-pressure profile distortion caused by low nozzle contraction ratios A_{max}/A_t .

CONCLUSIONS

An investigation has been conducted in the Langley 16-Foot Transonic Tunnel to determine and document the weight-flow measurement characteristics of a multiple critical venturi system and the nozzle discharge coefficient characteristics of a series of convergent calibration nozzles. The effects on model discharge coefficient of nozzle-throat area, model choke-plate open area, nozzle pressure ratio, jet total temperature, and number and combination of operating venturis were investigated. Tests were conducted at static conditions (tunnel wind off) at nozzle pressure ratios from 1.3 to 7.0. Results of this investigation indicate the following conclusions:

1. The Langley 16-Foot Transonic Tunnel multiple critical venturi system measures nozzle discharge coefficient to an uncertainty of 0.5 percent for nozzle pressure ratios equal to or above 1.75.

2. The measurement which was determined to have the largest effect on the multiple critical venturi system accuracy is the upstream venturi pressure. It is highly recommended that the average of multiple upstream venturi pressure measurements be used to compute weight flow from the venturi system. In addition, the pressure transducers used to measure the upstream venturi pressure should be carefully sized to cover the required pressure range only.

3. Discharge coefficients measured with the multiple critical venturi system are independent of the number or combination of venturis used. Discharge coefficients are also independent of small variations in venturi temperature.

4. Discharge coefficients measured for the Langley 16-Foot Transonic Tunnel Stratford choke nozzles fall within the expected range of 0.9925 to 0.9975 when nozzle-throat area is between 1.933 in² and 5.711 in².

5. A low nozzle-throat Reynolds number causes the discharge coefficient of the 0.999-in² throat area Stratford choke nozzle to be below the expected value.

6. Total-pressure profile distortion as a result of low contraction ratios is believed to cause the relatively low discharge coefficient levels of 0.986 and 0.979, respectively, for the 8.501-in² and the 11.352-in² throat area Stratford choke nozzles.

NASA Langley Research Center
Hampton, VA 23665-5225
May 16, 1985

REFERENCES

1. Beckwith, T. G.; and Buck, N. Lewis: **Mechanical Measurements.** Addison-Wesley Pub. Co., Inc., c.1961.
2. Berrier, Bobby L.: **Effect of Nonlifting Empennage Surfaces on Single-Engine Afterbody/Nozzle Drag at Mach Numbers From 0.5 to 2.2.** NASA TN D-8326, 1977.
3. Capone, Francis J.: **Static Performance of Five Twin-Engine Nonaxisymmetric Nozzles With Vectoring and Reversing Capability.** NASA TP-1224, 1978.
4. Capone, Francis J.; and Berrier, Bobby L.: **Investigation of Axisymmetric and Nonaxisymmetric Nozzles Installed on a 0.10-Scale F-18 Prototype Airplane Model.** NASA TP-1638, 1980.
5. Re, Richard J.; and Berrier, Bobby L.: **Static Internal Performance of Single Expansion-Ramp Nozzles With Thrust Vectoring and Reversing.** NASA TP-1962, 1982.
6. Stratford, B. S.: **The Calculation of the Discharge Coefficient of Profiled Choked Nozzles and the Optimum Profile for Absolute Air Flow Measurement.** J. R. Aeronaut. Soc., vol. 68, no. 640, Apr. 1964, pp. 237-245.
7. Smith, Robert E., Jr.; and Matz, Roy J.: **A Theoretical Method of Determining Discharge Coefficients for Venturis Operating at Critical Flow Conditions.** Trans. ASME, Ser. D: J. Basic Eng., vol. 84, no. 4, Dec. 1962, pp. 434-446.
8. Arnberg, B. T.: **Review of Critical Flowmeters for Gas Flow Measurements.** Trans. ASME, Ser. D: J. Basic Eng., vol. 84, no. 4, Dec. 1962, pp. 447-460.
9. Johnson, Robert C.: **Real-Gas Effects in Critical-Flow-Through Nozzles and Tabulated Thermodynamic Properties.** NASA TN D-2565, 1965.
10. Peddrew, Kathryn H., compiler: **A User's Guide to the Langley 16-Foot Transonic Tunnel.** NASA TM-83186, 1981.
11. Shapiro, Ascher H.: **The Dynamics and Thermodynamics of Compressible Fluid Flow.** Volume I. Ronald Press Co., c.1953.
12. Ames Research Staff: **Equations, Tables, and Charts for Compressible Flow.** NACA Rep. 1135, 1953. (Supersedes NACA TN 1428.)
13. Salters, Leland B., Jr.; and Chamales, Nicholas C.: **Studies of Flow Distortion in the Tailpipes of Hydrogen Peroxide Gas Generators Used for Jet-Engine Simulation.** NASA TM X-1671, 1968.

TABLE 1.- TEST NOZZLE GEOMETRY AND REFERENCE 6 DESIGN GUIDELINES

| Design feature | Reference 6 guidelines | Test nozzle geometry for A_t , in ² , of - | | | | | | | |
|--|------------------------|---|-----------------------|-----------------------|-----------------------|-----------------------|-----------------------|-----------------------|-----|
| | | 0.999 | 1.933 | 3.002 | 3.992 | 5.711 | 8.501 | 11.352 | |
| Choked flow | Yes | Yes | Yes | Yes | Yes | Yes | Yes | Yes | Yes |
| Continuously curving throat wall profile | Yes | Yes | Yes | Yes | Yes | Yes | Yes | Yes | Yes |
| D_{max}/D_t | 2 to 3 | 4.49 | 3.23 | 2.59 | 2.25 | 1.88 | 1.54 | 1.33 | |
| R_1/D_t | 2 | 2 | 2 | 2 | 2 | 2 | 2 | 2 | 2 |
| L_2/D_t | >.80 | .80 | 1.03 | .80 | .91 | .83 | .69 | .61 | |
| R_d at NPR = 2 | >1 x 10 ⁶ | 8.8 x 10 ⁵ | 1.2 x 10 ⁶ | 1.5 x 10 ⁶ | 1.8 x 10 ⁶ | 2.1 x 10 ⁶ | 2.6 x 10 ⁶ | 3.0 x 10 ⁶ | |
| R_d at NPR = 3 | >1 x 10 ⁶ | 1.3 x 10 ⁶ | 1.8 x 10 ⁶ | 2.3 x 10 ⁶ | 2.7 x 10 ⁶ | 3.2 x 10 ⁶ | 3.9 x 10 ⁶ | 4.5 x 10 ⁶ | |
| R_d at NPR = 5 | >1 x 10 ⁶ | 2.2 x 10 ⁶ | 3.1 x 10 ⁶ | 3.8 x 10 ⁶ | 4.4 x 10 ⁶ | 5.3 x 10 ⁶ | 6.4 x 10 ⁶ | 7.4 x 10 ⁶ | |
| R_d at NPR = 7 | >1 x 10 ⁶ | 3.1 x 10 ⁶ | 4.3 x 10 ⁶ | 5.4 x 10 ⁶ | 6.2 x 10 ⁶ | 7.4 x 10 ⁶ | 9.0 x 10 ⁶ | 1.0 x 10 ⁷ | |

TABLE II.- INDIVIDUAL CALIBRATED-VENTURI DISCHARGE COEFFICIENTS

| R _{d,v} per inch | Discharge coefficients for venturi number - | | | | | |
|---------------------------|---|--------|--------|--------|--------|--------|
| | 1 | 2 | 4 | 8 | 16.1 | 16.2 |
| 0.6 × 10 ⁶ | 0.9838 | 0.9857 | 0.9886 | 0.9892 | 0.9922 | 0.9921 |
| .9 | .9856 | .9880 | .9910 | .9912 | .9932 | .9930 |
| 1.4 | .9875 | .9902 | .9931 | .9930 | .9940 | .9938 |
| 2.1 | .9890 | .9920 | .9943 | .9939 | .9941 | .9938 |
| 3.2 | .9902 | .9931 | .9947 | .9939 | .9934 | .9932 |
| 4.8 | .9901 | .9934 | .9939 | .9932 | .9930 | .9928 |
| 7.3 | .9893 | .9930 | .9933 | .9931 | .9930 | .9927 |
| 11.0 | .9903 | .9938 | .9933 | .9934 | .9931 | .9927 |
| 17.0 | .9912 | .9938 | .9935 | .9932 | .9931 | .9928 |
| 26.0 | .9916 | .9939 | .9936 | .9933 | .9932 | .9928 |
| 40.0 | .9918 | .9939 | .9937 | .9934 | .9933 | .9929 |

TABLE III.- CONSTANTS FOR CRITICAL-FLOW FACTOR EQUATION

[From unpublished multiple critical venturi data,
Boeing Commercial Airplane Group]

| Constant | Value of constant | Constant | Value of constant |
|----------------|-----------------------------|-----------------|-----------------------------|
| K ₀ | 0.68493 | K ₈ | 3.8268 × 10 ⁻⁹ |
| K ₁ | -6.7865 × 10 ⁻⁷ | K ₉ | -7.3594 × 10 ⁻¹¹ |
| K ₂ | -4.9249 × 10 ⁻⁹ | K ₁₀ | 4.9408 × 10 ⁻¹³ |
| K ₃ | -1.0056 × 10 ⁻¹¹ | K ₁₁ | -1.1853 × 10 ⁻¹⁵ |
| K ₄ | 3.0262 × 10 ⁻⁵ | K ₁₂ | -1.4721 × 10 ⁻¹² |
| K ₅ | -1.9236 × 10 ⁻⁷ | K ₁₃ | 1.7692 × 10 ⁻¹⁴ |
| K ₆ | 5.4687 × 10 ⁻¹⁰ | K ₁₄ | -1.1238 × 10 ⁻¹⁶ |
| K ₇ | -6.5437 × 10 ⁻¹³ | K ₁₅ | 2.8935 × 10 ⁻¹⁹ |

ORIGINAL PAGE IS
OF POOR QUALITY

TABLE IV.- VALUES OF TOTAL PRESSURE MEASURED IN THE INSTRUMENTATION SECTION AND AT THE NOZZLE EXIT

[All pressure measurements in psi.]

(a) $A_t = 0.999 \text{ in}^2$; $A_{\text{choke}} = 1.750 \text{ in}^2$

| NPR | $P_{t,j}$ | $P_{t,j,1}$ | $P_{t,j,2}$ | $P_{t,j,3}$ | $P_{t,j,4}$ | $P_{t,j,5}$ |
|-------|-----------|-------------|-------------|-------------|-------------|-------------|
| 1.308 | 19.361 | 19.371 | 19.367 | 19.349 | 19.392 | 19.327 |
| 1.540 | 22.791 | 22.797 | 22.799 | 22.771 | 22.827 | 22.761 |
| 1.486 | 21.983 | 21.998 | 21.985 | 21.976 | 22.009 | 21.949 |
| 1.749 | 25.887 | 25.978 | 25.864 | 25.856 | 25.950 | 25.884 |
| 2.011 | 29.750 | 29.732 | 29.745 | 29.737 | 29.797 | 29.739 |
| 2.496 | 36.936 | 36.924 | 36.925 | 36.922 | 36.990 | 36.922 |
| 3.004 | 44.443 | 44.386 | 44.393 | 44.393 | 44.556 | 44.487 |
| 4.980 | 73.680 | 73.563 | 73.573 | 73.586 | 73.895 | 73.785 |
| 5.011 | 74.125 | 73.991 | 74.036 | 74.032 | 74.333 | 74.232 |
| 7.011 | 103.706 | 103.507 | 103.577 | 103.567 | 104.008 | 103.872 |

| NPR | $P_{t,j}$ | P_{rake} at r/r_t of - | | | | | |
|-------|-----------|-----------------------------------|---------|---------|---------|---------|---------|
| | | -.87 | -.53 | -.18 | .18 | .51 | .92 |
| 1.308 | 19.361 | 19.328 | 19.367 | 19.356 | 19.373 | 19.329 | 19.358 |
| 1.540 | 22.791 | 22.737 | 22.777 | 22.774 | 22.787 | 22.748 | 22.774 |
| 1.486 | 21.983 | 21.948 | 21.985 | 21.984 | 22.002 | 21.958 | 21.983 |
| 1.749 | 25.897 | 25.871 | 25.919 | 25.908 | 25.926 | 25.894 | 25.908 |
| 2.011 | 29.750 | 29.730 | 29.760 | 29.764 | 29.782 | 29.737 | 29.766 |
| 2.496 | 36.936 | 36.908 | 36.945 | 36.948 | 36.974 | 36.933 | 36.947 |
| 3.004 | 44.443 | 44.457 | 44.456 | 44.504 | 44.528 | 44.486 | 44.505 |
| 4.980 | 73.680 | 73.727 | 73.742 | 73.803 | 73.843 | 73.794 | 73.802 |
| 5.011 | 74.125 | 74.175 | 74.250 | 74.241 | 74.285 | 74.231 | 74.245 |
| 7.011 | 103.706 | 103.781 | 103.875 | 103.870 | 103.924 | 103.881 | 103.875 |

ORIGINAL PAGE IS
OF POOR QUALITY

TABLE IV.- Continued

(b) $A_t = 0.999 \text{ in}^2$; $A_{\text{choke}} = 3.853 \text{ in}^2$

| NPR | $P_{t,j}$ | $P_{t,j,1}$ | $P_{t,j,2}$ | $P_{t,j,3}$ | $P_{t,j,4}$ | $P_{t,j,5}$ |
|-------|-----------|-------------|-------------|-------------|-------------|-------------|
| 1.297 | 19.281 | 19.289 | 19.283 | 19.281 | 19.302 | 19.252 |
| 1.416 | 21.058 | 21.049 | 21.045 | 21.046 | 21.100 | 21.050 |
| 1.531 | 22.765 | 22.769 | 22.768 | 22.771 | 22.777 | 22.740 |
| 1.746 | 25.955 | 25.969 | 25.955 | 25.951 | 25.966 | 25.932 |
| 1.993 | 29.626 | 29.637 | 29.631 | 29.631 | 29.635 | 29.597 |
| 2.502 | 37.194 | 37.203 | 37.191 | 37.194 | 37.207 | 37.173 |
| 2.997 | 44.551 | 44.545 | 44.550 | 44.558 | 44.567 | 44.535 |
| 5.005 | 74.405 | 74.389 | 74.415 | 74.413 | 74.417 | 74.393 |
| 7.030 | 104.501 | 104.434 | 104.529 | 104.507 | 104.535 | 104.502 |

| NPR | $P_{t,j}$ | P_{rake} at r/r_t of - | | | | | |
|-------|-----------|-----------------------------------|---------|---------|---------|---------|---------|
| | | -.89 | -.56 | -.18 | .19 | .58 | .90 |
| 1.297 | 19.281 | 19.258 | 19.288 | 19.272 | 19.296 | 19.249 | 19.288 |
| 1.416 | 21.058 | 21.324 | 21.343 | 21.328 | 21.347 | 21.320 | 21.364 |
| 1.531 | 22.765 | 22.759 | 22.763 | 22.785 | 22.762 | 22.764 | 22.767 |
| 1.746 | 25.955 | 25.916 | 25.950 | 25.946 | 25.958 | 25.925 | 25.959 |
| 1.993 | 29.626 | 29.579 | 29.617 | 29.611 | 29.634 | 29.591 | 29.615 |
| 2.502 | 37.194 | 37.138 | 37.181 | 37.177 | 37.196 | 37.156 | 37.185 |
| 2.997 | 44.551 | 44.499 | 44.545 | 44.543 | 44.583 | 44.552 | 44.555 |
| 5.005 | 74.405 | 74.322 | 74.392 | 74.397 | 74.434 | 74.386 | 74.385 |
| 7.030 | 104.501 | 104.374 | 104.478 | 104.490 | 104.543 | 104.479 | 104.456 |

(c) $A_t = 0.999 \text{ in}^2$; $A_{\text{choke}} = 15.286 \text{ in}^2$

| NPR | $P_{t,j}$ | $P_{t,j,1}$ | $P_{t,j,2}$ | $P_{t,j,3}$ | $P_{t,j,4}$ | $P_{t,j,5}$ |
|-------|-----------|-------------|-------------|-------------|-------------|-------------|
| 1.302 | 19.149 | 19.141 | 19.173 | 19.149 | 19.162 | 19.119 |
| 1.513 | 22.253 | 22.262 | 22.280 | 22.248 | 22.258 | 22.218 |
| 1.756 | 25.828 | 25.838 | 25.848 | 25.832 | 25.831 | 25.791 |
| 2.009 | 29.552 | 29.548 | 29.580 | 29.552 | 29.556 | 29.526 |
| 2.516 | 37.003 | 36.996 | 37.032 | 37.006 | 37.008 | 36.972 |
| 2.988 | 43.950 | 43.940 | 43.970 | 43.951 | 43.960 | 43.931 |
| 5.024 | 73.890 | 73.859 | 73.917 | 73.894 | 73.904 | 73.876 |
| 7.009 | 103.096 | 103.013 | 103.137 | 103.131 | 103.114 | 103.082 |

| NPR | $P_{t,j}$ | P_{rake} at r/r_t of - | | | | |
|-------|-----------|-----------------------------------|---------|---------|---------|---------|
| | | -.91 | -.47 | .06 | .56 | .92 |
| 1.302 | 19.149 | 19.120 | 19.120 | 19.153 | 19.131 | 19.146 |
| 1.513 | 22.253 | 22.224 | 22.225 | 22.250 | 22.207 | 22.252 |
| 1.756 | 25.828 | 25.811 | 25.808 | 25.843 | 25.790 | 25.828 |
| 2.009 | 29.552 | 29.534 | 29.542 | 29.575 | 29.523 | 29.564 |
| 2.516 | 37.003 | 36.978 | 36.986 | 37.013 | 36.964 | 36.998 |
| 2.988 | 43.950 | 43.940 | 43.943 | 43.972 | 43.929 | 43.951 |
| 5.024 | 73.890 | 73.854 | 73.878 | 73.912 | 73.867 | 73.866 |
| 7.009 | 103.096 | 103.056 | 103.106 | 103.132 | 103.082 | 103.052 |

ORIGINAL PAGE IS
OF POOR QUALITY

TABLE IV.- Continued

(d) $A_t = 1.933 \text{ in}^2$; $A_{\text{choke}} = 1.750 \text{ in}^2$

| NPR | $P_{t,j}$ | $P_{t,j,1}$ | $P_{t,j,2}$ | $P_{t,j,3}$ | $P_{t,j,4}$ | $P_{t,j,5}$ |
|-------|-----------|-------------|-------------|-------------|-------------|-------------|
| 1.311 | 19.389 | 19.428 | 19.406 | 19.373 | 19.405 | 19.332 |
| 1.496 | 22.147 | 22.188 | 22.146 | 22.108 | 22.241 | 22.050 |
| 1.750 | 25.880 | 25.934 | 25.877 | 25.828 | 26.004 | 25.757 |
| 2.496 | 36.901 | 36.979 | 36.897 | 36.827 | 37.072 | 36.730 |
| 2.000 | 29.568 | 29.601 | 29.581 | 29.521 | 29.660 | 29.477 |
| 2.500 | 36.963 | 37.019 | 36.965 | 36.908 | 37.058 | 36.866 |
| 2.992 | 44.243 | 44.267 | 44.243 | 44.204 | 44.297 | 44.202 |
| 4.993 | 73.813 | 73.886 | 73.750 | 73.653 | 74.161 | 73.613 |
| 7.006 | 103.588 | 103.527 | 103.439 | 103.344 | 104.025 | 103.603 |

| NPR | $P_{t,j}$ | Prake at r/r_t of - | | | | | |
|-------|-----------|-----------------------|---------|---------|---------|---------|---------|
| | | -.94 | -.62 | -.33 | .10 | .54 | .88 |
| 1.311 | 19.389 | 19.389 | 19.400 | 19.421 | 19.428 | 19.394 | 19.417 |
| 1.498 | 22.147 | 22.142 | 22.175 | 22.172 | 22.194 | 22.145 | 22.176 |
| 1.750 | 25.880 | 25.869 | 25.867 | 25.904 | 25.925 | 25.878 | 25.913 |
| 2.496 | 36.901 | 36.908 | 36.930 | 36.944 | 36.972 | 36.917 | 36.952 |
| 2.000 | 29.568 | 29.557 | 29.579 | 29.570 | 29.602 | 29.544 | 29.570 |
| 2.500 | 36.963 | 36.925 | 36.957 | 36.958 | 36.985 | 36.931 | 36.952 |
| 2.992 | 44.243 | 44.208 | 44.215 | 44.214 | 44.249 | 44.184 | 44.201 |
| 4.993 | 73.813 | 73.898 | 73.915 | 73.923 | 73.959 | 73.899 | 73.922 |
| 7.006 | 103.588 | 103.732 | 103.740 | 103.741 | 103.799 | 103.691 | 103.717 |

(e) $A_t = 1.933 \text{ in}^2$; $A_{\text{choke}} = 3.853 \text{ in}^2$

| NPR | $P_{t,j}$ | $P_{r,j,1}$ | $P_{t,j,2}$ | $P_{t,j,3}$ | $P_{t,j,4}$ | $P_{t,j,5}$ |
|-------|-----------|-------------|-------------|-------------|-------------|-------------|
| 1.301 | 19.306 | 19.333 | 19.309 | 19.294 | 19.320 | 19.276 |
| 1.530 | 22.713 | 22.747 | 22.715 | 22.703 | 22.715 | 22.685 |
| 1.754 | 26.036 | 26.068 | 26.039 | 26.019 | 26.047 | 26.013 |
| 2.000 | 29.585 | 29.724 | 29.577 | 29.672 | 29.684 | 29.666 |
| 2.507 | 37.208 | 37.251 | 37.198 | 37.196 | 37.218 | 37.177 |
| 2.997 | 44.475 | 44.515 | 44.464 | 44.466 | 44.471 | 44.461 |
| 3.009 | 44.665 | 44.702 | 44.654 | 44.655 | 44.662 | 44.650 |
| 5.021 | 74.512 | 74.560 | 74.490 | 74.502 | 74.505 | 74.503 |
| 6.981 | 103.602 | 103.612 | 103.577 | 103.603 | 103.597 | 103.623 |
| 6.988 | 103.711 | 103.719 | 103.686 | 103.711 | 103.707 | 103.732 |

| NPR | $P_{t,j}$ | Prake at r/r_t of - | | | | | | |
|-------|-----------|-----------------------|---------|---------|---------|---------|---------|---------|
| | | -.90 | -.62 | -.35 | -.07 | .26 | .54 | .89 |
| 1.301 | 19.306 | 19.280 | 19.299 | 19.301 | 19.313 | 19.285 | 19.290 | 19.305 |
| 1.530 | 22.713 | 22.650 | 22.671 | 22.678 | 22.699 | 22.663 | 22.687 | 22.667 |
| 1.754 | 26.036 | 25.994 | 26.017 | 26.015 | 26.031 | 26.001 | 26.023 | 26.003 |
| 2.000 | 29.685 | 29.642 | 29.658 | 29.667 | 29.694 | 29.653 | 29.666 | 29.634 |
| 2.507 | 37.208 | 37.149 | 37.170 | 37.179 | 37.203 | 37.163 | 37.170 | 37.142 |
| 2.997 | 44.475 | 44.421 | 44.441 | 44.451 | 44.481 | 44.444 | 44.447 | 44.411 |
| 3.009 | 44.665 | 44.592 | 44.516 | 44.628 | 44.660 | 44.621 | 44.622 | 44.586 |
| 5.021 | 74.512 | 74.413 | 74.452 | 74.460 | 74.502 | 74.480 | 74.460 | 74.387 |
| 6.981 | 103.602 | 103.488 | 103.525 | 103.561 | 103.603 | 103.589 | 103.563 | 103.456 |
| 6.988 | 103.711 | 103.594 | 103.633 | 103.657 | 103.714 | 103.698 | 103.657 | 103.564 |

TABLE IV.- Continued

(f) $A_t = 1.933 \text{ in}^2$; $A_{\text{choke}} = 15.286 \text{ in}^2$

| NPR | $P_{t,j}$ | $P_{t,j,1}$ | $P_{t,j,2}$ | $P_{t,j,3}$ | $P_{t,j,4}$ | $P_{t,j,5}$ |
|-------|-----------|-------------|-------------|-------------|-------------|-------------|
| 1.339 | 19.706 | 19.705 | 19.735 | 19.704 | 19.719 | 19.668 |
| 1.497 | 22.035 | 22.039 | 22.068 | 22.037 | 22.036 | 21.994 |
| 1.772 | 26.077 | 26.081 | 26.112 | 26.081 | 26.073 | 26.038 |
| 1.982 | 29.163 | 29.163 | 29.193 | 29.169 | 29.155 | 29.136 |
| 2.491 | 36.665 | 36.637 | 36.713 | 36.680 | 36.661 | 36.632 |
| 3.005 | 44.236 | 44.221 | 44.276 | 44.261 | 44.213 | 44.212 |
| 5.037 | 74.135 | 74.128 | 74.181 | 74.164 | 74.097 | 74.103 |
| 7.011 | 103.187 | 103.168 | 103.246 | 103.225 | 103.137 | 103.158 |

| NPR | $P_{t,j}$ | P_{rake} at r/r_t of - | | | | | | |
|-------|-----------|-----------------------------------|---------|---------|---------|---------|---------|---------|
| | | -.94 | -.71 | -.40 | .02 | .34 | .67 | .96 |
| 1.339 | 19.706 | 19.651 | 19.692 | 19.685 | 19.710 | 19.667 | 19.710 | 19.704 |
| 1.497 | 22.035 | 21.995 | 22.029 | 22.014 | 22.050 | 22.011 | 22.040 | 22.048 |
| 1.772 | 26.077 | 26.012 | 26.058 | 26.060 | 26.083 | 26.044 | 26.085 | 26.067 |
| 1.982 | 29.163 | 29.108 | 29.148 | 29.140 | 29.168 | 29.137 | 29.179 | 29.149 |
| 2.491 | 36.665 | 36.617 | 36.658 | 36.651 | 36.688 | 36.648 | 36.681 | 36.654 |
| 3.005 | 44.236 | 44.167 | 44.210 | 44.208 | 44.240 | 44.200 | 44.237 | 44.203 |
| 5.037 | 74.135 | 74.054 | 74.110 | 74.111 | 74.135 | 74.101 | 74.135 | 74.079 |
| 7.011 | 103.187 | 103.096 | 103.185 | 103.166 | 103.185 | 103.170 | 103.191 | 103.126 |

(g) $A_t = 3.002 \text{ in}^2$; $A_{\text{choke}} = 1.750 \text{ in}^2$

| NPR | $P_{t,j}$ | $P_{t,j,1}$ | $P_{t,j,2}$ | $P_{t,j,3}$ | $P_{t,j,4}$ | $P_{t,j,5}$ |
|-------|-----------|-------------|-------------|-------------|-------------|-------------|
| 1.305 | 19.293 | 19.333 | 19.293 | 19.266 | 19.296 | 19.274 |
| 1.496 | 22.111 | 22.172 | 22.114 | 22.082 | 22.163 | 22.085 |
| 1.747 | 25.819 | 25.918 | 25.804 | 25.788 | 25.810 | 25.776 |
| 1.998 | 29.539 | 29.638 | 29.521 | 29.508 | 29.532 | 29.494 |
| 2.495 | 36.880 | 37.015 | 36.863 | 36.828 | 36.871 | 36.824 |
| 3.019 | 44.634 | 44.797 | 44.616 | 44.592 | 44.612 | 44.564 |
| 4.980 | 73.610 | 73.880 | 73.565 | 73.527 | 73.584 | 73.495 |
| 5.004 | 73.968 | 74.214 | 73.932 | 73.992 | 73.941 | 73.961 |
| 6.007 | 88.798 | 89.114 | 88.751 | 88.694 | 88.762 | 88.670 |

| NPR | $P_{t,j}$ | P_{rake} at r/r_t of - | | | | | | |
|-------|-----------|-----------------------------------|--------|--------|--------|--------|--------|--------|
| | | -.95 | -.65 | -.34 | .02 | .33 | .63 | .94 |
| 1.305 | 19.293 | 19.242 | 19.272 | 19.251 | 19.263 | 19.220 | 19.250 | 19.240 |
| 1.496 | 22.111 | 22.072 | 22.092 | 22.057 | 22.082 | 22.040 | 22.049 | 22.064 |
| 1.747 | 25.819 | 25.785 | 25.784 | 25.761 | 25.797 | 25.745 | 25.771 | 25.772 |
| 1.998 | 29.539 | 29.498 | 29.504 | 29.494 | 29.499 | 29.465 | 29.467 | 29.481 |
| 2.495 | 36.880 | 36.847 | 36.838 | 36.814 | 36.838 | 36.798 | 36.807 | 36.809 |
| 3.019 | 44.634 | 44.607 | 44.591 | 44.562 | 44.595 | 44.555 | 44.537 | 44.543 |
| 4.980 | 73.610 | 73.628 | 73.535 | 73.498 | 73.546 | 73.509 | 73.467 | 73.433 |
| 5.004 | 73.968 | 73.984 | 73.884 | 73.854 | 73.905 | 73.864 | 73.829 | 73.782 |
| 6.007 | 88.798 | 88.918 | 88.696 | 88.665 | 88.725 | 88.682 | 88.627 | 88.440 |

TABLE IV.- Continued

(h) $A_t = 3.002 \text{ in}^2$; $A_{\text{choke}} = 3.853 \text{ in}^2$

| NPR | $P_{t,j}$ | $P_{t,j,1}$ | $P_{t,j,2}$ | $P_{t,j,3}$ | $P_{t,j,4}$ | $P_{t,j,5}$ |
|-------|-----------|-------------|-------------|-------------|-------------|-------------|
| 1.288 | 19.102 | 19.144 | 19.099 | 19.085 | 19.115 | 19.067 |
| 1.498 | 22.219 | 22.264 | 22.205 | 22.211 | 22.223 | 22.191 |
| 1.754 | 26.016 | 26.077 | 26.003 | 25.997 | 26.014 | 25.991 |
| 1.995 | 29.588 | 29.652 | 29.557 | 29.56. | 29.597 | 29.576 |
| 2.503 | 37.121 | 37.204 | 37.075 | 37.104 | 37.107 | 37.113 |
| 3.004 | 44.543 | 44.627 | 44.502 | 44.521 | 44.523 | 44.545 |
| 4.997 | 74.097 | 74.232 | 74.218 | 74.062 | 74.050 | 74.121 |
| 6.979 | 103.483 | 103.639 | 103.376 | 103.436 | 103.414 | 103.551 |

| NPR | $P_{t,j}$ | P_{rake} at r/r_t of - | | | | | | | |
|-------|-----------|-----------------------------------|---------|---------|---------|---------|---------|---------|---------|
| | | -.94 | -.75 | -.56 | -.25 | .10 | .44 | .67 | .92 |
| 1.288 | 19.102 | 19.097 | 19.043 | 19.059 | 19.071 | 19.101 | 19.055 | 19.076 | 19.070 |
| 1.498 | 22.219 | 22.178 | 22.151 | 22.176 | 22.190 | 22.213 | 22.175 | 22.183 | 22.178 |
| 1.754 | 26.016 | 25.969 | 25.944 | 25.964 | 25.979 | 26.014 | 25.963 | 25.973 | 25.956 |
| 1.995 | 29.588 | 29.543 | 29.514 | 29.525 | 29.550 | 29.596 | 29.547 | 29.536 | 29.521 |
| 2.503 | 37.121 | 37.060 | 37.036 | 37.050 | 37.078 | 37.121 | 37.072 | 37.052 | 37.042 |
| 3.004 | 44.543 | 44.470 | 44.455 | 44.469 | 44.501 | 44.552 | 44.503 | 44.462 | 44.446 |
| 4.997 | 74.097 | 73.971 | 73.943 | 73.983 | 74.029 | 74.100 | 74.044 | 73.975 | 73.937 |
| 6.979 | 103.483 | 103.290 | 103.279 | 103.330 | 103.390 | 103.463 | 103.427 | 103.316 | 103.243 |

(i) $A_t = 3.002 \text{ in}^2$; $A_{\text{choke}} = 15.286 \text{ in}^2$

| NPR | $P_{t,j}$ | $P_{t,j,1}$ | $P_{t,j,2}$ | $P_{t,j,3}$ | $P_{t,j,4}$ | $P_{t,j,5}$ |
|-------|-----------|-------------|-------------|-------------|-------------|-------------|
| 1.310 | 19.293 | 19.285 | 19.316 | 19.305 | 19.290 | 19.270 |
| 1.517 | 22.338 | 22.340 | 22.368 | 22.338 | 22.330 | 22.313 |
| 1.757 | 25.869 | 25.876 | 25.882 | 25.883 | 25.849 | 25.857 |
| 1.994 | 29.353 | 29.359 | 29.370 | 29.375 | 29.327 | 29.334 |
| 2.501 | 36.827 | 36.834 | 36.848 | 36.845 | 36.792 | 36.816 |
| 3.009 | 44.304 | 44.311 | 44.329 | 44.330 | 44.244 | 44.301 |
| 3.504 | 51.580 | 51.590 | 51.609 | 51.614 | 51.504 | 51.585 |
| 5.021 | 73.919 | 73.922 | 73.953 | 73.962 | 73.820 | 73.937 |
| 6.988 | 102.879 | 102.875 | 102.936 | 102.931 | 102.739 | 102.914 |

| NPR | $P_{t,j}$ | P_{rake} at r/r_t of - | | | | | | | | |
|-------|-----------|-----------------------------------|---------|---------|---------|---------|---------|---------|---------|---------|
| | | -.96 | -.80 | -.58 | -.33 | 0.0 | .26 | .51 | .73 | .93 |
| 1.310 | 19.293 | 19.266 | 19.227 | 19.265 | 19.267 | 19.286 | 19. | 19.292 | 19.305 | 19.266 |
| 1.517 | 22.338 | 22.280 | 22.256 | 22.288 | 22.292 | 22.313 | 22.300 | 22.332 | 22.332 | 22.314 |
| 1.757 | 25.869 | 25.811 | 25.798 | 25.834 | 25.835 | 25.850 | 25.833 | 25.890 | 25.882 | 25.855 |
| 1.994 | 29.353 | 29.289 | 29.276 | 29.314 | 29.312 | 29.333 | 29.321 | 29.362 | 29.365 | 29.329 |
| 2.501 | 36.827 | 36.750 | 36.745 | 36.785 | 36.785 | 36.811 | 36.791 | 36.837 | 36.831 | 36.805 |
| 3.009 | 44.304 | 44.214 | 44.216 | 44.243 | 44.262 | 4.280 | 44.275 | 44.299 | 44.312 | 44.270 |
| 3.504 | 51.580 | 51.475 | 51.478 | 51.515 | 51.524 | 51.546 | 51.544 | 51.589 | 51.569 | 51.522 |
| 5.021 | 73.919 | 73.788 | 73.799 | 73.833 | 73.850 | 73.881 | 73.894 | 73.938 | 73.919 | 73.794 |
| 6.988 | 102.879 | 102.682 | 102.732 | 102.767 | 102.769 | 102.859 | 102.861 | 102.903 | 102.886 | 100.269 |

ORIGINAL PAGE IS
OF POOR QUALITY

TABLE IV.- Continued

(j) $A_t = 3.992 \text{ in}^2$; $A_{\text{choke}} = 1.750 \text{ in}^2$

| NPR | $P_{t,j}$ | $P_{t,j,1}$ | $P_{t,j,2}$ | $P_{t,j,3}$ | $P_{t,j,4}$ | $P_{t,j,5}$ |
|-------|-----------|-------------|-------------|-------------|-------------|-------------|
| 1.259 | 19.049 | 19.137 | 19.041 | 19.020 | 19.065 | 18.992 |
| 1.496 | 22.103 | 22.215 | 22.080 | 22.064 | 22.104 | 22.052 |
| 1.753 | 25.904 | 26.042 | 25.866 | 25.863 | 25.907 | 25.841 |
| 2.018 | 29.811 | 29.962 | 29.761 | 29.757 | 29.808 | 29.765 |
| 2.510 | 37.092 | 37.287 | 37.037 | 37.022 | 37.081 | 37.033 |
| 3.001 | 44.339 | 44.561 | 44.261 | 44.263 | 44.319 | 44.290 |
| 3.992 | 58.980 | 59.297 | 58.893 | 58.875 | 58.960 | 58.904 |
| 4.505 | 66.562 | 66.905 | 66.450 | 66.449 | 66.542 | 66.465 |

| NPR | $P_{t,j}$ | P_{rake} at r/r_t of - | | | | | | | | |
|-------|-----------|-----------------------------------|--------|--------|--------|--------|--------|--------|--------|--------|
| | | -.96 | -.68 | -.41 | -.17 | .01 | .23 | .48 | .71 | .94 |
| 1.289 | 19.049 | 19.046 | 18.967 | 18.997 | 18.992 | 19.019 | 18.972 | 19.006 | 18.992 | 19.004 |
| 1.496 | 22.103 | 22.102 | 22.008 | 22.046 | 22.041 | 22.060 | 22.024 | 22.046 | 22.045 | 22.058 |
| 1.753 | 25.904 | 25.908 | 25.787 | 25.821 | 25.815 | 25.846 | 25.812 | 25.836 | 25.808 | 25.839 |
| 2.018 | 29.811 | 29.823 | 29.685 | 29.717 | 29.712 | 29.742 | 29.709 | 29.720 | 29.706 | 29.742 |
| 2.510 | 37.092 | 37.083 | 36.930 | 36.973 | 36.965 | 37.001 | 36.974 | 36.981 | 36.943 | 37.000 |
| 3.001 | 44.339 | 44.357 | 44.177 | 44.217 | 44.208 | 44.250 | 44.228 | 44.217 | 44.183 | 44.235 |
| 3.992 | 58.986 | 58.980 | 58.756 | 58.803 | 58.803 | 58.857 | 58.824 | 58.800 | 58.742 | 58.838 |
| 4.505 | 66.562 | 66.559 | 66.327 | 66.374 | 66.360 | 66.423 | 66.399 | 66.362 | 66.303 | 66.396 |

(k) $A_t = 3.992 \text{ in}^2$; $A_{\text{choke}} = 3.853 \text{ in}^2$

| NPR | $P_{t,j}$ | $P_{t,j,1}$ | $P_{t,j,2}$ | $P_{t,j,3}$ | $P_{t,j,4}$ | $P_{t,j,5}$ |
|-------|-----------|-------------|-------------|-------------|-------------|-------------|
| 1.314 | 19.389 | 19.443 | 19.462 | 19.276 | 19.474 | 19.293 |
| 1.501 | 22.141 | 22.772 | 22.202 | 22.024 | 22.227 | 22.052 |
| 1.743 | 25.712 | 25.771 | 25.757 | 25.594 | 25.785 | 25.638 |
| 1.991 | 29.371 | 29.455 | 29.408 | 29.245 | 29.440 | 29.305 |
| 2.499 | 36.871 | 36.980 | 36.887 | 36.739 | 36.931 | 36.816 |
| 3.010 | 44.401 | 44.521 | 44.396 | 44.263 | 44.442 | 44.384 |
| 5.006 | 73.842 | 74.035 | 73.779 | 73.689 | 73.829 | 73.879 |
| 7.012 | 103.408 | 103.695 | 103.283 | 103.243 | 103.343 | 103.475 |

| NPR | $P_{t,j}$ | P_{rake} at r/r_t of - | | | | | | | | |
|-------|-----------|-----------------------------------|---------|---------|---------|---------|---------|---------|---------|---------|
| | | -.96 | -.83 | -.64 | -.36 | -.05 | .26 | .53 | .74 | .96 |
| 1.314 | 19.389 | 19.346 | 19.190 | 19.252 | 19.263 | 19.419 | 19.313 | 19.311 | 19.394 | 19.219 |
| 1.501 | 22.141 | 22.098 | 21.968 | 22.006 | 22.028 | 22.184 | 22.078 | 22.099 | 22.139 | 21.963 |
| 1.743 | 25.712 | 25.648 | 25.523 | 25.552 | 25.597 | 25.749 | 25.648 | 25.648 | 25.674 | 25.489 |
| 1.991 | 29.371 | 29.291 | 29.171 | 29.207 | 29.249 | 29.398 | 29.314 | 29.305 | 29.318 | 29.136 |
| 2.499 | 36.871 | 36.782 | 36.640 | 36.691 | 36.733 | 36.891 | 36.811 | 36.793 | 36.782 | 36.582 |
| 3.010 | 44.401 | 44.289 | 44.163 | 44.204 | 44.249 | 44.429 | 44.351 | 44.311 | 44.290 | 44.086 |
| 5.006 | 73.842 | 73.622 | 73.530 | 73.570 | 73.634 | 73.854 | 73.798 | 73.685 | 73.613 | 73.310 |
| 7.012 | 103.408 | 102.924 | 103.026 | 103.040 | 103.115 | 103.402 | 103.350 | 103.180 | 103.081 | 102.182 |

TABLE IV.- Continued

(l) $A_t = 3.992 \text{ in}^2$; $A_{\text{choke}} = 5.779 \text{ in}^2$

| NPR | $P_{t,j}$ | $P_{t,j,1}$ | $P_{t,j,2}$ | $P_{t,j,3}$ | $P_{t,j,4}$ | $P_{t,j,5}$ |
|-------|-----------|-------------|-------------|-------------|-------------|-------------|
| 1.301 | 19.173 | 19.213 | 19.173 | 19.168 | 19.158 | 19.152 |
| 1.500 | 22.115 | 22.173 | 22.116 | 22.107 | 22.090 | 22.086 |
| 1.751 | 25.805 | 25.881 | 25.793 | 25.801 | 25.772 | 25.778 |
| 2.007 | 29.583 | 29.669 | 29.566 | 29.590 | 29.538 | 29.553 |
| 2.452 | 36.135 | 36.234 | 36.109 | 36.144 | 36.076 | 36.115 |
| 2.499 | 36.827 | 36.928 | 36.801 | 36.831 | 36.772 | 36.805 |
| 3.001 | 44.229 | 44.336 | 44.202 | 44.237 | 44.161 | 44.208 |
| 5.013 | 73.856 | 74.030 | 73.818 | 73.859 | 73.739 | 73.847 |
| 6.993 | 103.038 | 103.278 | 102.985 | 103.035 | 102.857 | 103.036 |

| NPR | $P_{t,j}$ | P_{rake} at r/r_t of - | | | | | | | | |
|-------|-----------|-----------------------------------|---------|---------|---------|---------|---------|---------|---------|--------|
| | | -0.96 | -0.71 | -0.42 | -0.20 | -0.01 | .22 | .45 | .69 | .92 |
| 1.301 | 19.173 | 19.167 | 19.176 | 19.152 | | | | | | |
| 1.500 | 22.115 | 22.076 | 22.047 | 22.082 | 22.069 | 22.081 | 22.064 | 22.112 | 22.109 | 22.099 |
| 1.751 | 25.805 | 25.757 | 25.734 | 25.775 | 25.758 | 25.784 | 25.755 | 25.808 | 25.792 | 25.788 |
| 2.007 | 29.583 | 29.521 | 29.500 | 29.548 | 29.531 | 29.542 | 29.528 | 29.571 | 29.556 | 29.571 |
| 2.452 | 36.135 | 36.068 | 36.032 | 36.076 | 36.058 | 36.085 | 36.069 | 36.121 | 36.096 | 36.103 |
| 2.499 | 36.827 | 36.750 | 36.730 | 36.775 | 36.753 | 36.774 | 36.764 | 36.805 | 36.793 | 36.804 |
| 3.001 | 44.229 | 44.146 | 44.121 | 44.164 | 44.144 | 44.175 | 44.165 | 44.214 | 44.194 | 44.202 |
| 5.013 | 73.856 | 73.744 | 73.707 | 73.755 | 73.720 | 73.780 | 73.766 | 73.828 | 73.795 | 73.786 |
| 6.993 | 103.038 | 102.854 | 102.892 | 102.863 | 102.926 | 102.946 | 102.988 | 102.959 | 102.926 | |

(m) $A_t = 3.992 \text{ in}^2$; $A_{\text{choke}} = 15.286 \text{ in}^2$

| NPR | $P_{t,j}$ | $P_{t,j,1}$ | $P_{t,j,2}$ | $P_{t,j,3}$ | $P_{t,j,4}$ | $P_{t,j,5}$ |
|-------|-----------|-------------|-------------|-------------|-------------|-------------|
| 1.344 | 19.804 | 19.834 | 19.853 | 19.825 | 19.791 | 19.719 |
| 1.513 | 22.298 | 22.327 | 22.351 | 22.331 | 22.286 | 22.195 |
| 1.760 | 25.938 | 25.981 | 26.003 | 25.984 | 25.914 | 25.808 |
| 2.008 | 29.592 | 29.636 | 29.669 | 29.637 | 29.570 | 29.448 |
| 2.491 | 36.710 | 36.775 | 36.798 | 36.769 | 36.691 | 36.527 |
| 2.986 | 43.996 | 44.064 | 44.092 | 44.079 | 43.961 | 43.783 |
| 5.023 | 74.012 | 74.135 | 74.182 | 74.164 | 73.936 | 73.642 |
| 7.014 | 103.333 | 103.482 | 103.564 | 103.568 | 103.236 | 102.815 |

| NPR | $P_{t,j}$ | P_{rake} at r/r_t of - | | | | | | | | |
|-------|-----------|-----------------------------------|---------|---------|---------|---------|---------|---------|---------|---------|
| | | -0.96 | -0.76 | -0.50 | -0.28 | -0.04 | .20 | .41 | .71 | .96 |
| 1.344 | 19.804 | 19.771 | 19.738 | 19.759 | 19.773 | 19.794 | 19.754 | 19.805 | 19.801 | 19.777 |
| 1.513 | 22.298 | 22.270 | 22.240 | 22.272 | 22.280 | 22.299 | 22.275 | 22.310 | 22.307 | 22.280 |
| 1.760 | 25.938 | 25.917 | 25.886 | 25.928 | 25.919 | 25.946 | 25.913 | 25.966 | 25.966 | 25.928 |
| 2.008 | 29.592 | 29.563 | 29.547 | 29.571 | 29.573 | 29.595 | 29.566 | 29.623 | 29.626 | 29.577 |
| 2.491 | 36.710 | 36.671 | 36.672 | 36 | 36.705 | 36.717 | 36.695 | 36.751 | 36.759 | 36.702 |
| 2.986 | 43.996 | 43.980 | 43.958 | 43.9 | 43.991 | 44.008 | 43.991 | 44.053 | 44.070 | 43.992 |
| 5.023 | 74.012 | 73.909 | 73.967 | 74.008 | 73.991 | 74.009 | 74.004 | 74.097 | 74.105 | 74.002 |
| 7.014 | 103.333 | 102.647 | 103.326 | 103.348 | 103.297 | 103.300 | 103.300 | 103.465 | 103.486 | 103.276 |

ORIGINAL PAGE IS
OF POOR QUALITY

TABLE IV.- Continued

(n) $A_t = 5.711 \text{ in}^2$; $A_{\text{choke}} = 3.853 \text{ in}^2$

| NPR | $P_{t,j}$ | $P_{t,j,1}$ | $P_{t,j,2}$ | $P_{t,j,3}$ | $P_{t,j,4}$ | $P_{t,j,5}$ |
|-------|-----------|-------------|-------------|-------------|-------------|-------------|
| 1.249 | 17.362 | 19.440 | 19.296 | 19.321 | 19.332 | 19.421 |
| 1.506 | 22.436 | 22.546 | 22.350 | 22.380 | 22.358 | 22.545 |
| 1.754 | 26.129 | 26.271 | 26.096 | 26.059 | 26.011 | 26.293 |
| 2.002 | 29.833 | 29.999 | 29.688 | 29.752 | 29.767 | 29.828 |
| 2.503 | 37.266 | 37.502 | 37.096 | 37.208 | 37.117 | 37.566 |
| 2.943 | 44.566 | 44.877 | 44.346 | 44.491 | 44.368 | 44.891 |
| 5.007 | 74.596 | 74.987 | 74.196 | 74.438 | 74.233 | 75.133 |
| 5.998 | 87.364 | 89.517 | 88.660 | 89.176 | 88.931 | 89.997 |

| NPR | $P_{t,j}$ | P_{rake} at r/r_t of - | | | | | |
|-------|-----------|-----------------------------------|--------|--------|--------|--------|--------|
| | | -.98 | -.84 | -.70 | -.48 | -.25 | -.04 |
| 1.249 | 17.362 | 19.731 | 19.267 | 19.217 | 19.258 | 19.292 | 19.326 |
| 1.506 | 22.436 | 22.735 | 22.293 | 22.259 | 22.306 | 22.356 | 22.395 |
| 1.754 | 26.129 | 25.953 | 25.947 | 25.844 | 25.973 | 26.021 | 26.070 |
| 2.002 | 29.833 | 29.576 | 29.643 | 29.595 | 29.681 | 29.741 | 29.768 |
| 2.503 | 37.266 | 36.734 | 37.065 | 37.024 | 37.111 | 37.185 | 37.254 |
| 2.943 | 44.566 | 43.586 | 44.310 | 44.264 | 44.367 | 44.469 | 44.545 |
| 5.007 | 74.596 | 70.644 | 74.135 | 74.107 | 74.259 | 74.414 | 74.535 |
| 5.998 | 87.364 | 79.925 | 88.817 | 88.766 | 88.952 | 89.140 | 89.284 |

| NPR | $P_{t,j}$ | P_{rake} at r/r_t of - | | | | |
|-------|-----------|-----------------------------------|--------|--------|--------|--------|
| | | .21 | .41 | .64 | .85 | .96 |
| 1.249 | 17.362 | 19.305 | 19.334 | 19.294 | 19.272 | 19.162 |
| 1.506 | 22.436 | 22.369 | 22.401 | 22.335 | 22.300 | 22.210 |
| 1.754 | 26.129 | 26.060 | 26.085 | 25.993 | 25.947 | 25.872 |
| 2.002 | 29.833 | 29.774 | 29.809 | 29.691 | 29.650 | 29.562 |
| 2.503 | 37.266 | 37.262 | 37.271 | 37.131 | 37.057 | 36.983 |
| 2.943 | 44.566 | 44.556 | 44.561 | 44.374 | 44.320 | 44.232 |
| 5.007 | 74.596 | 74.591 | 74.566 | 74.276 | 74.149 | 74.072 |
| 5.998 | 87.364 | 89.372 | 89.323 | 88.962 | 88.836 | 88.743 |

TABLE IV.- Continued

(o) $A_t = 5.711 \text{ in}^2$; $A_{\text{choke}} = 5.779 \text{ in}^2$

| NPR | $P_{t,j}$ | $P_{t,j,1}$ | $P_{t,j,2}$ | $P_{t,j,3}$ | $P_{t,j,4}$ | $P_{t,j,5}$ |
|-------|-----------|-------------|-------------|-------------|-------------|-------------|
| 1.290 | 19.992 | 19.077 | 18.982 | 18.999 | 18.952 | 18.956 |
| 1.480 | 21.764 | 21.909 | 21.753 | 21.788 | 21.719 | 21.744 |
| 1.695 | 22.614 | 22.136 | 21.993 | 22.017 | 21.950 | 21.974 |
| 1.749 | 25.753 | 25.910 | 25.738 | 25.750 | 25.659 | 25.709 |
| 1.998 | 29.418 | 29.635 | 29.389 | 29.417 | 29.315 | 29.363 |
| 2.487 | 36.608 | 36.624 | 36.570 | 36.603 | 36.486 | 36.565 |
| 2.995 | 44.085 | 44.352 | 44.039 | 44.087 | 43.908 | 44.039 |
| 4.998 | 73.565 | 74.022 | 73.469 | 73.575 | 73.253 | 73.537 |
| 6.967 | 102.537 | 103.177 | 102.427 | 102.543 | 102.162 | 102.445 |

| NPR | $P_{t,j}$ | P_{rake} at r/r_t of - | | | | | |
|-------|-----------|-----------------------------------|---------|---------|---------|---------|---------|
| | | -.96 | -.78 | -.58 | -.34 | -.15 | .01 |
| 1.290 | 18.992 | 18.950 | 18.944 | 18.926 | 18.930 | 18.925 | 18.938 |
| 1.480 | 21.764 | 21.779 | 21.725 | 21.731 | 21.737 | 21.730 | 21.732 |
| 1.695 | 22.614 | 21.942 | 21.924 | 21.928 | 21.930 | 21.935 | 21.938 |
| 1.749 | 25.753 | 25.655 | 25.651 | 25.655 | 25.672 | 25.653 | 25.655 |
| 1.998 | 29.418 | 29.301 | 29.292 | 29.316 | 29.325 | 29.304 | 29.316 |
| 2.487 | 36.608 | 36.472 | 36.467 | 36.482 | 36.486 | 36.474 | 36.481 |
| 2.995 | 44.085 | 43.934 | 43.930 | 43.953 | 43.944 | 43.921 | 43.938 |
| 4.998 | 73.565 | 73.352 | 73.348 | 73.368 | 73.341 | 73.307 | 73.335 |
| 6.967 | 102.537 | 102.255 | 102.261 | 102.257 | 102.231 | 102.177 | 102.200 |

| NPR | $P_{t,j}$ | P_{rake} at r/r_t of - | | | | |
|-------|-----------|-----------------------------------|---------|---------|---------|--------|
| | | .19 | .39 | .60 | .79 | .97 |
| 1.290 | 18.992 | 18.911 | 18.965 | 18.976 | 18.978 | 18.954 |
| 1.480 | 21.764 | 21.714 | 21.778 | 21.788 | 21.776 | 21.650 |
| 1.695 | 22.614 | 21.919 | 21.978 | 21.976 | 21.964 | 21.852 |
| 1.749 | 25.753 | 25.636 | 25.715 | 25.713 | 25.705 | 25.581 |
| 1.998 | 29.418 | 29.299 | 29.372 | 29.383 | 29.366 | 29.230 |
| 2.487 | 36.608 | 36.466 | 36.552 | 36.553 | 36.543 | 36.408 |
| 2.995 | 44.085 | 43.922 | 44.015 | 44.022 | 43.993 | 43.859 |
| 4.998 | 73.565 | 73.337 | 73.443 | 73.438 | 73.416 | 73.124 |
| 6.967 | 102.537 | 102.281 | 102.359 | 102.371 | 102.349 | 99.745 |

ORIGINAL PAGE IS
OF POOR QUALITY

TABLE IV.- Continued

(p) $A_t = 5.71 \text{ in}^2$; $A_{\text{choke}} = 7.549 \text{ in}^2$

| NPR | $P_{t,j}$ | $P_{t,j,1}$ | $P_{t,j,2}$ | $P_{t,j,3}$ | $P_{t,j,4}$ | $P_{t,j,5}$ |
|-------|-----------|-------------|-------------|-------------|-------------|-------------|
| 1.293 | 19.074 | 19.141 | 19.092 | 19.090 | 19.022 | 19.037 |
| 1.506 | 22.210 | 22.294 | 22.240 | 22.257 | 22.136 | 22.175 |
| 1.779 | 26.241 | 26.343 | 26.257 | 26.301 | 26.125 | 26.160 |
| 1.746 | 25.782 | 25.875 | 25.809 | 25.825 | 25.662 | 25.733 |
| 1.996 | 29.433 | 29.531 | 29.460 | 29.496 | 29.290 | 29.337 |
| 2.479 | 36.540 | 36.671 | 36.574 | 36.625 | 36.372 | 36.432 |
| 2.997 | 44.193 | 44.347 | 44.220 | 44.291 | 43.974 | 44.128 |
| 4.991 | 73.588 | 73.759 | 73.606 | 73.754 | 73.226 | 73.490 |
| 5.015 | 73.946 | 74.205 | 73.987 | 74.123 | 73.562 | 73.642 |
| 7.009 | 103.357 | 103.727 | 103.399 | 103.588 | 102.643 | 103.227 |

| NPR | $P_{t,j}$ | P_{rake} at r/r_t of - | | | | | |
|-------|-----------|-----------------------------------|---------|---------|---------|---------|---------|
| | | -.95 | -.82 | -.63 | -.41 | -.23 | -.03 |
| 1.293 | 19.076 | 19.037 | 19.039 | 19.021 | 19.046 | 19.021 | 19.032 |
| 1.506 | 22.210 | 22.155 | 22.176 | 22.174 | 22.178 | 22.154 | 22.155 |
| 1.779 | 26.241 | 26.139 | 26.160 | 26.151 | 26.168 | 26.146 | 26.132 |
| 1.746 | 25.782 | 25.697 | 25.725 | 25.717 | 25.724 | 25.696 | 25.692 |
| 1.996 | 29.433 | 29.337 | 29.367 | 29.365 | 29.379 | 29.348 | 29.326 |
| 2.479 | 36.540 | 36.429 | 36.490 | 36.460 | 36.488 | 36.436 | 36.419 |
| 2.997 | 44.193 | 44.042 | 44.107 | 44.122 | 44.122 | 44.078 | 44.040 |
| 4.991 | 73.588 | 73.510 | 73.430 | 73.463 | 73.476 | 73.386 | 73.326 |
| 5.015 | 73.946 | 73.679 | 73.786 | 73.826 | 73.634 | 73.742 | 73.667 |
| 7.009 | 103.357 | 102.939 | 103.137 | 103.198 | 103.189 | 103.058 | 102.991 |

| NPR | $P_{t,j}$ | P_{rake} at r/r_t of - | | | | |
|-------|-----------|-----------------------------------|---------|---------|---------|---------|
| | | .18 | .36 | .56 | .75 | .96 |
| 1.293 | 19.076 | 19.015 | 19.056 | 19.066 | 19.063 | 18.961 |
| 1.506 | 22.210 | 22.149 | 22.179 | 22.186 | 22.200 | 22.098 |
| 1.779 | 26.241 | 26.178 | 26.171 | 26.177 | 26.200 | 26.083 |
| 1.746 | 25.782 | 25.679 | 25.729 | 25.735 | 25.756 | 25.639 |
| 1.996 | 29.433 | 29.331 | 29.385 | 29.393 | 29.419 | 29.238 |
| 2.479 | 36.540 | 36.433 | 36.472 | 36.482 | 36.520 | 36.400 |
| 2.997 | 44.193 | 44.055 | 44.110 | 44.125 | 44.162 | 44.040 |
| 4.991 | 73.588 | 73.371 | 73.431 | 73.460 | 73.536 | 73.434 |
| 5.015 | 73.946 | 73.712 | 73.793 | 73.909 | 73.837 | 73.785 |
| 7.009 | 103.357 | 103.014 | 103.127 | 103.192 | 103.257 | 103.134 |

ORIGINAL PAGE IS
OF POOR QUALITY

TABLE IV.- Continued

(q) $A_t = 5.711 \text{ in}^2$; $A_{\text{choke}} = 15.286 \text{ in}^2$

| NPR | $P_{t,j}$ | $P_{t,j,1}$ | $P_{t,j,2}$ | $P_{t,j,3}$ | $P_{t,j,4}$ | $P_{t,j,5}$ |
|-------|-----------|-------------|-------------|-------------|-------------|-------------|
| 1.316 | 19.406 | 19.438 | 19.454 | 19.421 | 19.361 | 19.382 |
| 1.497 | 22.079 | 22.105 | 22.127 | 22.116 | 22.001 | 22.047 |
| 1.751 | 25.329 | 25.690 | 25.965 | 25.663 | 25.737 | 25.701 |
| 1.999 | 29.477 | 29.523 | 29.555 | 29.530 | 29.364 | 29.434 |
| 2.523 | 37.208 | 37.277 | 37.234 | 37.269 | 37.047 | 37.152 |
| 3.008 | 44.369 | 44.447 | 44.455 | 44.445 | 44.176 | 44.324 |
| 4.996 | 73.691 | 73.794 | 73.827 | 73.830 | 73.371 | 73.632 |
| 7.022 | 103.570 | 103.712 | 103.775 | 103.776 | 103.103 | 103.490 |

| NPR | $P_{t,j}$ | P_{rake} at r/r_t of - | | | | | |
|-------|-----------|-----------------------------------|---------|---------|---------|---------|---------|
| | | -.97 | -.81 | -.62 | -.40 | -.21 | -.02 |
| 1.316 | 19.406 | 19.364 | 19.380 | 19.351 | 19.359 | 19.351 | 19.367 |
| 1.497 | 22.079 | 22.033 | 22.053 | 22.024 | 22.033 | 22.021 | 22.022 |
| 1.751 | 25.329 | 25.730 | 25.790 | 25.776 | 25.783 | 25.756 | 25.780 |
| 1.999 | 29.477 | 29.376 | 29.445 | 29.426 | 29.425 | 29.376 | 29.414 |
| 2.523 | 37.208 | 37.052 | 37.154 | 37.120 | 37.127 | 37.101 | 37.114 |
| 3.008 | 44.369 | 44.201 | 44.319 | 44.286 | 44.275 | 44.251 | 44.266 |
| 4.996 | 73.691 | 73.404 | 73.630 | 73.598 | 73.568 | 73.491 | 73.512 |
| 7.022 | 103.570 | 103.112 | 103.524 | 103.463 | 103.364 | 103.273 | 103.295 |

| NPR | $P_{t,j}$ | P_{rake} at r/r_t of - | | | | |
|-------|-----------|-----------------------------------|---------|---------|---------|---------|
| | | .19 | .37 | .58 | .76 | .96 |
| 1.316 | 19.406 | 19.333 | 19.341 | 19.423 | 19.395 | 19.235 |
| 1.497 | 22.079 | 22.013 | 22.057 | 22.102 | 22.077 | 21.951 |
| 1.751 | 25.329 | 25.754 | 25.622 | 25.853 | 25.832 | 25.694 |
| 1.999 | 29.477 | 29.410 | 29.474 | 29.511 | 29.494 | 29.344 |
| 2.523 | 37.208 | 37.117 | 37.184 | 37.230 | 37.197 | 37.050 |
| 3.008 | 44.369 | 44.271 | 44.354 | 44.404 | 44.380 | 44.219 |
| 4.996 | 73.691 | 73.553 | 73.663 | 73.717 | 73.729 | 73.484 |
| 7.022 | 103.570 | 103.372 | 103.515 | 103.602 | 103.642 | 102.990 |

ORIGINAL PAGE IS
OF POOR QUALITY

TABLE IV.- Continued

(r) $A_t = 8.501 \text{ in}^2$; $A_{choke} = 3.853 \text{ in}^2$

| NPR | $P_{t,j}$ | $P_{t,j,1}$ | $P_{t,j,2}$ | $P_{t,j,3}$ | $P_{t,j,4}$ | $P_{t,j,5}$ |
|-------|-----------|-------------|-------------|-------------|-------------|-------------|
| 1.274 | 19.008 | 19.182 | 18.867 | 18.892 | 18.986 | 19.111 |
| 1.506 | 22.466 | 22.796 | 22.163 | 22.354 | 22.555 | 22.463 |
| 1.759 | 26.244 | 26.650 | 25.825 | 26.099 | 26.398 | 26.248 |
| 2.003 | 29.883 | 30.346 | 29.407 | 29.710 | 30.052 | 29.899 |
| 1.993 | 29.723 | 30.199 | 29.257 | 29.535 | 29.888 | 29.737 |
| 2.492 | 37.168 | 37.726 | 36.586 | 36.947 | 37.391 | 37.189 |
| 2.998 | 44.716 | 45.375 | 44.011 | 44.457 | 44.968 | 44.767 |
| 4.256 | 63.490 | 64.399 | 62.473 | 63.130 | 63.820 | 63.630 |

| NPR | $P_{t,j}$ | P_{rake} at r/r_t of - | | | | | |
|-------|-----------|----------------------------|--------|--------|--------|--------|--------|
| | | -.96 | -.82 | -.66 | -.56 | -.39 | -.20 |
| 1.274 | 19.008 | 18.750 | 18.861 | 18.860 | 18.859 | 18.931 | 18.966 |
| 1.506 | 22.466 | 22.234 | 22.384 | 22.406 | 22.399 | 22.448 | 22.466 |
| 1.759 | 26.244 | 25.957 | 26.124 | 26.184 | 26.163 | 26.194 | 26.225 |
| 2.003 | 29.883 | 29.575 | 29.743 | 29.812 | 29.796 | 29.820 | 29.863 |
| 1.993 | 29.723 | 29.416 | 29.594 | 29.648 | 29.638 | 29.658 | 29.713 |
| 2.492 | 37.168 | 36.812 | 37.011 | 37.084 | 37.078 | 37.085 | 37.155 |
| 2.998 | 44.716 | 44.304 | 44.526 | 44.630 | 44.639 | 44.622 | 44.698 |
| 4.256 | 63.490 | 63.065 | 63.343 | 63.442 | 63.436 | 63.346 | 63.420 |

| NPR | $P_{t,j}$ | P_{rake} at r/r_t of - | | | | | | |
|-------|-----------|----------------------------|--------|--------|--------|--------|--------|--------|
| | | -.03 | .17 | .33 | .53 | .71 | .84 | .97 |
| 1.274 | 19.008 | 19.010 | 19.000 | 19.032 | 18.988 | 18.918 | 18.812 | 18.808 |
| 1.506 | 22.466 | 22.530 | 22.542 | 22.581 | 22.577 | 22.443 | 22.337 | 22.365 |
| 1.759 | 26.244 | 26.340 | 26.357 | 26.412 | 26.380 | 26.211 | 26.079 | 26.110 |
| 2.003 | 29.883 | 30.013 | 30.036 | 30.082 | 30.051 | 29.845 | 29.700 | 29.760 |
| 1.993 | 29.723 | 29.848 | 29.873 | 29.921 | 29.890 | 29.670 | 29.539 | 29.608 |
| 2.492 | 37.168 | 37.337 | 37.382 | 37.424 | 37.382 | 37.116 | 36.972 | 37.046 |
| 2.998 | 44.716 | 44.914 | 44.990 | 45.035 | 44.971 | 44.661 | 44.480 | 44.599 |
| 4.256 | 63.490 | 63.770 | 63.909 | 63.950 | 63.840 | 63.405 | 63.213 | 63.320 |

TABLE IV.- Continued

(s) $A_t = 8.501 \text{ in}^2$; $A_{\text{choke}} = 5.779 \text{ in}^2$

| NPR | $P_{t,j}$ | $P_{t,j,1}$ | $P_{t,j,2}$ | $P_{t,j,3}$ | $P_{t,j,4}$ | $P_{t,j,5}$ |
|-------|-----------|-------------|-------------|-------------|-------------|-------------|
| 1.304 | 19.164 | 19.389 | 19.146 | 19.146 | 19.647 | 19.105 |
| 1.501 | 22.060 | 22.422 | 22.037 | 22.010 | 21.870 | 21.960 |
| 1.751 | 25.740 | 26.224 | 25.728 | 25.676 | 25.472 | 25.600 |
| 2.000 | 29.399 | 29.987 | 29.395 | 29.316 | 29.074 | 29.227 |
| 2.503 | 36.780 | 37.515 | 36.765 | 36.664 | 36.391 | 36.563 |
| 3.003 | 44.130 | 45.020 | 44.114 | 43.986 | 43.665 | 43.875 |
| 4.999 | 73.463 | 74.925 | 73.496 | 73.276 | 72.672 | 73.042 |
| 5.991 | 86.038 | 87.809 | 87.956 | 87.826 | 87.074 | 87.521 |
| 5.969 | 87.702 | 89.444 | 87.618 | 87.504 | 86.722 | 87.209 |

| NPR | $P_{t,j}$ | P_{rake} at r/r_t of - | | | | | |
|-------|-----------|-----------------------------------|--------|--------|--------|--------|--------|
| | | -.96 | -.79 | -.65 | -.48 | -.29 | -.13 |
| 1.304 | 19.164 | 19.293 | 19.045 | 19.046 | 19.043 | 19.039 | 19.022 |
| 1.501 | 22.060 | 21.806 | 21.874 | 21.910 | 21.901 | 21.874 | 21.842 |
| 1.751 | 25.740 | 25.399 | 25.479 | 25.512 | 25.511 | 25.488 | 25.453 |
| 2.000 | 29.399 | 29.019 | 29.072 | 29.127 | 29.134 | 29.103 | 29.065 |
| 2.503 | 36.780 | 36.320 | 36.362 | 36.455 | 36.460 | 36.400 | 36.374 |
| 3.003 | 44.130 | 43.595 | 43.606 | 43.730 | 43.760 | 43.665 | 43.646 |
| 4.999 | 73.463 | 72.749 | 72.667 | 72.807 | 72.868 | 72.714 | 72.655 |
| 5.991 | 86.038 | 85.259 | 85.125 | 87.253 | 87.323 | 87.148 | 87.083 |
| 5.969 | 87.702 | 86.941 | 86.798 | 86.925 | 86.993 | 86.811 | 86.740 |

| NPR | $P_{t,j}$ | P_{rake} at $1/r_t$ of - | | | | | | |
|-------|-----------|-----------------------------------|--------|--------|--------|--------|--------|--------|
| | | 0.0 | .15 | .32 | .49 | .66 | .80 | .95 |
| 1.304 | 19.164 | 19.033 | 19.066 | 19.062 | 19.104 | 19.082 | 19.966 | 18.957 |
| 1.501 | 22.060 | 21.855 | 21.826 | 21.924 | 21.958 | 21.922 | 21.813 | 21.770 |
| 1.751 | 25.740 | 25.462 | 25.423 | 25.543 | 25.575 | 25.530 | 25.449 | 25.358 |
| 2.000 | 29.399 | 29.083 | 29.034 | 29.175 | 29.207 | 29.152 | 29.056 | 28.961 |
| 2.503 | 36.780 | 36.395 | 36.350 | 36.507 | 36.540 | 36.494 | 36.413 | 36.279 |
| 3.003 | 44.130 | 43.675 | 43.622 | 43.813 | 43.862 | 43.785 | 43.730 | 43.556 |
| 4.999 | 73.463 | 72.698 | 72.676 | 72.920 | 73.007 | 72.945 | 72.966 | 72.639 |
| 5.991 | 86.038 | 85.103 | 85.102 | 87.389 | 87.463 | 87.459 | 87.503 | 86.984 |
| 5.969 | 87.702 | 86.782 | 86.774 | 87.053 | 87.160 | 87.121 | 87.179 | 86.665 |

ORIGINAL PAGE IS
OF POOR QUALITY

TABLE IV.- Continued

(t) $A_t = 8.501 \text{ in}^2$; $A_{\text{choke}} = 7.549 \text{ in}^2$

| NPR | $P_{t,j}$ | $P_{t,j,1}$ | $P_{t,j,2}$ | $P_{t,j,3}$ | $P_{t,j,4}$ | $P_{t,j,5}$ |
|-------|-----------|-------------|-------------|-------------|-------------|-------------|
| 1.299 | 19.148 | 19.253 | 19.183 | 19.199 | 19.618 | 19.677 |
| 1.500 | 22.116 | 22.243 | 22.167 | 22.191 | 21.921 | 22.039 |
| 1.747 | 25.750 | 25.932 | 25.804 | 25.843 | 25.493 | 25.679 |
| 2.003 | 29.531 | 29.735 | 29.577 | 29.657 | 29.230 | 29.454 |
| 2.505 | 35.935 | 37.203 | 36.962 | 37.066 | 36.571 | 36.845 |
| 2.998 | 44.204 | 44.520 | 44.220 | 44.382 | 43.768 | 44.116 |
| 5.003 | 73.770 | 74.343 | 73.795 | 74.682 | 73.031 | 73.616 |
| 5.440 | 80.209 | 80.843 | 80.217 | 80.541 | 79.391 | 80.045 |

| NPR | $P_{t,j}$ | P_{rake} at r/r_t of - | | | | | |
|-------|-----------|-----------------------------------|--------|--------|--------|--------|--------|
| | | -.95 | -.79 | -.66 | -.49 | -.31 | -.17 |
| 1.299 | 19.148 | 19.016 | 19.110 | 19.106 | 19.077 | 19.074 | 19.039 |
| 1.500 | 22.116 | 21.945 | 22.062 | 22.064 | 22.019 | 22.016 | 21.967 |
| 1.747 | 25.750 | 25.524 | 25.653 | 25.678 | 25.619 | 25.618 | 25.550 |
| 2.003 | 29.531 | 29.302 | 29.436 | 29.450 | 29.398 | 29.391 | 29.324 |
| 2.505 | 35.935 | 35.674 | 36.601 | 36.636 | 36.787 | 36.760 | 36.672 |
| 2.998 | 44.204 | 43.839 | 44.032 | 44.083 | 44.033 | 43.992 | 43.904 |
| 5.003 | 73.770 | 73.249 | 73.466 | 73.574 | 73.506 | 73.415 | 73.260 |
| 5.440 | 80.209 | 79.598 | 79.869 | 79.972 | 79.920 | 79.804 | 79.653 |

| NPR | $P_{t,j}$ | P_{rake} at r/r_t of - | | | | | | |
|-------|-----------|-----------------------------------|--------|--------|--------|--------|--------|--------|
| | | .01 | .17 | .32 | .50 | .64 | .76 | .95 |
| 1.299 | 19.148 | 19.027 | 19.035 | 19.104 | 19.100 | 19.112 | 19.046 | 19.066 |
| 1.500 | 22.116 | 21.963 | 21.964 | 22.035 | 22.021 | 22.046 | 22.009 | 21.989 |
| 1.747 | 25.750 | 25.540 | 25.560 | 25.636 | 25.625 | 25.658 | 25.618 | 25.592 |
| 2.003 | 29.531 | 29.300 | 29.334 | 29.413 | 29.391 | 29.431 | 29.390 | 29.368 |
| 2.505 | 35.935 | 35.644 | 36.694 | 36.779 | 36.765 | 36.817 | 36.788 | 36.789 |
| 2.998 | 44.204 | 43.869 | 43.933 | 44.027 | 43.995 | 44.070 | 44.039 | 44.054 |
| 5.003 | 73.770 | 73.199 | 73.338 | 73.456 | 73.436 | 73.536 | 73.567 | 73.579 |
| 5.440 | 80.209 | 79.593 | 79.729 | 79.847 | 79.829 | 79.946 | 79.960 | 79.980 |

TABLE IV.- Continued

(u) $A_t = 8.501 \text{ in}^2$; $A_{\text{choke}} = 15.286 \text{ in}^2$

| NPR | $P_{t,j}$ | $P_{t,j,1}$ | $P_{t,j,2}$ | $P_{t,j,3}$ | $P_{t,j,4}$ | $P_{t,j,5}$ |
|-------|-----------|-------------|-------------|-------------|-------------|-------------|
| 1.306 | 19.224 | 19.224 | 19.252 | 19.253 | 19.131 | 19.225 |
| 1.500 | 22.073 | 22.054 | 22.077 | 22.096 | 21.965 | 22.173 |
| 1.756 | 25.844 | 25.815 | 25.850 | 25.868 | 25.700 | 25.997 |
| 2.009 | 29.556 | 29.523 | 29.555 | 29.601 | 29.382 | 29.720 |
| 2.497 | 36.737 | 36.702 | 36.736 | 36.786 | 36.517 | 36.945 |
| 3.010 | 44.284 | 44.245 | 44.286 | 44.337 | 44.013 | 44.538 |
| 5.003 | 73.597 | 73.500 | 73.586 | 73.705 | 73.137 | 74.055 |
| 5.420 | 79.729 | 79.623 | 79.719 | 79.851 | 79.206 | 80.237 |

| NPR | $P_{t,j}$ | P_{rake} at r/r_t of - | | | | | |
|-------|-----------|-----------------------------------|--------|--------|--------|--------|--------|
| | | -.96 | -.81 | -.65 | -.51 | -.34 | -.18 |
| 1.306 | 19.224 | 19.115 | 19.209 | 19.211 | 19.169 | 19.136 | 19.144 |
| 1.500 | 22.073 | 21.919 | 22.050 | 22.047 | 22.027 | 22.034 | 22.004 |
| 1.756 | 25.844 | 25.653 | 25.777 | 25.798 | 25.767 | 25.768 | 25.738 |
| 2.009 | 29.556 | 29.301 | 29.463 | 29.481 | 29.454 | 29.462 | 29.445 |
| 2.497 | 36.737 | 36.447 | 36.621 | 36.657 | 36.633 | 36.637 | 36.603 |
| 3.010 | 44.284 | 43.939 | 44.122 | 44.150 | 44.176 | 44.149 | 44.107 |
| 5.003 | 73.597 | 73.066 | 73.350 | 73.451 | 73.411 | 73.374 | 73.316 |
| 5.420 | 79.729 | 79.147 | 79.471 | 79.572 | 79.545 | 79.500 | 79.417 |

| NPR | $P_{t,j}$ | P_{rake} at r/r_t of - | | | | | | |
|-------|-----------|-----------------------------------|--------|--------|--------|--------|--------|--------|
| | | -.02 | .16 | .34 | .50 | .66 | .81 | .96 |
| 1.306 | 19.224 | 19.174 | 19.136 | 19.222 | 19.251 | 19.236 | 19.150 | 19.137 |
| 1.500 | 22.073 | 22.035 | 22.011 | 22.086 | 22.103 | 22.088 | 21.977 | 21.922 |
| 1.756 | 25.844 | 25.777 | 25.757 | 25.834 | 25.853 | 25.815 | 25.710 | 25.635 |
| 2.009 | 29.556 | 29.465 | 29.463 | 29.524 | 29.537 | 29.516 | 29.409 | 29.306 |
| 2.497 | 36.737 | 36.625 | 36.631 | 36.720 | 36.734 | 36.692 | 36.574 | 36.457 |
| 3.010 | 44.284 | 44.147 | 44.156 | 44.247 | 44.268 | 44.236 | 44.106 | 43.957 |
| 5.003 | 73.597 | 73.354 | 73.437 | 73.563 | 73.568 | 73.522 | 73.370 | 73.047 |
| 5.420 | 79.729 | 79.466 | 79.569 | 79.721 | 79.708 | 79.554 | 79.498 | 79.127 |

TABLE IV.- Continued

(v) $A_t = 11.352 \text{ in}^2$; $A_{\text{choke}} = 3.853 \text{ in}^2$

| NPR | $P_{t,j}$ | $P_{t,j,1}$ | $P_{t,j,2}$ | $P_{t,j,3}$ | $P_{t,j,4}$ | $P_{t,j,5}$ |
|-------|-----------|-------------|-------------|-------------|-------------|-------------|
| 1.296 | 19.335 | 19.819 | 18.863 | 19.091 | 19.531 | 19.348 |
| 1.523 | 22.721 | 23.432 | 21.881 | 22.217 | 22.884 | 23.189 |
| 1.751 | 26.120 | 27.233 | 25.164 | 25.585 | 26.251 | 26.367 |
| 1.994 | 29.754 | 31.075 | 28.692 | 29.157 | 29.879 | 29.365 |
| 2.498 | 37.261 | 38.895 | 35.954 | 36.544 | 37.412 | 37.501 |
| 2.995 | 44.686 | 46.625 | 43.165 | 43.953 | 44.995 | 44.891 |
| 3.037 | 45.313 | 47.267 | 43.776 | 44.473 | 45.523 | 45.528 |

| NPR | $P_{t,j}$ | P_{rake} at r/r_t of - | | | | | |
|-------|-----------|-----------------------------------|--------|--------|--------|--------|--------|
| | | -.97 | -.82 | -.63 | -.47 | -.30 | -.15 |
| 1.296 | 19.335 | 19.057 | 19.278 | 19.258 | 19.209 | 19.220 | 19.301 |
| 1.523 | 22.721 | 22.144 | 22.447 | 22.368 | 22.303 | 22.364 | 22.475 |
| 1.751 | 26.120 | 25.511 | 25.820 | 25.668 | 25.569 | 25.602 | 25.828 |
| 1.994 | 29.754 | 29.116 | 29.425 | 29.229 | 29.125 | 29.242 | 29.412 |
| 2.498 | 37.261 | 36.541 | 36.870 | 36.624 | 36.489 | 36.632 | 36.958 |
| 2.995 | 44.686 | 43.902 | 44.263 | 43.953 | 43.788 | 43.957 | 44.239 |
| 3.037 | 45.313 | 44.525 | 44.876 | 44.553 | 44.408 | 44.575 | 44.953 |

| NPR | $P_{t,j}$ | P_{rake} at r/r_t of - | | | | | | |
|-------|-----------|-----------------------------------|--------|--------|--------|--------|--------|--------|
| | | -.01 | .16 | .36 | .52 | .70 | .86 | .97 |
| 1.296 | 19.335 | 19.439 | 19.447 | 19.443 | 19.427 | 19.248 | 19.133 | 19.139 |
| 1.523 | 22.721 | 22.645 | 22.662 | 22.691 | 22.628 | 22.381 | 22.283 | 22.229 |
| 1.751 | 26.120 | 26.003 | 26.013 | 26.054 | 26.017 | 25.717 | 25.690 | 25.541 |
| 1.994 | 29.754 | 29.596 | 29.623 | 29.671 | 29.635 | 29.310 | 29.298 | 29.117 |
| 2.498 | 37.261 | 37.074 | 37.132 | 37.198 | 37.142 | 36.727 | 36.747 | 36.533 |
| 2.995 | 44.686 | 44.502 | 44.562 | 44.612 | 44.572 | 44.081 | 44.144 | 43.909 |
| 3.037 | 45.313 | 45.109 | 45.169 | 45.242 | 45.202 | 44.701 | 44.764 | 44.533 |

TABLE IV.- Continued

(w) $A_t = 11.352 \text{ in}^2$; $A_{\text{choke}} = 5.779 \text{ in}^2$

| NPR | $P_{t,j}$ | $P_{t,j,1}$ | $P_{t,j,2}$ | $P_{t,j,3}$ | $P_{t,j,4}$ | $P_{t,j,5}$ |
|-------|-----------|-------------|-------------|-------------|-------------|-------------|
| 1.304 | 14.238 | 14.784 | 19.290 | 14.156 | 16.940 | 19.016 |
| 1.446 | 22.081 | 22.873 | 27.111 | 21.990 | 21.631 | 21.769 |
| 1.744 | 23.308 | 26.923 | 25.814 | 25.604 | 25.108 | 23.454 |
| 1.999 | 29.507 | 30.403 | 29.518 | 29.336 | 28.775 | 29.080 |
| 2.501 | 35.903 | 38.513 | 36.929 | 36.730 | 35.979 | 36.361 |
| 2.997 | 44.228 | 46.157 | 44.261 | 44.039 | 43.120 | 43.563 |
| 3.446 | 53.963 | 51.533 | 58.986 | 58.719 | 57.487 | 58.033 |
| 4.067 | 60.013 | 62.622 | 60.048 | 59.758 | 58.513 | 59.126 |

| NPR | $P_{t,j}$ | P_{rake} at r/r_t of - | | | | | |
|-------|-----------|-----------------------------------|--------|--------|--------|--------|--------|
| | | -.98 | -.82 | -.63 | -.47 | -.30 | -.15 |
| 1.304 | 14.238 | 18.843 | 18.966 | 14.020 | 14.984 | 13.955 | 18.925 |
| 1.446 | 22.081 | 21.645 | 21.824 | 21.870 | 21.828 | 21.749 | 21.778 |
| 1.744 | 23.308 | 23.264 | 25.496 | 25.566 | 25.502 | 25.362 | 23.305 |
| 1.999 | 29.507 | 28.896 | 29.143 | 29.235 | 29.176 | 28.984 | 28.930 |
| 2.501 | 35.903 | 34.202 | 36.465 | 36.575 | 36.487 | 36.257 | 36.164 |
| 2.997 | 44.228 | 43.403 | 45.723 | 43.835 | 43.733 | 43.450 | 43.345 |
| 3.446 | 53.963 | 57.976 | 58.331 | 58.443 | 58.325 | 57.940 | 57.791 |
| 4.067 | 60.013 | 58.441 | 59.369 | 59.494 | 59.367 | 58.962 | 58.815 |

| NPR | $P_{t,j}$ | P_{rake} at r/r_t of - | | | | | | |
|-------|-----------|-----------------------------------|--------|--------|--------|--------|--------|--------|
| | | -.01 | .17 | .33 | .52 | .67 | .82 | .98 |
| 1.304 | 14.238 | 18.932 | 18.910 | 19.031 | 19.054 | 19.007 | 18.856 | 18.666 |
| 1.446 | 22.081 | 21.648 | 21.660 | 21.817 | 21.800 | 21.900 | 21.872 | 21.622 |
| 1.744 | 23.308 | 25.274 | 25.240 | 25.421 | 25.551 | 25.570 | 25.575 | 25.294 |
| 1.999 | 29.507 | 28.844 | 28.844 | 29.052 | 29.197 | 29.252 | 29.251 | 28.910 |
| 2.501 | 35.903 | 34.145 | 36.097 | 36.342 | 36.530 | 36.593 | 36.620 | 36.186 |
| 2.997 | 44.228 | 43.313 | 43.267 | 43.538 | 43.772 | 43.857 | 43.923 | 43.351 |
| 3.446 | 53.963 | 57.755 | 57.712 | 58.056 | 58.375 | 58.489 | 58.591 | 57.792 |
| 4.067 | 60.013 | 58.776 | 58.735 | 59.088 | 59.420 | 59.528 | 59.643 | 58.818 |

TABLE IV.- Continued

(x) $A_t = 11.352 \text{ in}^2$; $A_{\text{choke}} = 7.549 \text{ in}^2$

| NPR | $P_{t,j}$ | $P_{t,j,1}$ | $P_{t,j,2}$ | $P_{t,j,3}$ | $P_{t,j,4}$ | $P_{t,j,5}$ |
|-------|-----------|-------------|-------------|-------------|-------------|-------------|
| 1.302 | 19.199 | 19.368 | 19.303 | 19.302 | 19.927 | 19.098 |
| 1.503 | 22.164 | 22.450 | 22.247 | 22.334 | 21.743 | 22.046 |
| 1.749 | 25.784 | 26.199 | 25.829 | 26.000 | 25.246 | 25.644 |
| 2.006 | 29.583 | 30.082 | 29.616 | 29.828 | 28.956 | 29.433 |
| 2.503 | 36.906 | 37.531 | 36.933 | 37.203 | 36.133 | 36.727 |
| 2.997 | 44.185 | 44.942 | 44.199 | 44.541 | 43.275 | 43.970 |
| 4.162 | 61.359 | 62.434 | 61.347 | 61.843 | 60.092 | 61.079 |

| NPR | $P_{t,j}$ | P_{rake} at r/r_t of - | | | | | |
|-------|-----------|-----------------------------------|--------|--------|--------|--------|--------|
| | | -.97 | -.82 | -.69 | -.52 | -.32 | -.16 |
| 1.302 | 19.199 | 18.879 | 19.093 | 19.119 | 19.061 | 19.032 | 18.998 |
| 1.503 | 22.164 | 21.715 | 22.004 | 22.036 | 21.971 | 21.934 | 21.886 |
| 1.749 | 25.784 | 25.188 | 25.568 | 25.609 | 25.540 | 25.482 | 25.416 |
| 2.006 | 29.583 | 28.900 | 29.323 | 29.386 | 29.294 | 29.232 | 29.165 |
| 2.503 | 36.906 | 36.087 | 36.570 | 36.671 | 36.553 | 36.477 | 36.379 |
| 2.997 | 44.185 | 43.210 | 43.761 | 43.890 | 43.761 | 43.656 | 43.542 |
| 4.162 | 61.359 | 60.063 | 60.831 | 60.958 | 60.781 | 60.611 | 60.449 |

| NPR | $P_{t,j}$ | P_{rake} at r/r_t of - | | | | | | |
|-------|-----------|-----------------------------------|--------|--------|--------|--------|--------|--------|
| | | 0.0 | .17 | .33 | .52 | .67 | .81 | .97 |
| 1.302 | 19.199 | 18.971 | 18.792 | 19.043 | 19.047 | 19.074 | 19.029 | 18.922 |
| 1.503 | 22.164 | 21.833 | 21.980 | 21.935 | 21.927 | 21.995 | 21.978 | 21.830 |
| 1.749 | 25.784 | 25.344 | 25.423 | 25.470 | 25.464 | 25.564 | 25.574 | 25.431 |
| 2.006 | 29.583 | 29.062 | 29.171 | 29.220 | 29.190 | 29.308 | 29.345 | 29.199 |
| 2.503 | 36.906 | 36.267 | 36.410 | 36.453 | 36.415 | 36.570 | 36.634 | 36.460 |
| 2.997 | 44.185 | 43.407 | 43.594 | 43.635 | 43.590 | 43.782 | 43.885 | 43.652 |
| 4.162 | 61.359 | 60.280 | 60.569 | 60.605 | 60.540 | 60.808 | 60.971 | 60.674 |

TABLE IV.- Concluded

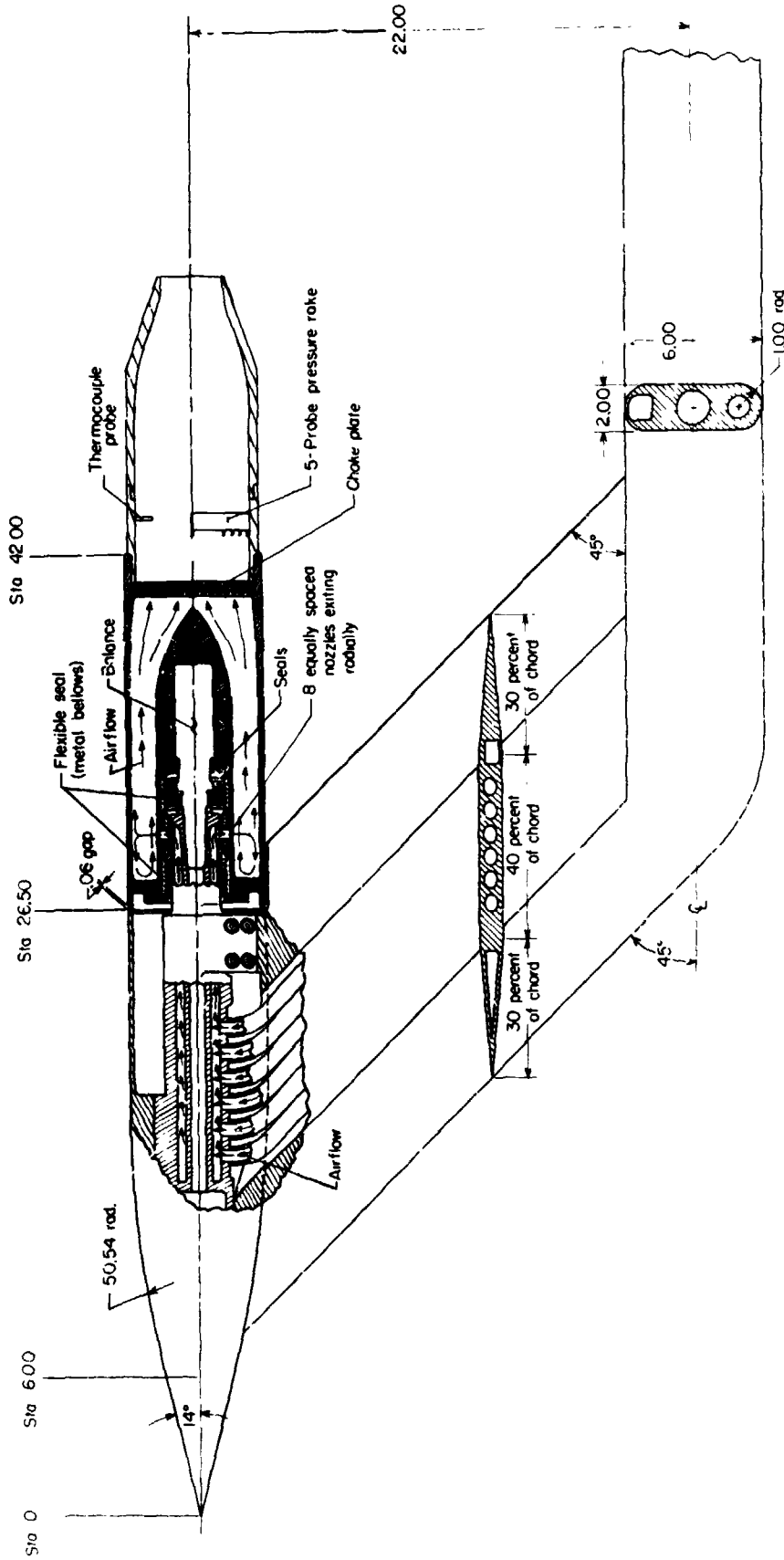
(y) $A_t = 11.352 \text{ in}^2$; $A_{\text{choke}} = 15.286 \text{ in}^2$

| NPR | $P_{t,j}$ | $P_{t,j,1}$ | $P_{t,j,2}$ | $P_{t,j,3}$ | $P_{t,j,4}$ | $P_{t,j,5}$ |
|-------|-----------|-------------|-------------|-------------|-------------|-------------|
| 1.299 | 19.115 | 19.111 | 19.130 | 19.146 | 19.035 | 19.154 |
| 1.495 | 21.999 | 21.990 | 22.005 | 22.029 | 21.870 | 22.102 |
| 1.757 | 25.853 | 25.842 | 25.844 | 25.896 | 25.686 | 25.998 |
| 2.023 | 29.776 | 29.749 | 29.765 | 29.831 | 29.572 | 29.962 |
| 2.495 | 36.718 | 36.686 | 36.700 | 36.787 | 36.461 | 36.957 |
| 2.516 | 37.029 | 36.993 | 37.012 | 37.097 | 36.775 | 37.269 |
| 3.001 | 44.164 | 44.133 | 44.139 | 44.258 | 43.833 | 44.456 |
| 3.808 | 56.035 | 55.980 | 56.010 | 56.157 | 55.598 | 56.428 |
| 4.117 | 60.584 | 60.510 | 60.561 | 60.732 | 60.111 | 61.007 |

| NPR | $P_{t,j}$ | P_{rake} at r/r_t of - | | | | | |
|-------|-----------|-----------------------------------|--------|--------|--------|--------|--------|
| | | -.96 | -.83 | -.65 | -.48 | -.32 | -.17 |
| 1.299 | 19.115 | 18.905 | 19.071 | 19.079 | 19.067 | 19.070 | 19.043 |
| 1.495 | 21.999 | 21.714 | 21.939 | 21.992 | 21.977 | 21.958 | 21.918 |
| 1.757 | 25.853 | 25.491 | 25.772 | 25.827 | 25.836 | 25.814 | 25.761 |
| 2.023 | 29.776 | 29.387 | 29.675 | 29.754 | 29.761 | 29.723 | 29.673 |
| 2.495 | 36.718 | 36.267 | 36.600 | 36.697 | 36.716 | 36.670 | 36.600 |
| 2.516 | 37.029 | 36.572 | 36.913 | 37.010 | 37.032 | 36.980 | 36.913 |
| 3.001 | 44.164 | 43.626 | 44.018 | 44.132 | 44.161 | 44.102 | 44.021 |
| 3.808 | 56.035 | 55.353 | 55.814 | 55.980 | 56.010 | 55.932 | 55.831 |
| 4.117 | 60.584 | 59.864 | 60.366 | 60.540 | 60.585 | 60.489 | 60.380 |

| NPR | $P_{t,j}$ | P_{rake} at r/r_t of - | | | | | | |
|-------|-----------|-----------------------------------|--------|--------|--------|--------|--------|--------|
| | | -.01 | .18 | .34 | .51 | .68 | .83 | .96 |
| 1.299 | 19.115 | 19.072 | 19.062 | 19.125 | 19.155 | 19.104 | 18.989 | 18.878 |
| 1.495 | 21.999 | 21.934 | 21.936 | 22.016 | 22.048 | 21.983 | 21.844 | 21.662 |
| 1.757 | 25.853 | 25.774 | 25.778 | 25.871 | 25.905 | 25.832 | 25.668 | 25.417 |
| 2.023 | 29.776 | 29.671 | 29.688 | 29.794 | 29.816 | 29.749 | 29.574 | 29.297 |
| 2.495 | 36.718 | 36.599 | 36.639 | 36.757 | 36.784 | 36.696 | 36.498 | 36.157 |
| 2.516 | 37.029 | 36.902 | 36.939 | 37.065 | 37.097 | 36.993 | 36.821 | 36.462 |
| 3.001 | 44.164 | 44.013 | 44.068 | 44.204 | 44.238 | 44.132 | 43.922 | 43.504 |
| 3.808 | 56.035 | 55.819 | 55.891 | 56.062 | 56.081 | 55.980 | 55.743 | 55.193 |
| 4.117 | 60.584 | 60.359 | 60.461 | 60.632 | 60.657 | 60.539 | 60.287 | 59.688 |

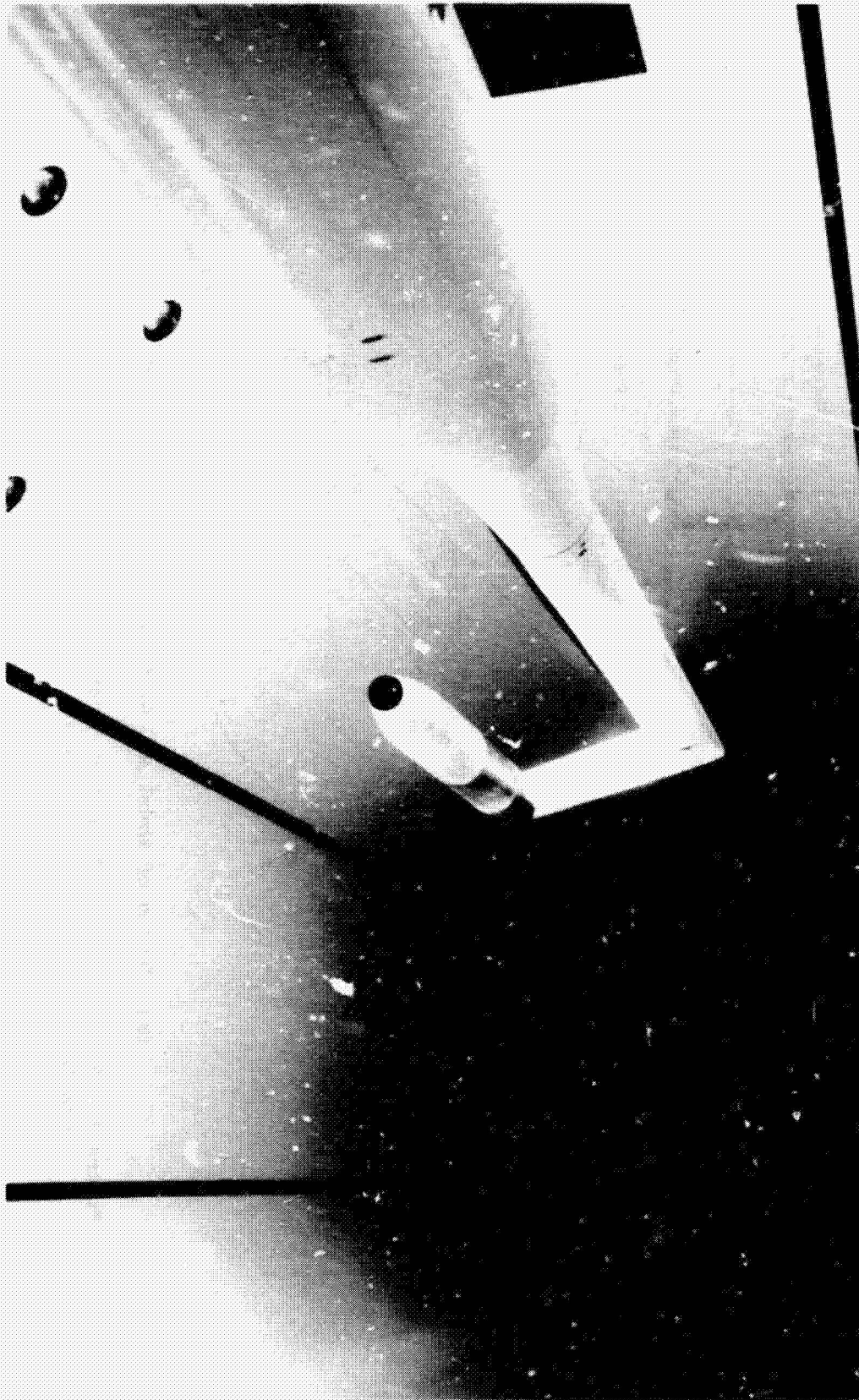
ORIGINAL PAGE IS
OF POOR QUALITY



(a) Sketch of model and propulsion-simulation system.

Figure 1.- Air-powered single-engine propulsion-simulation system with a typical nozzle installed. Dimensions are in inches unless otherwise noted.

ORIGINAL PAGE IS
OF POOR QUALITY



L-73-5555

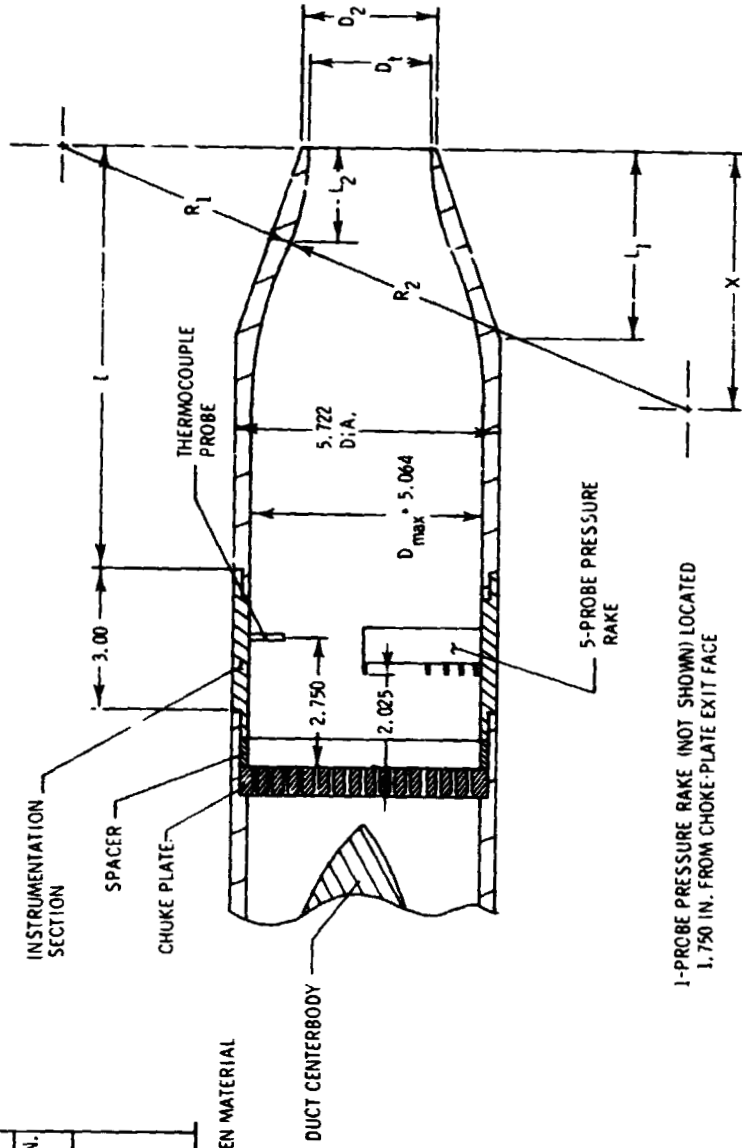
(b) Photograph of model and propulSION-simulation system installed in
Langley 16-Foot Transonic Tunnel.

Figure 1.- Concluded.

| STRATFORD CHOKE NOZZLES | | | | | | | | | | | |
|---|----------------------|-----------------|----------------------|----------------------|----------------------|----------------------|--------|----------------------|----------------------|--------|----------------------|
| MEASURED THROAT AREA (IN ²) | | DESIGN GEOMETRY | | | | | | | | | |
| R ₁ , IN. | R ₂ , IN. | X, IN. | D ₁ , IN. | D ₂ , IN. | L ₁ , IN. | L ₂ , IN. | L, IN. | L ₁ , IN. | L ₂ , IN. | L, IN. | L ₂ , IN. |
| 0.999 | 1.257 | 21.314 | 9.428 | 1.128 | 1.378 | 1.378 | 11.88 | 5.500 | 11.88 | 0.903 | 0.903 |
| 1.933 | 1.140 | 9.000 | 6.274 | 1.369 | 1.820 | 1.820 | 9.00 | 4.000 | 9.00 | 1.623 | 1.623 |
| 3.002 | 1.909 | 14.715 | 7.450 | 1.955 | 2.204 | 2.204 | 9.00 | 4.500 | 9.00 | 1.564 | 1.564 |
| 3.992 | 1.510 | 8.320 | 5.837 | 2.255 | 2.505 | 2.505 | 9.00 | 4.000 | 9.00 | 2.052 | 2.052 |
| 5.711 | 1.400 | 7.700 | 5.432 | 2.700 | 2.950 | 2.950 | 9.00 | 4.000 | 9.00 | 2.239 | 2.239 |
| 8.501 | 1.580 | 7.868 | 4.988 | 3.290 | 3.540 | 3.540 | 9.00 | 4.000 | 9.00 | 2.270 | 2.270 |
| 11.352 | .600 | 5.900 | 4.086 | 3.800 | 4.050 | 4.050 | 9.00 | 3.500 | 9.00 | 2.300 | 2.300 |

| CHOKE PLATES | | |
|------------------------------|-------------------|----------------|
| OPEN AREA (IN ²) | PERCENT DUCT AREA | HOLE DIA., IN. |
| 1.750 | 2.7 | 0.098 |
| 3.853 | 19.1 | 0.147 |
| 5.779 | 28.0 | 0.180 |
| 7.549 | 37.1 | 0.206 |
| 15.286 | 75.9 | |

NOTE: 15.286-IN² CHOKE PLATE IS ACTUALLY WIRE SCREEN MATERIAL SUPPORTED BY AN OPEN METAL LATTICEWORK

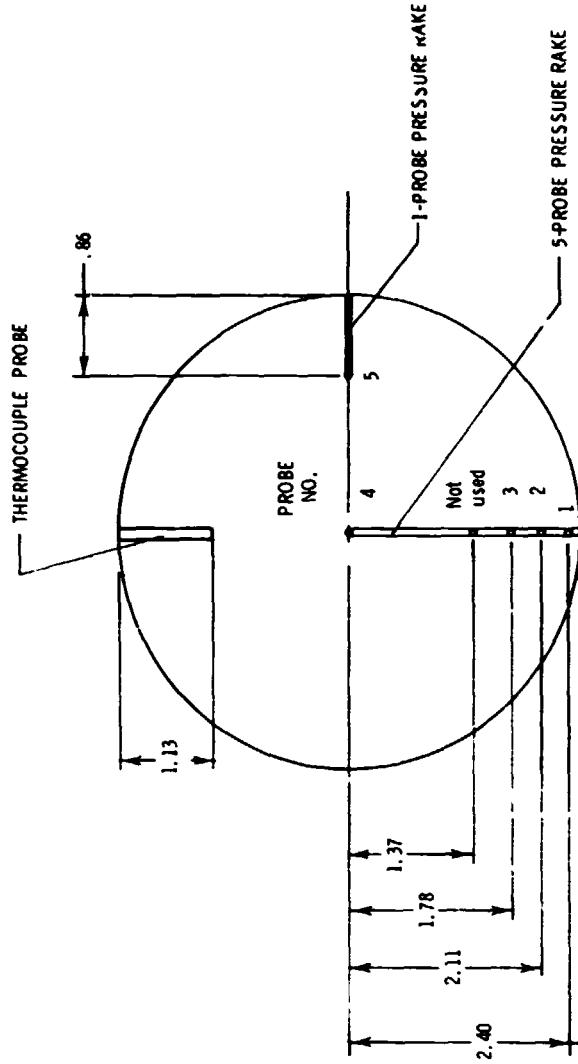


(a) Nozzle and choke-plate geometry.
Figure 2.- Nozzle and instrumentation section sketches.

SUMMARY OF RAKE CONSTANTS

| A_t (in ²) | A_{choke} (in ²) | $K_{R,1}$ | $K_{R,2}$ | $K_{R,3}$ | $K_{R,4}$ | $K_{R,5}$ |
|-----------------------------|-----------------------------------|-----------|-----------|-----------|-----------|-----------|
| .999 | 1.750 | .9984 | .9978 | .9978 | .9936 | .9950 |
| ↓ | 3.853 | .9955 | .9948 | .9950 | .9951 | .9949 |
| ↓ | 15.286 | .9970 | .9959 | .9961 | .9962 | .9965 |
| 1.933 | 1.750 | .9967 | .9962 | .9976 | .9920 | .9988 |
| ↓ | 3.853 | .9938 | .9944 | .9942 | .9942 | .9941 |
| ↓ | 15.286 | .9959 | .9950 | .9954 | .9961 | .9952 |
| 3.002 | 1.750 | .9880 | .9920 | .9926 | .9919 | .9929 |
| ↓ | 3.853 | .9909 | .9936 | .9930 | .9932 | .9920 |
| ↓ | 15.286 | .9909 | .9904 | .9904 | .9918 | .9907 |
| 5.992 | 1.750 | .9840 | .9909 | .9910 | .9896 | .9907 |
| ↓ | 3.853 | .9881 | .9919 | .9926 | .9913 | .9903 |
| ↓ | 15.286 | .9923 | .9963 | .9955 | .9972 | .9956 |
| ↓ | 15.286 | .9948 | .9940 | .9941 | .9974 | 1.0004 |
| 5.711 | 3.853 | .9802 | .9905 | .9880 | .9901 | .9784 |
| ↓ | 7.549 | .9839 | .9915 | .9901 | .9948 | .9908 |
| ↓ | 15.286 | .9901 | .9932 | .9914 | .9986 | .9949 |
| ↓ | 15.286 | .9923 | .9918 | .9918 | .9981 | .9946 |
| 8.501 | 3.853 | .9760 | 1.0061 | .9960 | .9850 | .9888 |
| ↓ | 7.549 | .9684 | .9857 | .9880 | .9957 | .9907 |
| ↓ | 15.286 | .9830 | .9905 | .9871 | 1.0009 | .9931 |
| ↓ | 15.286 | .9904 | .9899 | .9879 | .9955 | .9830 |
| 11.352 | 3.853 | .9425 | 1.0177 | 1.0016 | .9778 | .9759 |
| ↓ | 7.549 | .9393 | .9803 | .9844 | 1.0050 | .9947 |
| ↓ | 15.286 | .9630 | .9802 | .9717 | 1.0001 | .9842 |
| ↓ | 15.286 | .9902 | .9895 | .9859 | .9967 | .9824 |

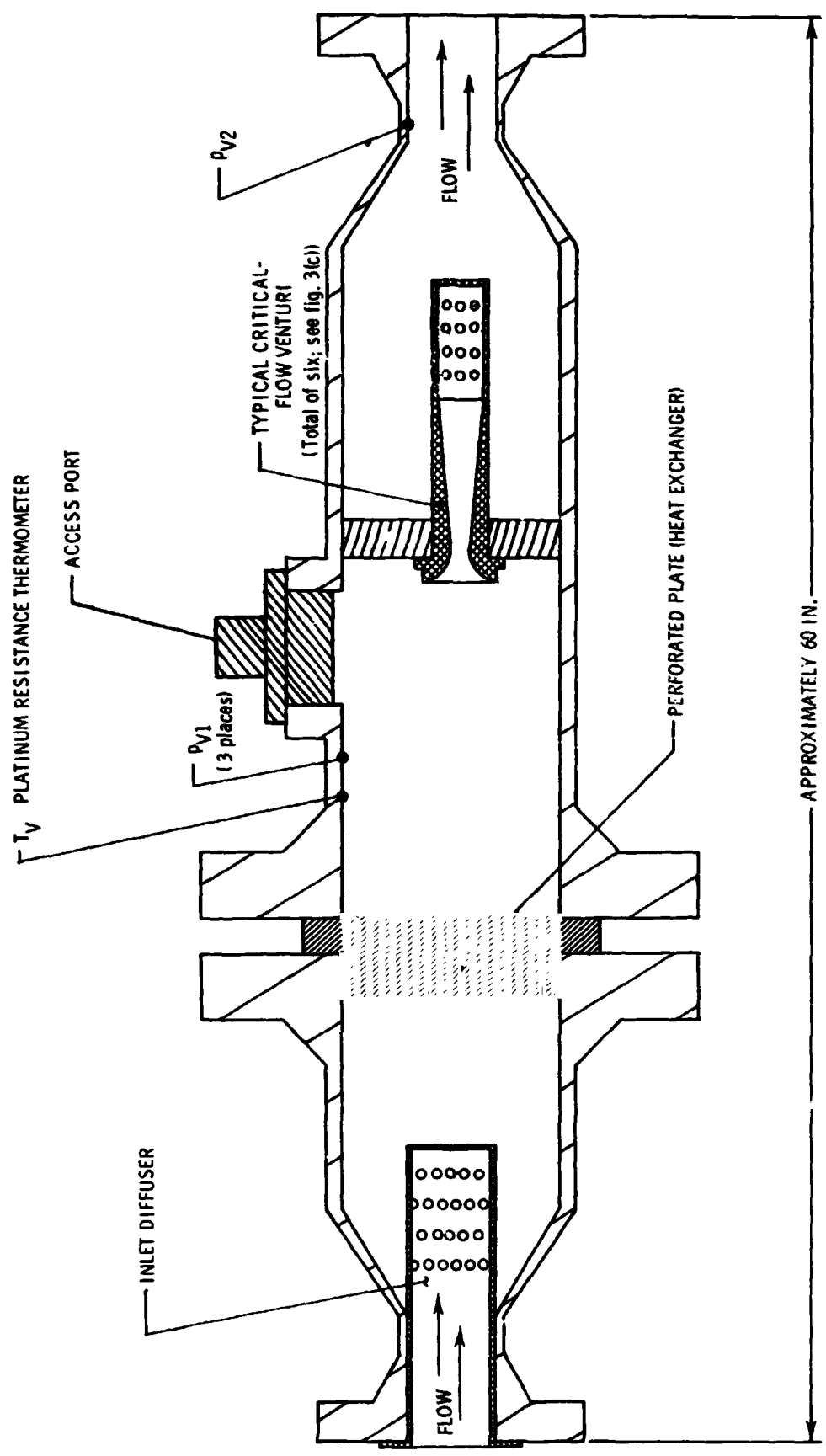
NOTE: $K_{R,1}$ represents rake constant for probe number 1.



(b) Total-pressure-probe orientation and summary of rake correction factors.

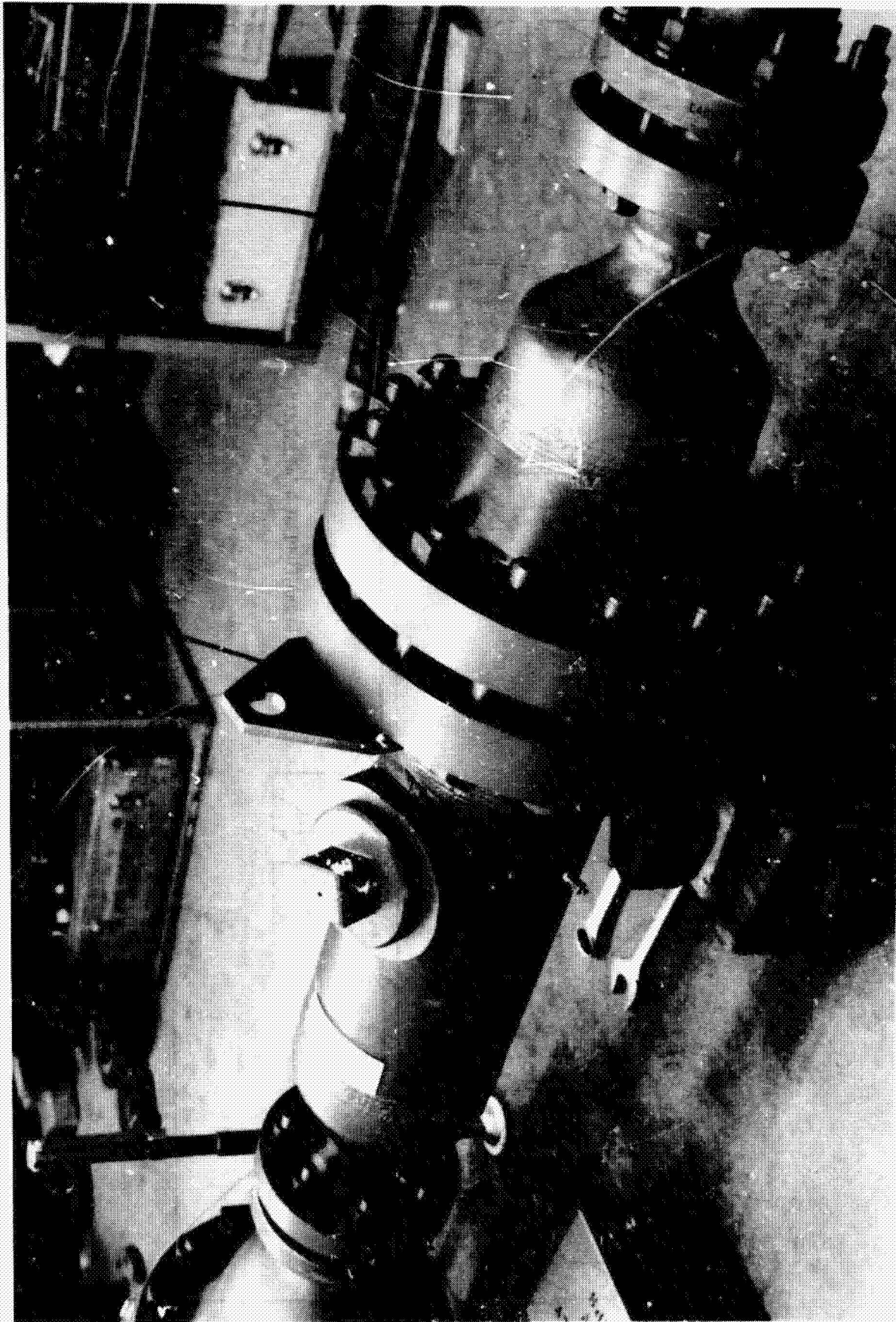
Figure 2.- Concluded.

ORIGINAL PAGE IS
OF POOR QUALITY



(a) Sketch of multiple critical venturi system.
Figure 3.- Geometry of multiple critical venturi system.

ORIGINAL PAGE IS
OF POOR QUALITY

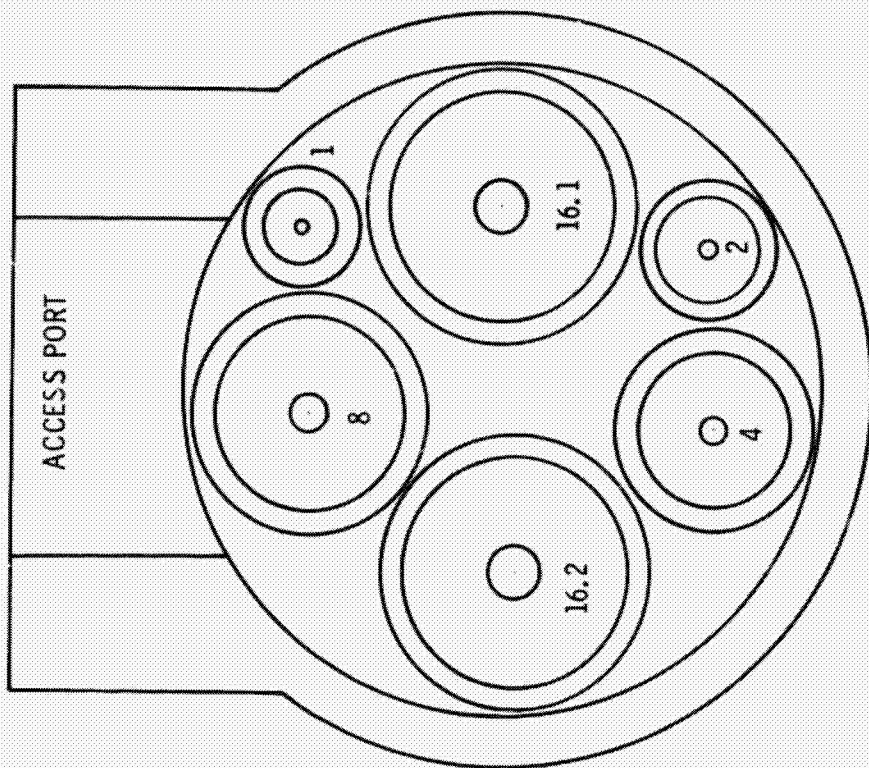


L-85-110

(b) Photograph of multiple critical venturi system.

Figure 3.- Continued.

| VENTURI GEOMETRY | | |
|------------------|------------------|------------------------------|
| VENTURI NO. | THROAT DIA., IN. | THROAT AREA, IN ² |
| 1 | 0.1877 | 0.0277 |
| 2 | 0.2639 | 0.0547 |
| 4 | 0.3741 | 0.1099 |
| 8 | 0.5281 | 0.2190 |
| 16.1 | 0.7475 | 0.4388 |
| 16.2 | 0.7478 | 0.4392 |



(c) Individual venturi geometry and orientation.

Figure 3.- Concluded.

ORIGINAL FILED
OF POOR QUALITY

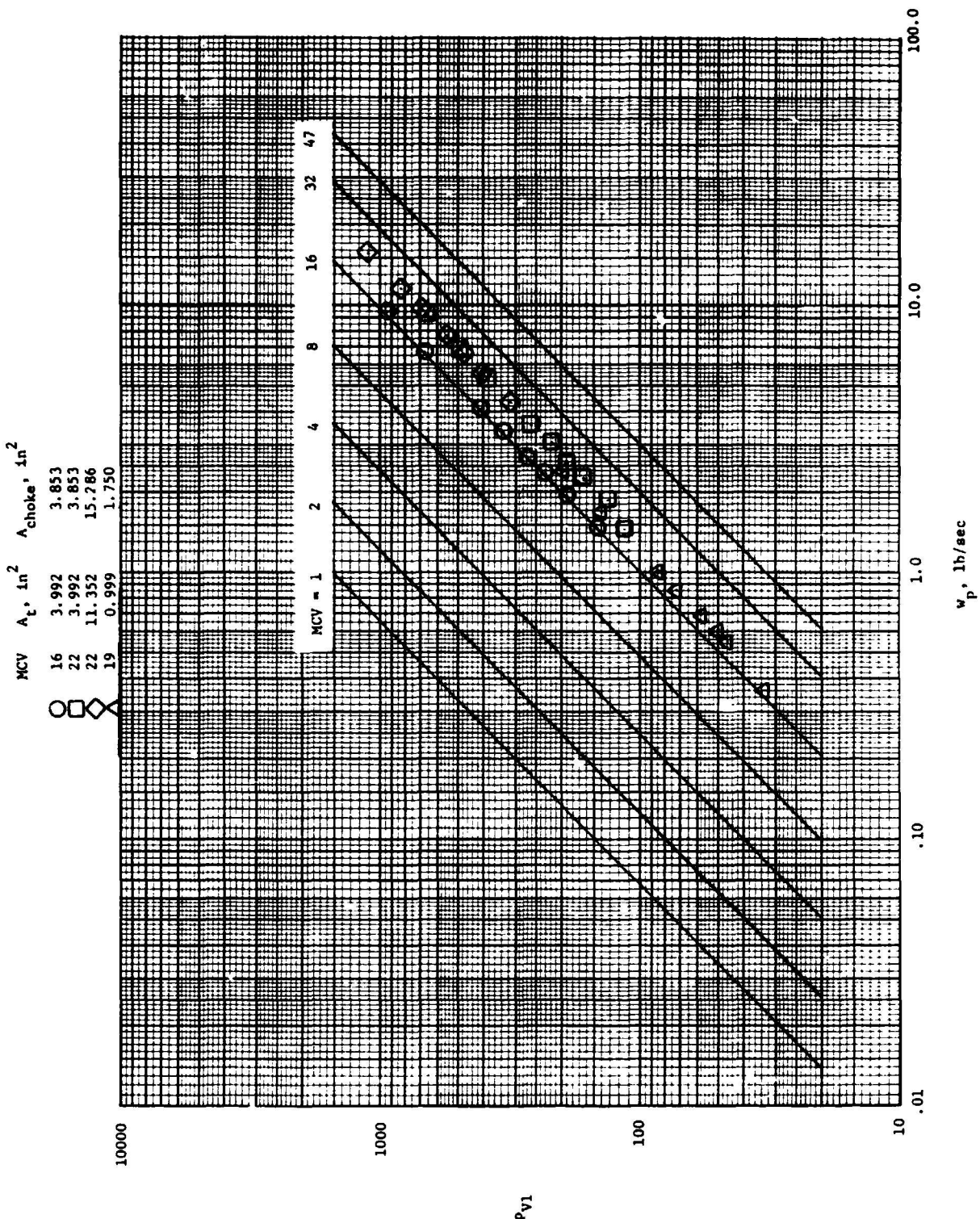
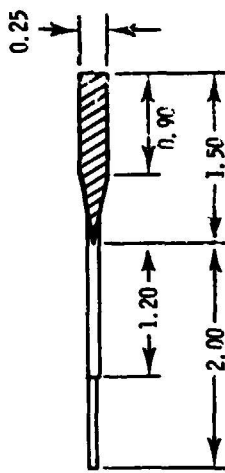
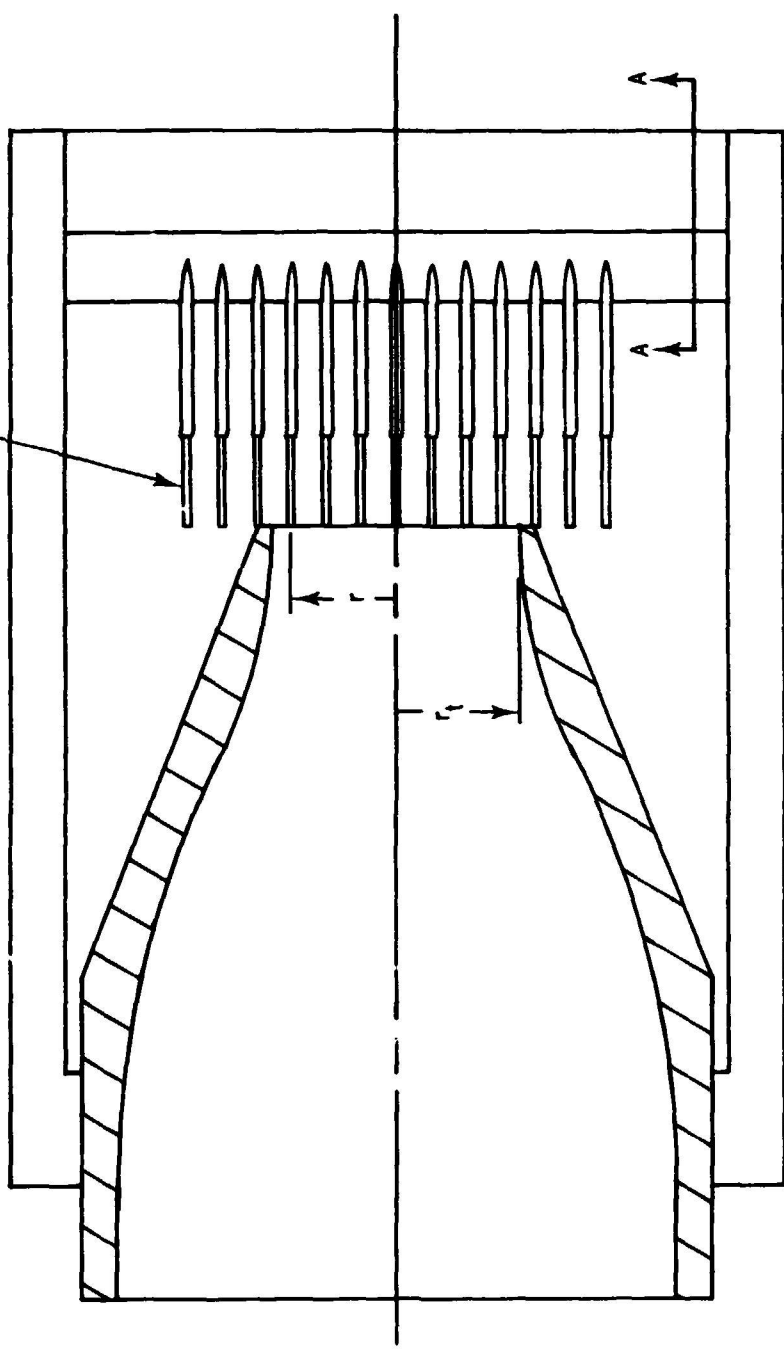


Figure 4.- Multiple critical venturi operating envelope.

0.06 Dia. tube inserted through 0.09 Dia. tube

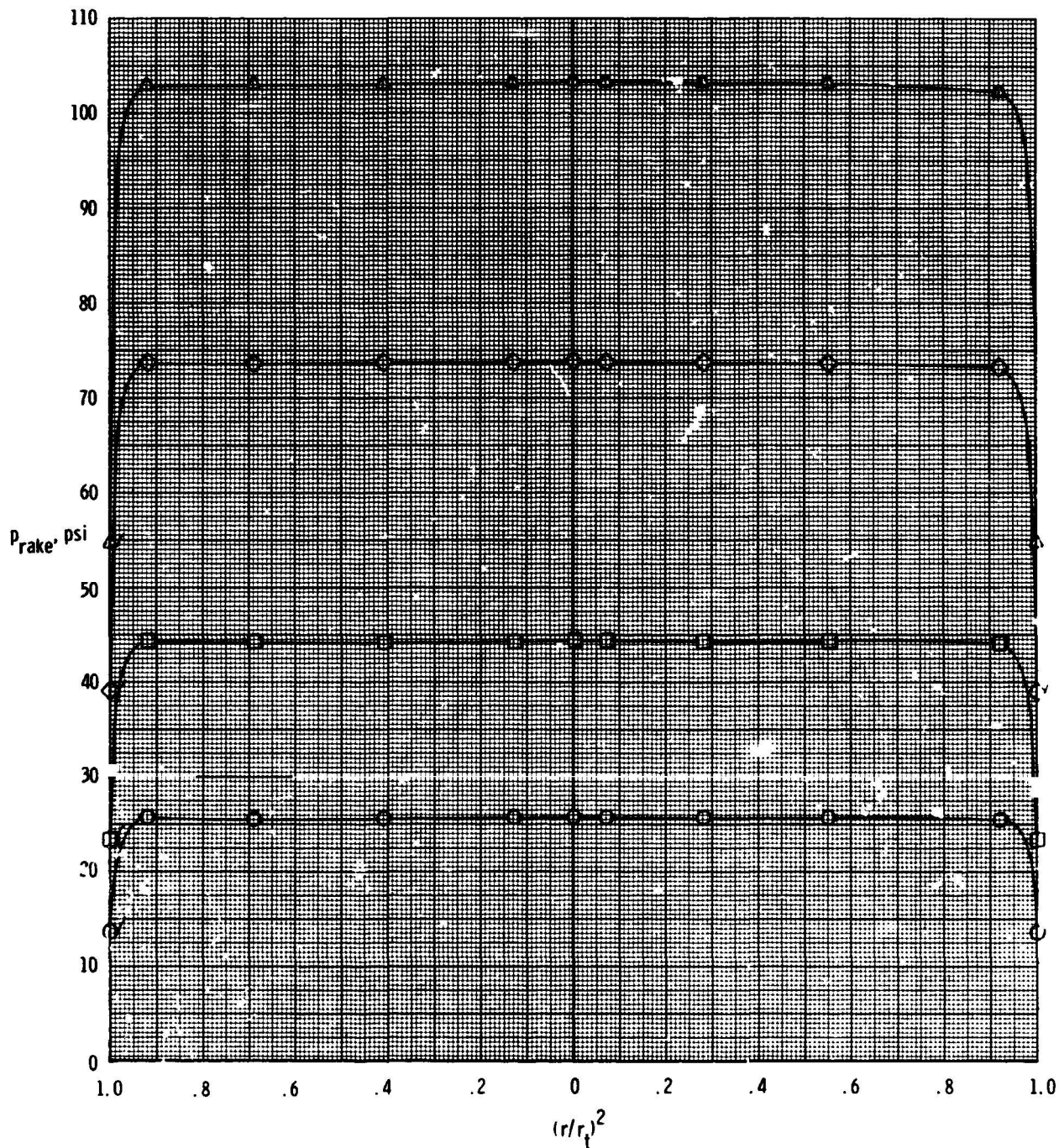


Section A-A

Figure 5.- Sketch of jet total-pressure rake mounted at throat of typical Stratford choke nozzle.

| | NPR | $P_{t,j}$, psi |
|---|------|-----------------|
| ○ | 1.74 | 25,712 |
| □ | 3.01 | 44,401 |
| ◇ | 5.01 | 73,842 |
| △ | 7.01 | 103,408 |

ORIGINAL FILE
OF POOR QUALITY

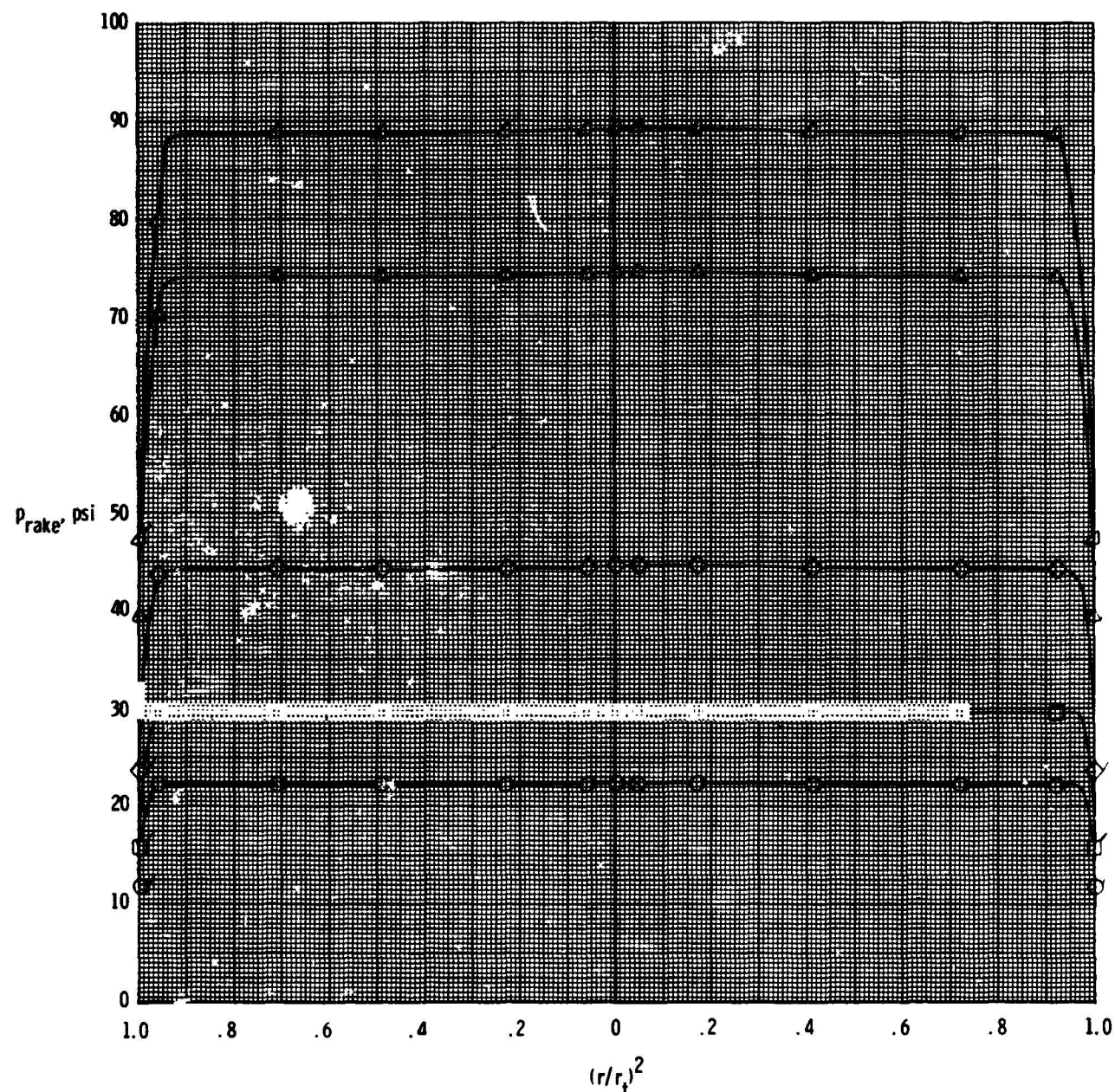


(a) $A_t = 3.992 \text{ in}^2$; $A_{choke} = 3.853 \text{ in}^2$.

Figure 6.- Typical exhaust total-pressure profiles measured with rake located at nozzle throat. Flagged symbols indicate wall static pressure.

ORIGINAL PAGE IS
OF POOR QUALITY

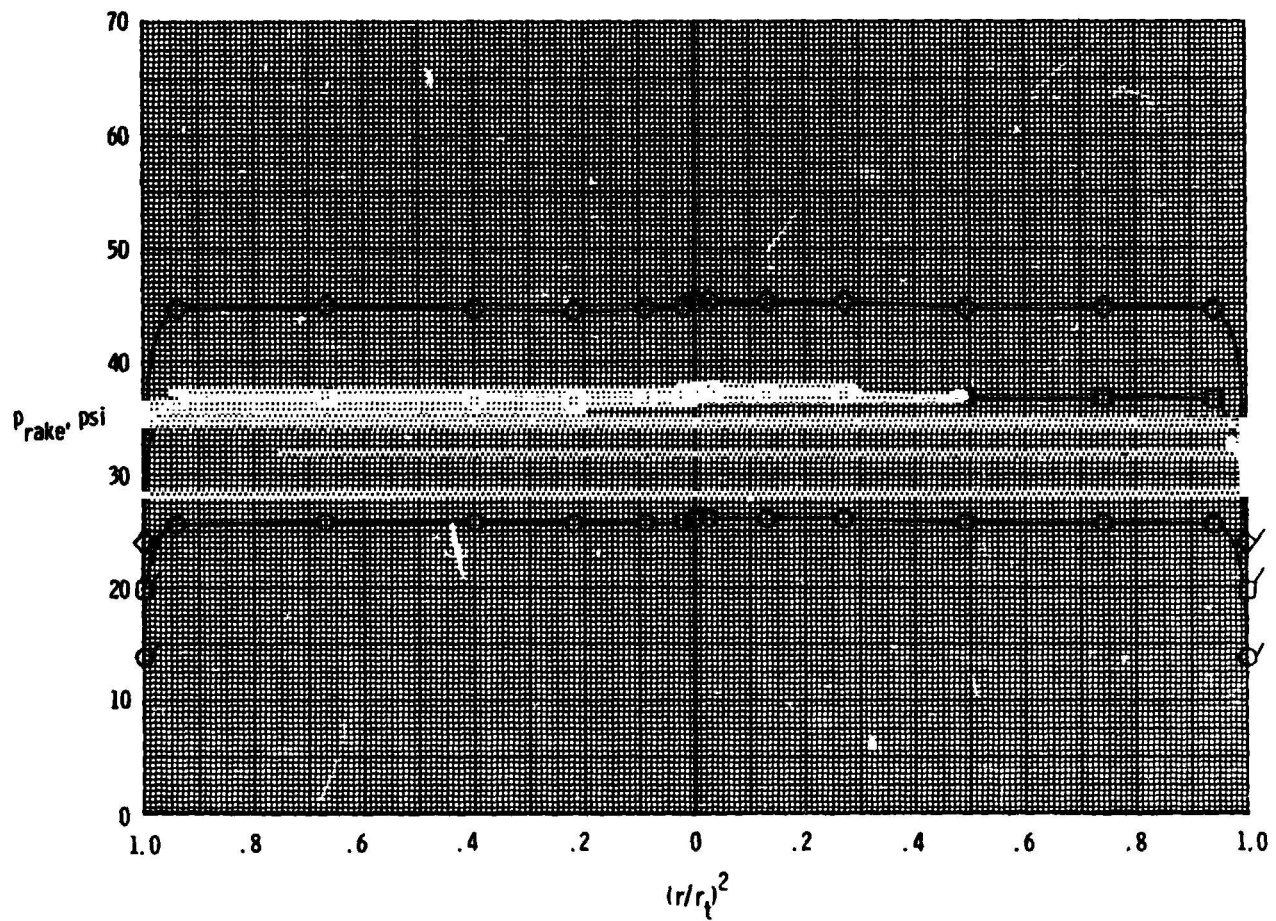
| | NPR | $P_{t,j}$ psi |
|---|------|---------------|
| ○ | 1.51 | 22,436 |
| □ | 2.00 | 29,833 |
| ◇ | 2.99 | 44,586 |
| △ | 5.01 | 74,598 |
| ▽ | 6.00 | 89,364 |



(b) $A_t = 5.711 \text{ in}^2$; $A_{choke} = 3.853 \text{ in}^2$.

Figure 6.- Continued.

| | NPR | $P_{t,j}$, psi |
|---|------|-----------------|
| ○ | 1.75 | 26.120 |
| □ | 2.50 | 37.261 |
| ◇ | 3.04 | 45.313 |



(c) $A_c = 11.352 \text{ in}^2$; $A_{choke} = 3.853 \text{ in}^2$.

Figure 6.- Concluded.

ORIGINAL PAGES 15
OF POOR QUALITY

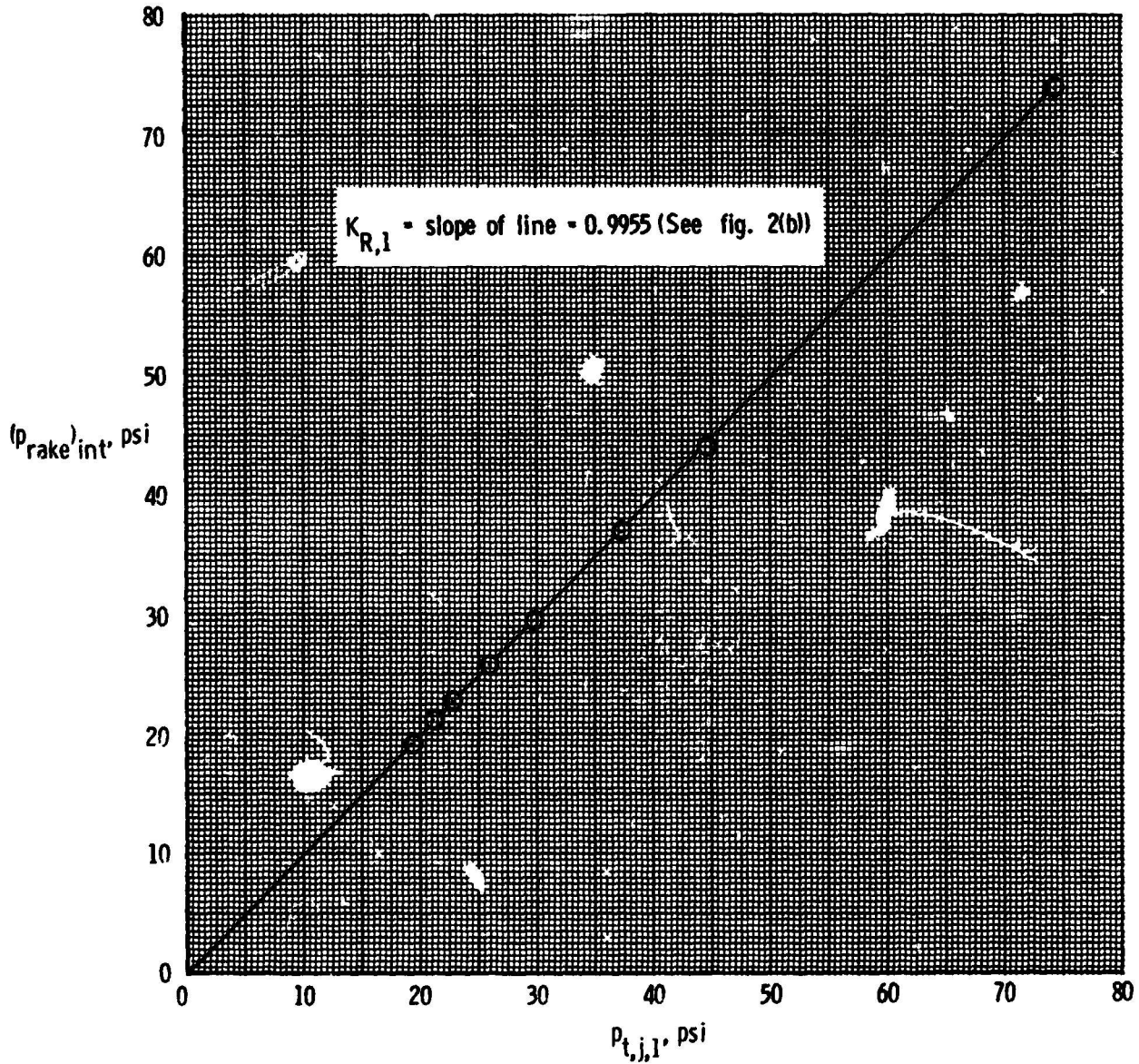


Figure 7.- Typical variation of total pressure obtained by integrating exhaust total-pressure profiles measured with rake (see fig. 6) as a function of jet total pressure measured with an individual probe (see fig. 2(b)) located in the instrumentation section. $A_t = 0.999 \text{ in}^2$; $A_{\text{choke}} = 3.853 \text{ in}^2$.

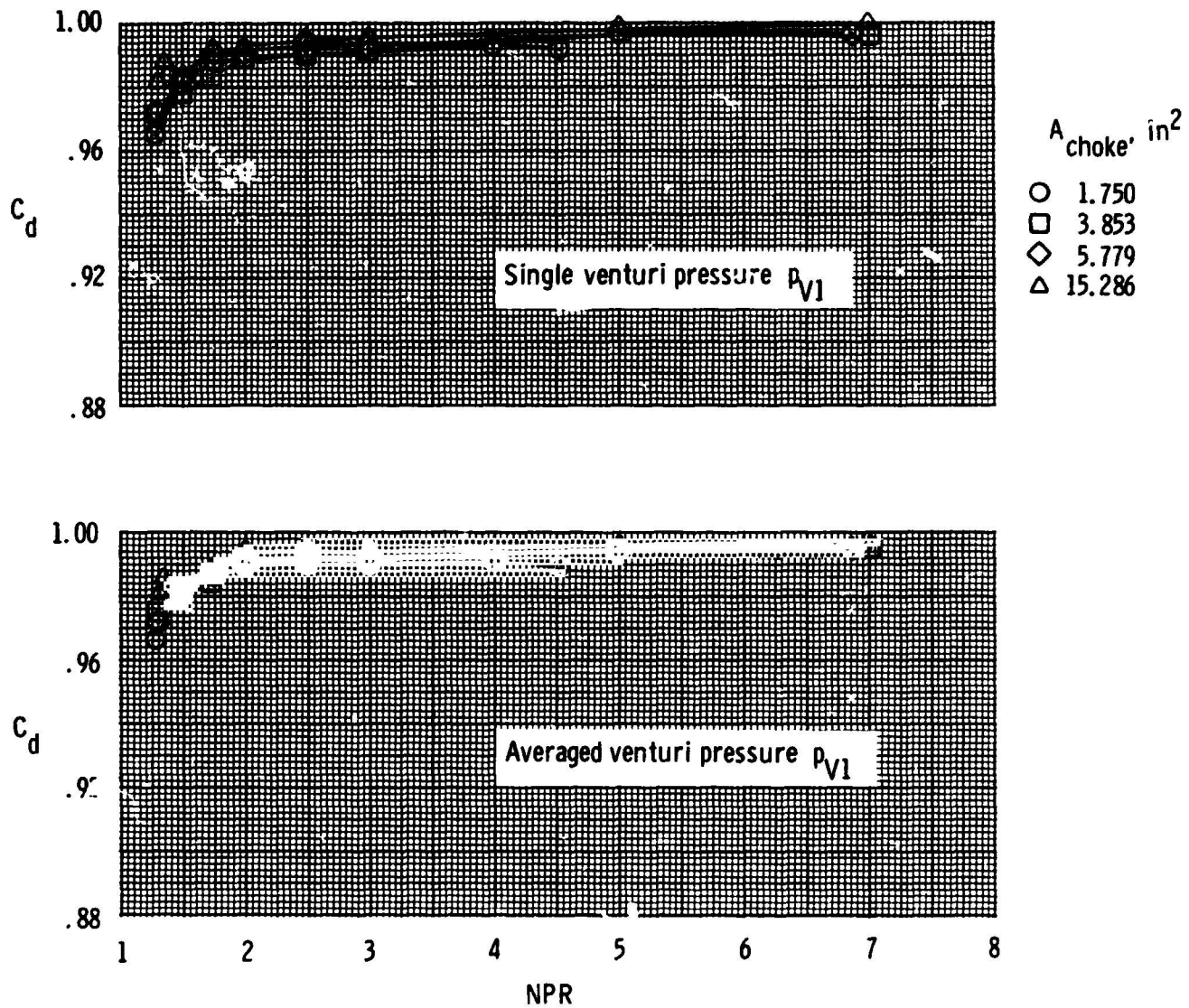


Figure 8.- Comparison of nozzle discharge coefficient calculations for single and averaged p_{V1} measurements. $A_t = 3.992 \text{ in}^2$; $K_{R,1}$ to $K_{R,5} = 1.0$; $(T_{t,j})_{nom} = 530^\circ\text{R}$; $MCV = 22$.

ORIGINAL PAGE IS
OF POOR QUALITY

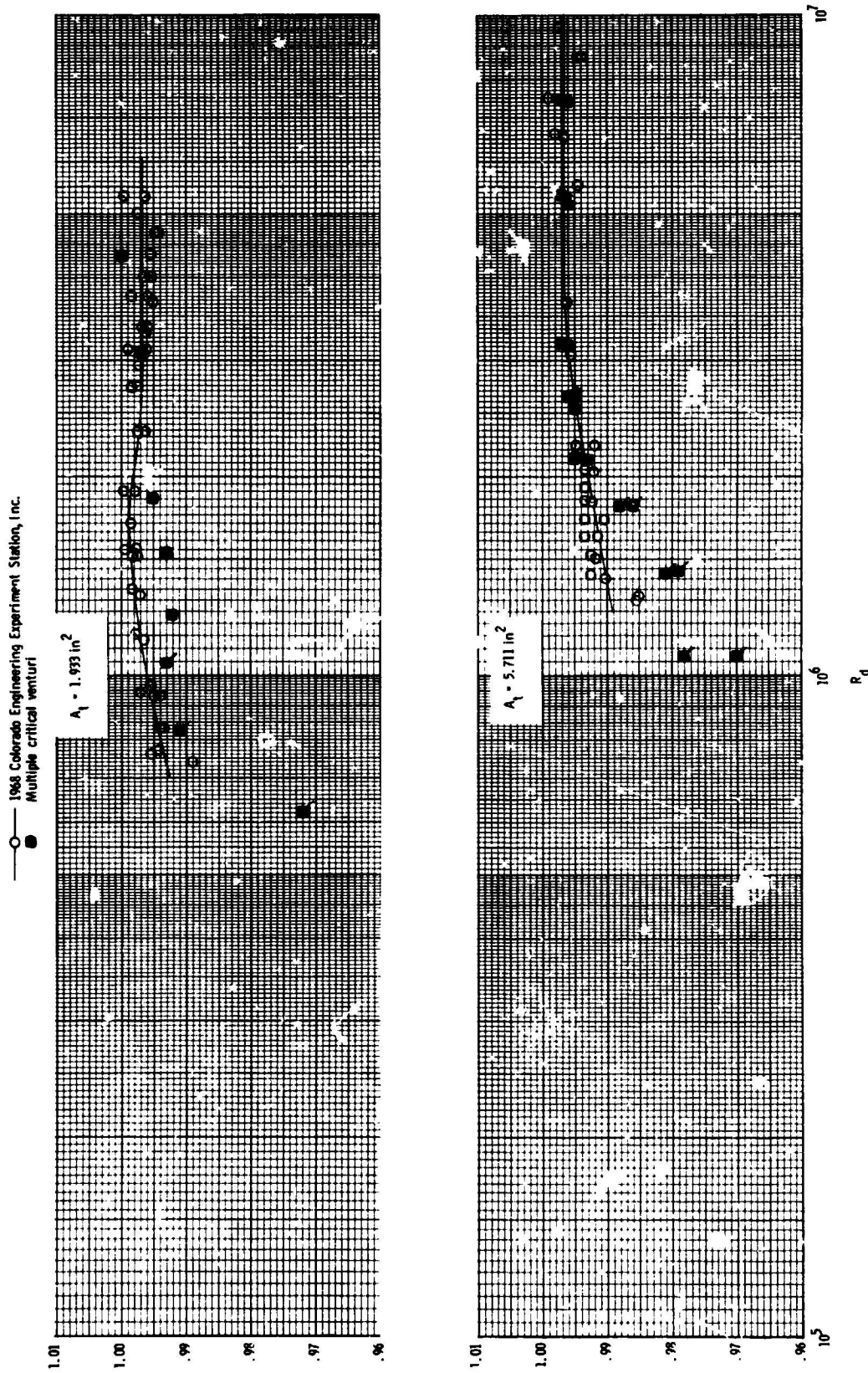
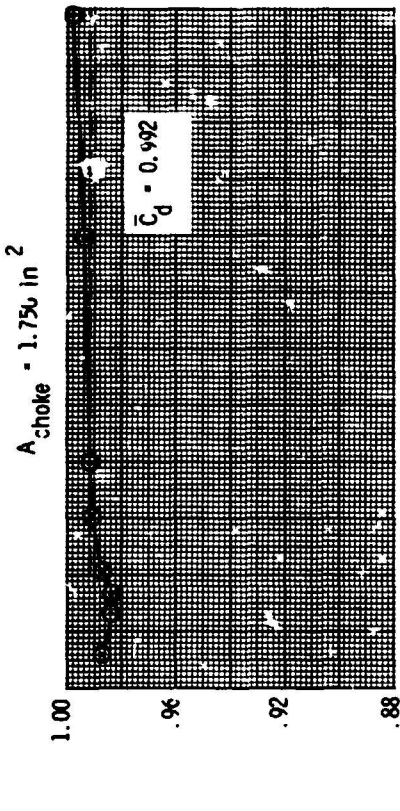
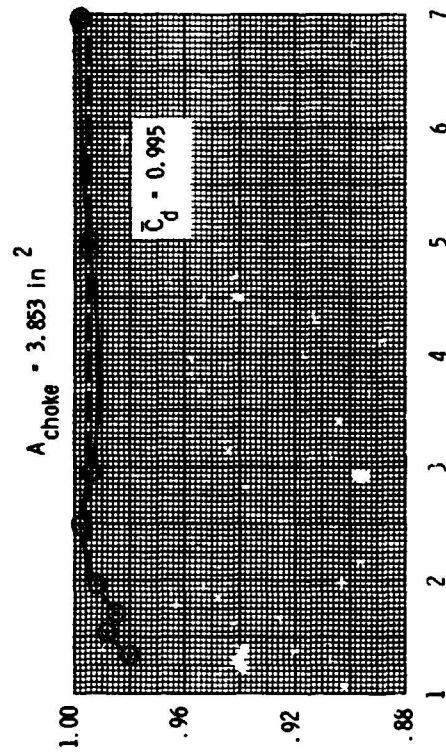


Figure 9.- Comparison of discharge coefficients obtained from multiple critical venturis with discharge coefficients obtained from standard-nozzle calibration in 1968 at Colorado Engineering Experiment Station, Inc. Flagged symbols indicate $NPR < (NPR)_c$. $K_{R,1}$ to $K_{R,5} = 1.0$; $A_{choke} = 15.286 \text{ in}^2$ (screens).

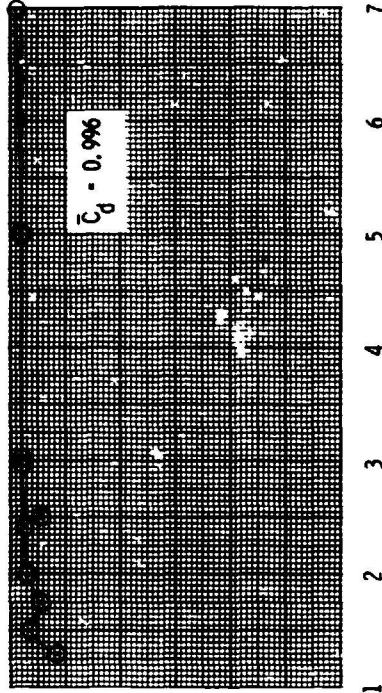


$K_{R,1}$ to K_p = (See fig. 2(b))
 $(T_{t,j})_{\text{noir}}$ 30°R
 MCV = 19

C_d



$A_{\text{choke}} = 15.286 \text{ in}^2$ (screens)



NPR

(a) $A_t = 0.999 \text{ in}^2$.

Figure 10.- Variation of standard-nozzle discharge coefficient with nozzle pressure ratio for jet total pressure corrected with rake factors measured at throat.



ORIGINAL PAGE IS
OF POOR QUALITY

$K_{R,1}$ to $K_{R,5}$ - (See fig. 2(b))

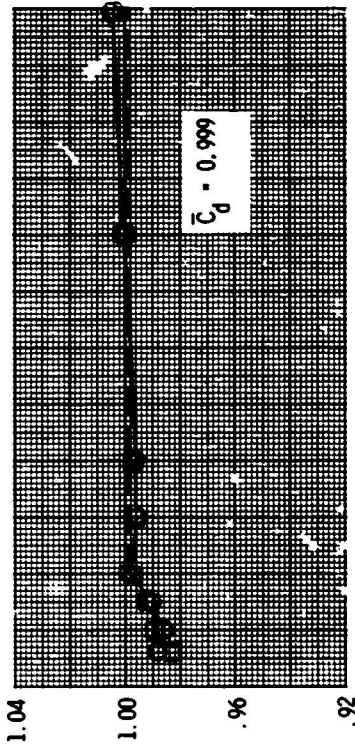
$(\tau_{t,j})_{nom} = 530^{\circ}R$

MCV

○ 22

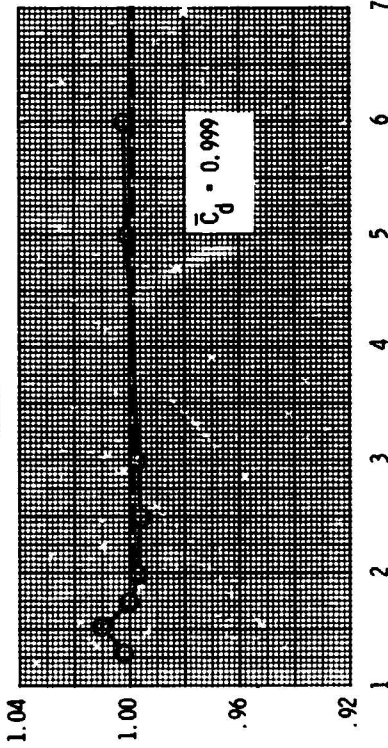
□ 21

$A_{choke} = 1.750 \text{ in}^2$

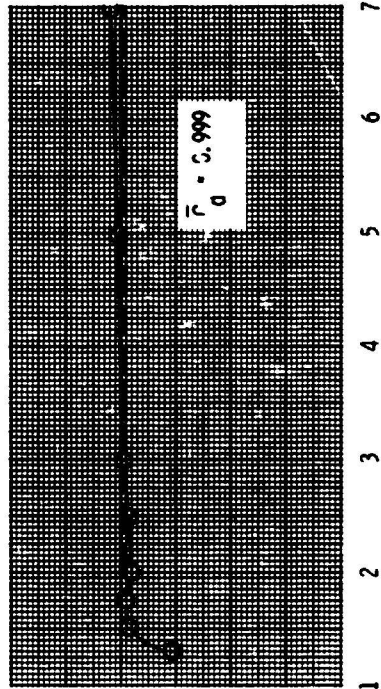


C_d

$A_{choke} = 3.853 \text{ in}^2$



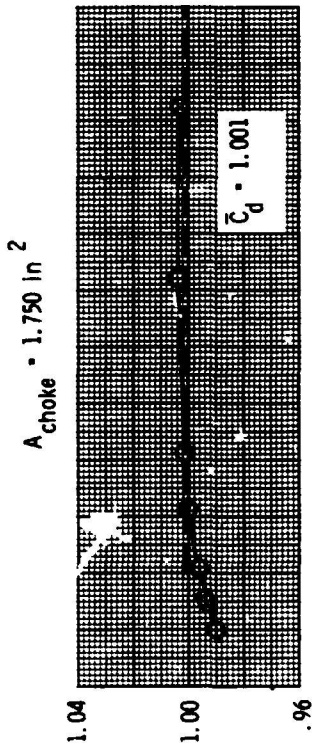
$A_{choke} = 15.286 \text{ in}^2$ (screens)



NPR

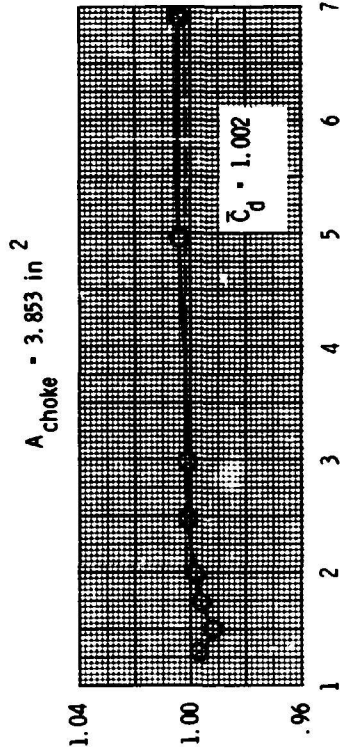
(b) $A_t = 1.933 \text{ in}^2$.

Figure 10.- Continued.

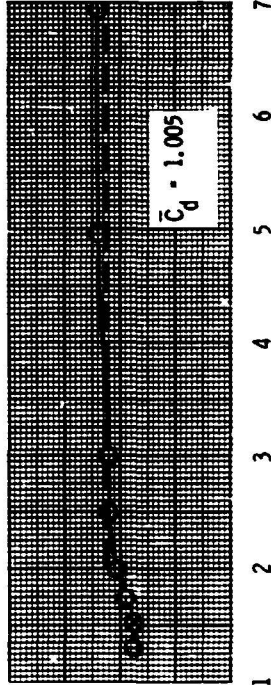


$K_{R,1}$ to $K_{R,5}$ - (See fig. 2(b))
 $(T_{t,1})_{nom} = 530^\circ\text{R}$
 $MCV = 22$

C_d



$A_{choke} = 15.286 \text{ in}^2$ (screens)



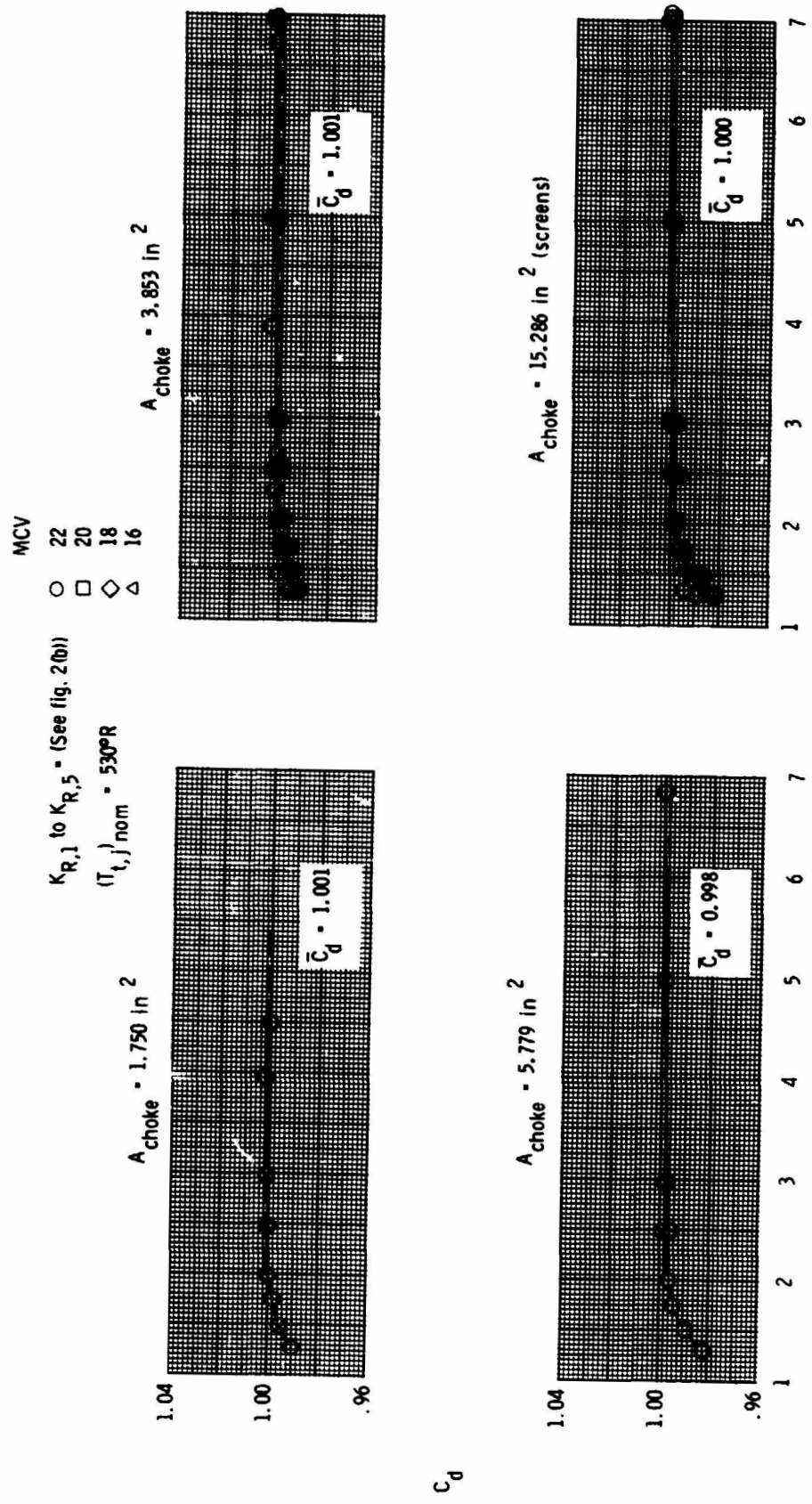
NPR

(c) $A_t = 3.002 \text{ in}^2$.

Figure 10.- Continued.



ORIGINAL PAGE IS
OF POOR QUALITY



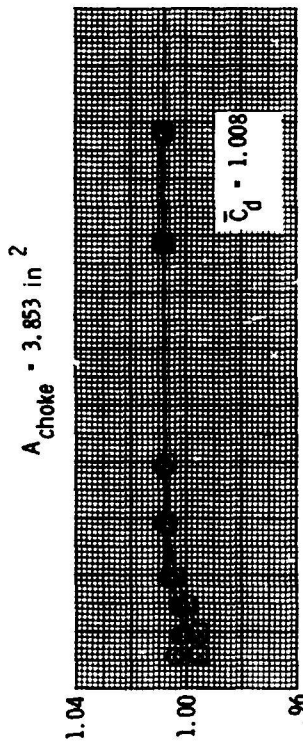
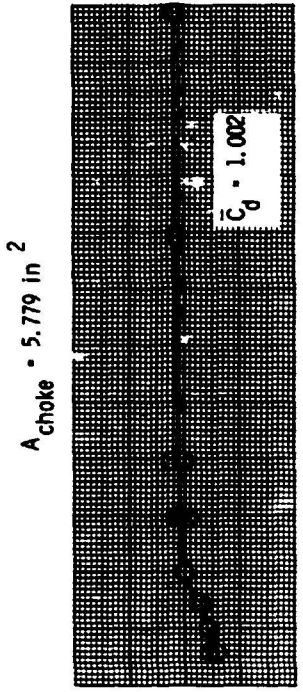
NPR
 (d) $A_t = 3.992 \text{ in}^2$.
 Figure 10.- Continued.

$(T_{t,j})_{nom} \text{ } ^\circ R$ $(T_{V,j})_{nom} \text{ } ^\circ R$

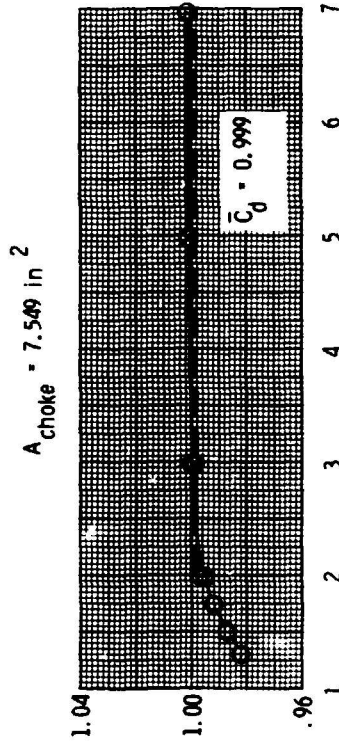
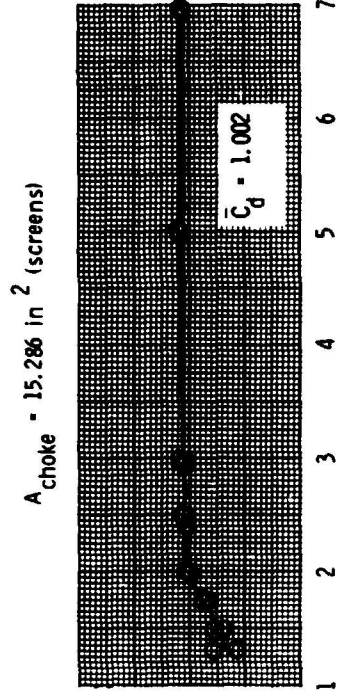
○ 530 542
 □ 550 562

$K_{R,1}$ to $K_{R,5}$ (See fig. 2(b))

MCV = 22



C_d



NPR

(e) $A_t = 5.711 \text{ in}^2$.

Figure 10.- Continued.

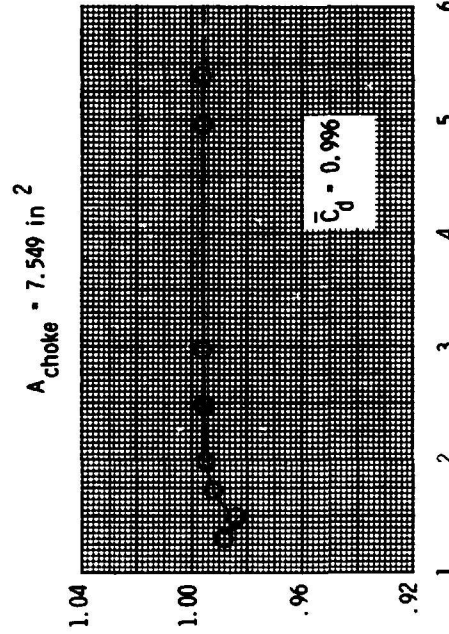
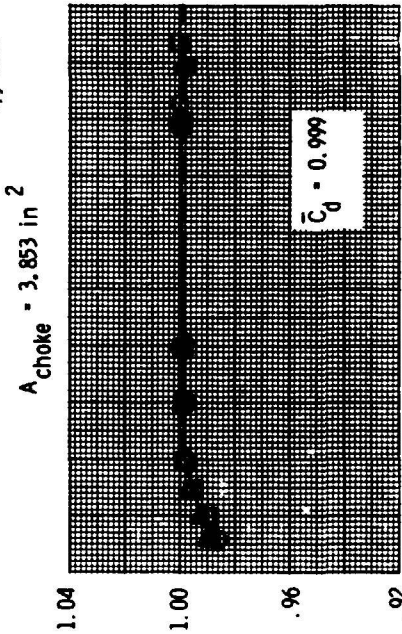
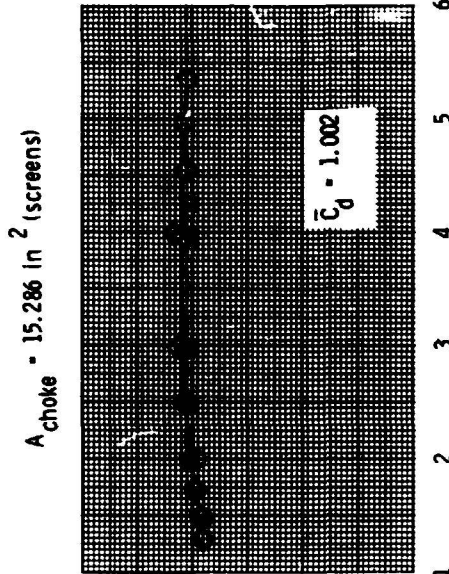
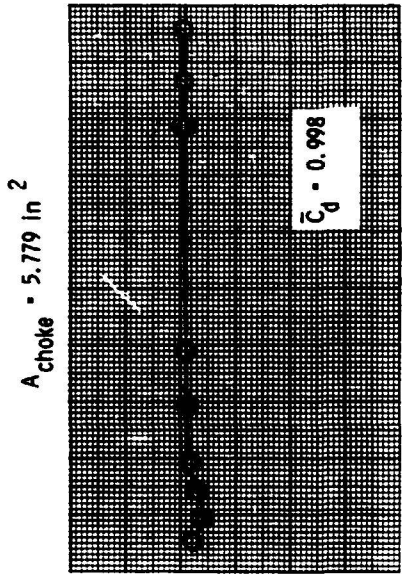
ORIGINAL PAGE IS
OF POOR QUALITY

MCV

- 22
- 20
- ◇ 19
- △ 18
- ▽ 16

$K_{R,1}$ to $K_{R,5}$ - (See fig. 2(b))

$(T_{t,j})_{nom} = 529^{\circ}R$



NPR

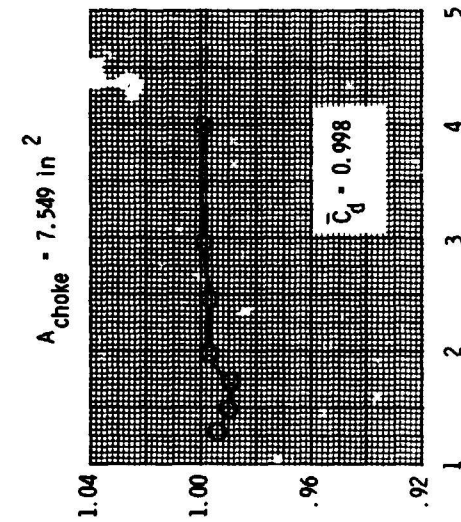
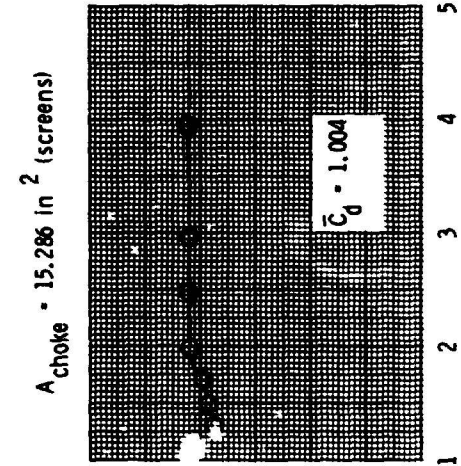
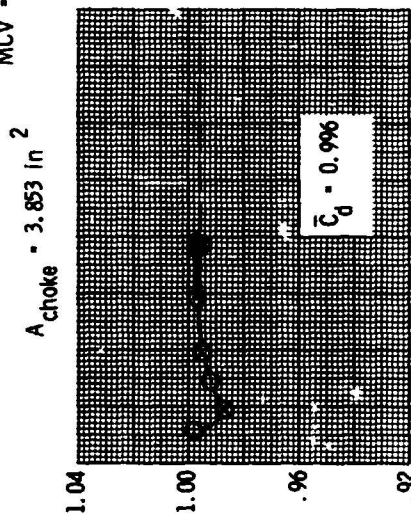
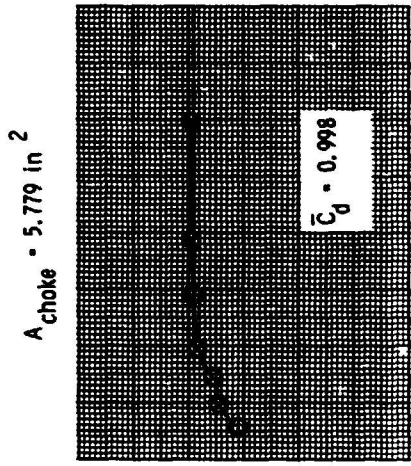
(£) $A_E = 8.501 \text{ in}^2$.

Figure 10.- Continued.

$K_{R,1}$ to $K_{R,5}$ - (See fig. 2(b))

$(T_{t,j})_{nom} = 530^{\circ}R$

MCV - 22



NPR

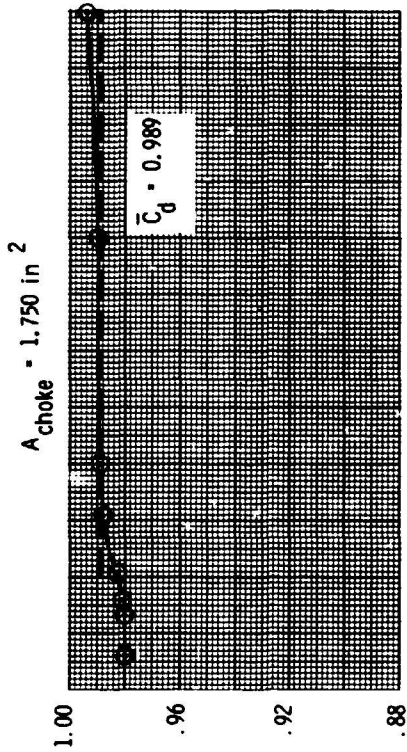
(g) $A_c = 11.352 \text{ in}^2$.

Figure 10.- Concluded.

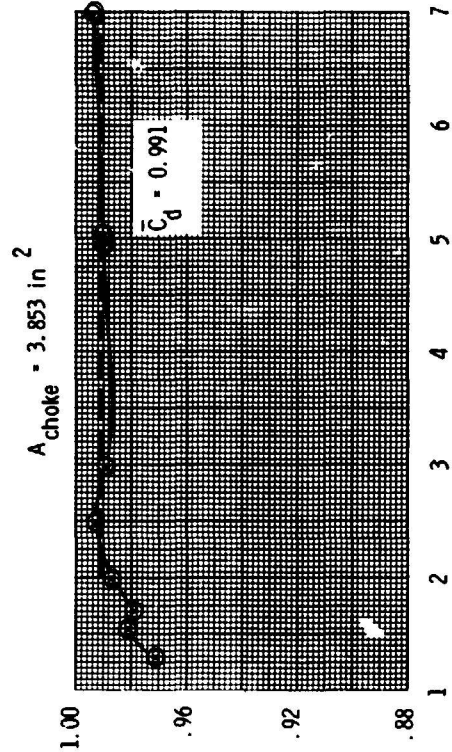


ORIGINAL PAGE IS
OF POOR QUALITY

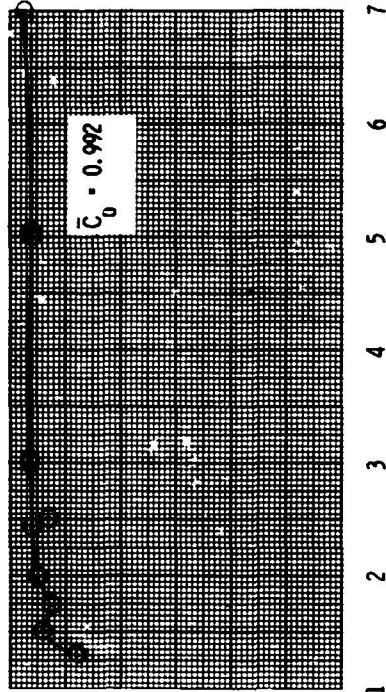
$K_{R,1}$ to $K_{R,5} = 1.0$
 $(T_{t,j})_{nom} = 530^\circ R$
MCV = 19



C_d



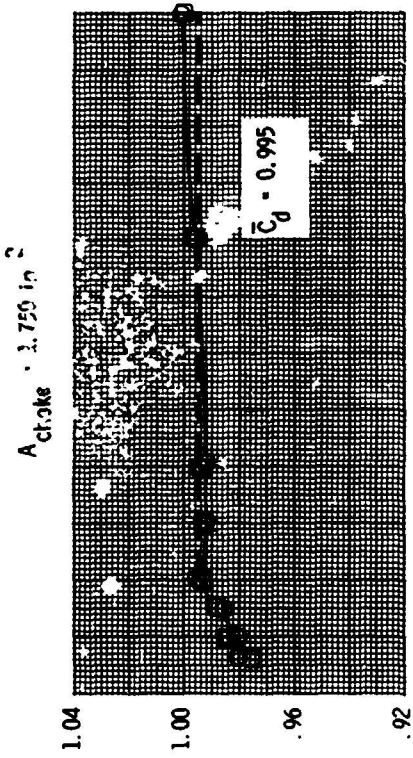
$A_{choke} = 15.286 \text{ in}^2$ (screens)



NPR

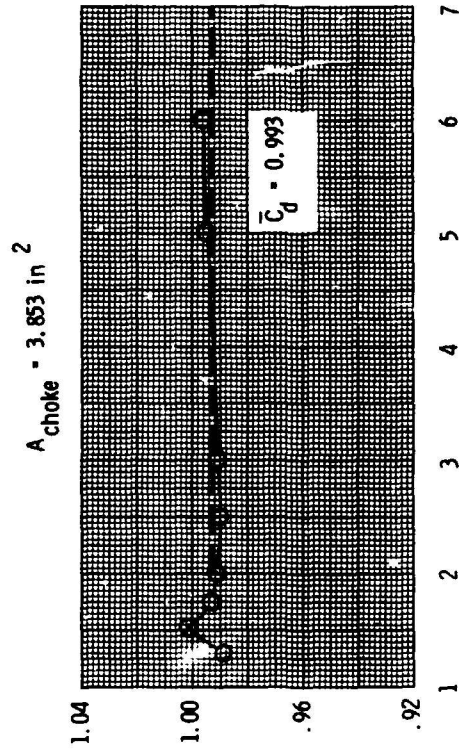
(a) $A_t = 0.999 \text{ in}^2$.

Figure 11.- Variation of standard-nozzle discharge coefficient with nozzle pressure ratio for average jet total pressure measured in instrumentation section.

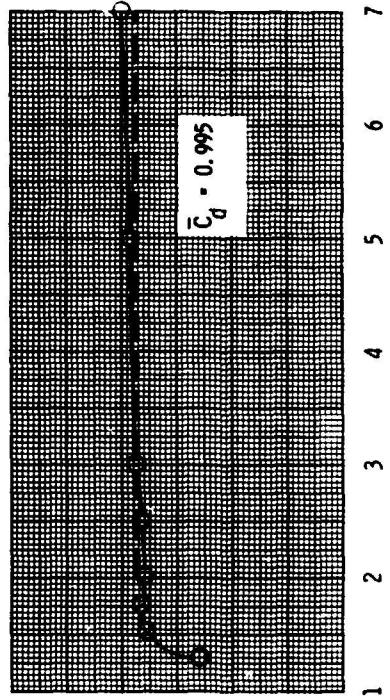


$K_{R,1}$ to $K_{R,5} = 1.0$
 $(T_{t,j})_{nom} = 530^\circ R$
 MCV
 ○ 22
 □ 21

C_d



$A_{choke} = 15.286 \text{ in}^2$ (screens)



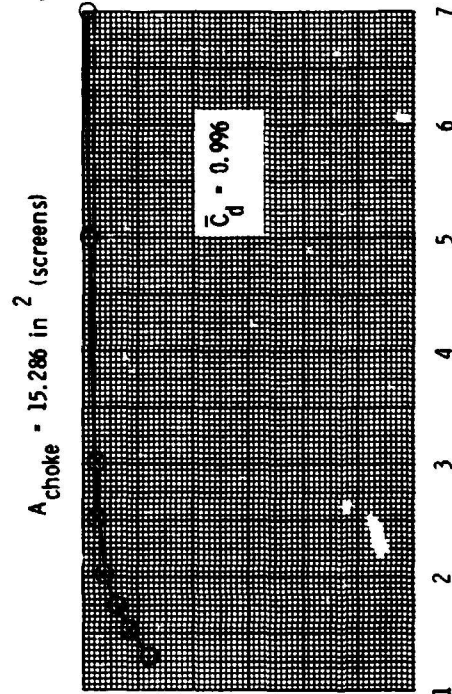
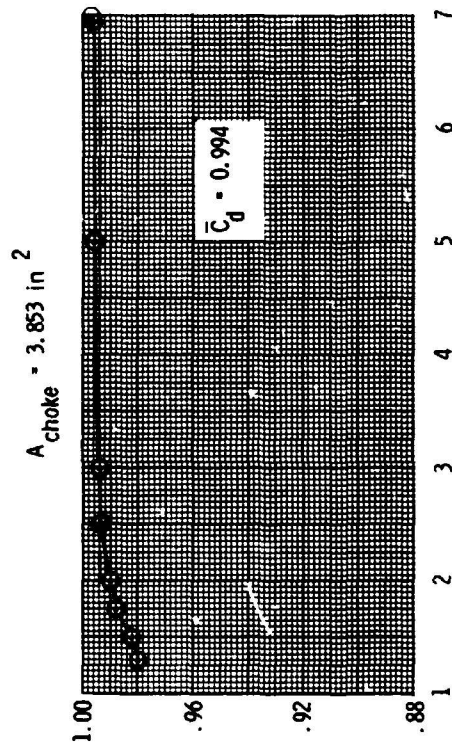
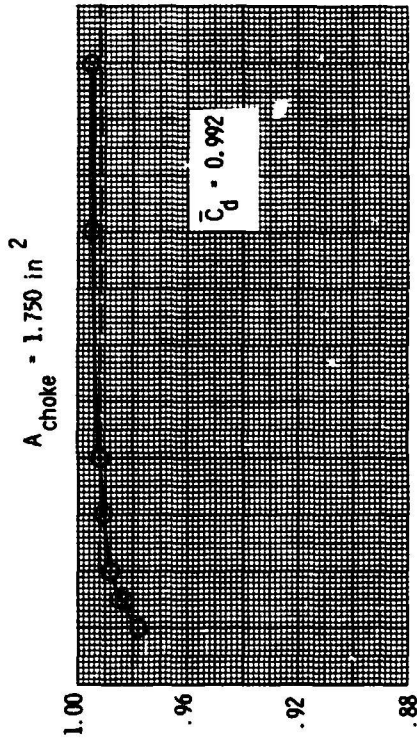
NPR

(b) $A_t = 1.933 \text{ in}^2$.

Figure 11.- Continued.

ORIGINAL
OF POOR

$K_{R,1}$ to $K_{R,5} = 1.0$
 $(T_{t,j})_{nom} = 530^{\circ}R$
 $MCV = 22$



NPR

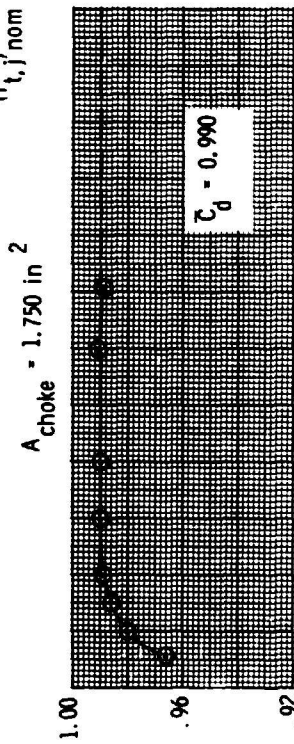
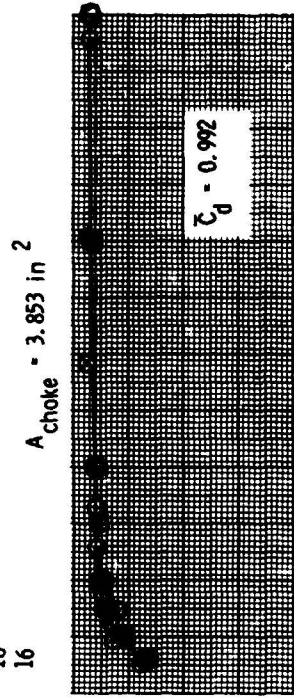
(c) $A_t = 3.002 \text{ in}^2$.

Figure 11.- Continued.

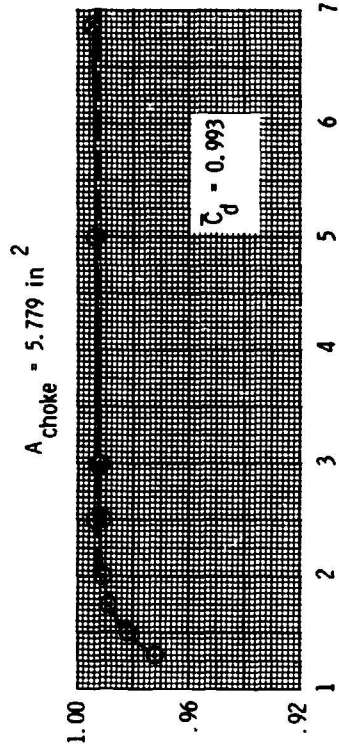
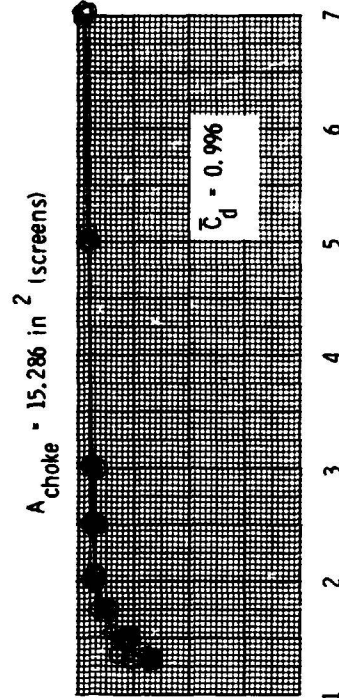
MCV

- 22
- 20
- ◇ 18
- △ 16

$K_{R,1}$ to $K_{R,5} = 1.0$
 $(T_{t,j})_{nom} = 530^{\circ}R$



C_d



NPR

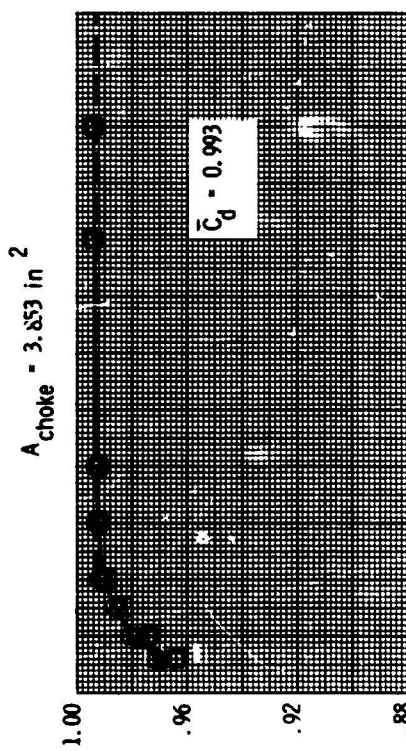
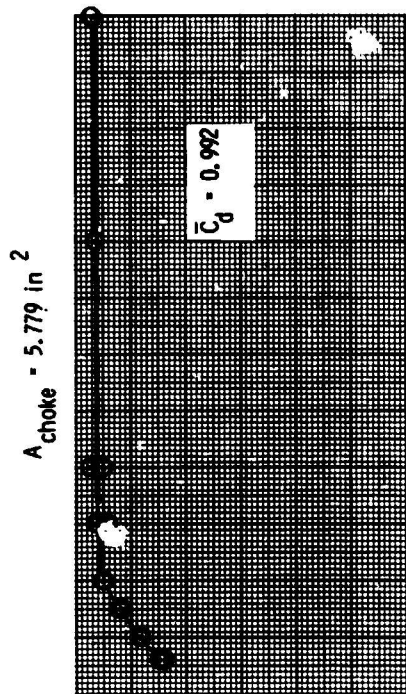
(d) $A_t = 3.992 \text{ in}^2$.

Figure 11.- Continued.

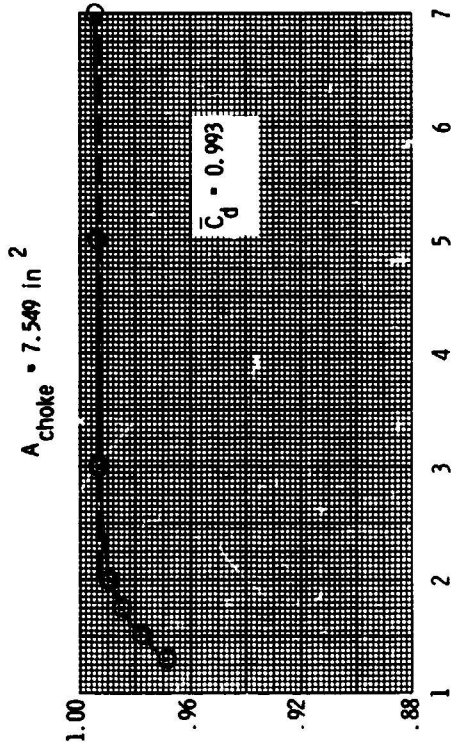
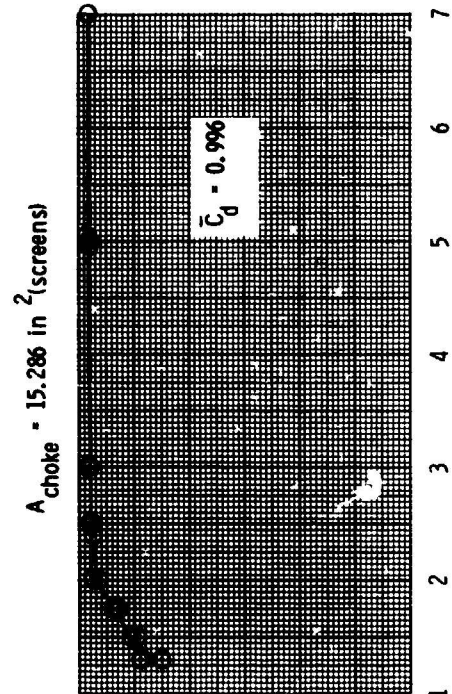
ORIGINAL PAGE IS
OF POOR QUALITY

$(T_{t,j})_{nom}$ °R $(T_V)_{nom}$ °R
 ○ 530 542
 □ 550 562

$K_{R,1}$ to $K_{R,5}$ = 1.0
 MCV = 22



C_d



NPR

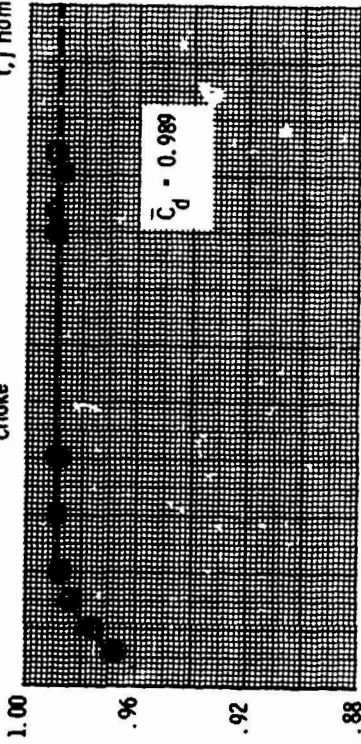
(e) $A_t = 5.711 \text{ in}^2$.

Figure 11.- Continued.

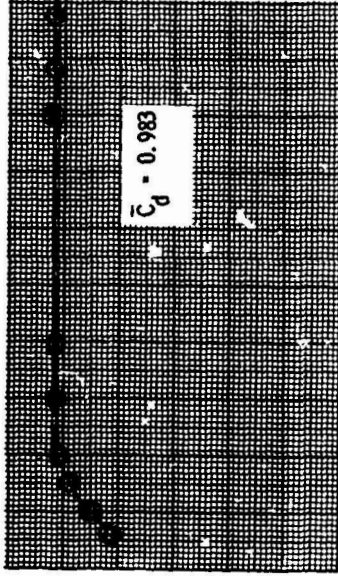
- MCV
 ○ 22
 □ 20
 ◇ 19
 △ 18
 ▽ 16

$K_{R,1}$ to $K_{R,5} = 1.0$
 $(T_{t,j})_{nom} = 529PR$

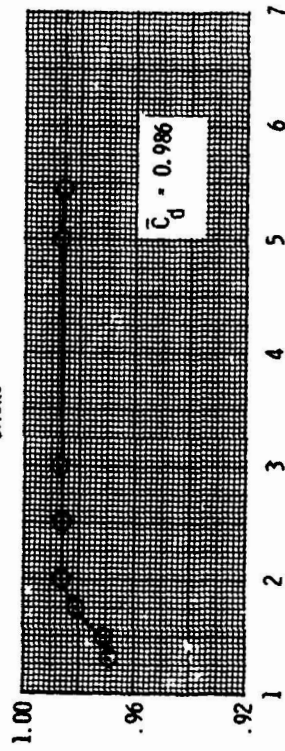
$A_{choke} = 3.853 \text{ in}^2$



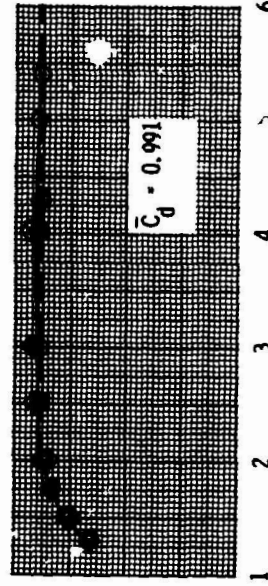
$A_{choke} = 5.779 \text{ in}^2$



$A_{choke} = 7.549 \text{ in}^2$



$A_{choke} = 15.286 \text{ in}^2$ (screens)



NPR

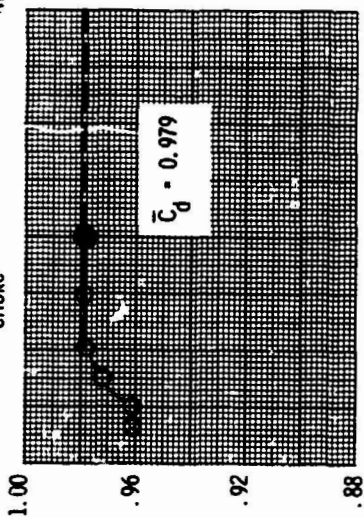
(f) $A_t = 8.501 \text{ in}^2$.

Figure 11.- Continued.

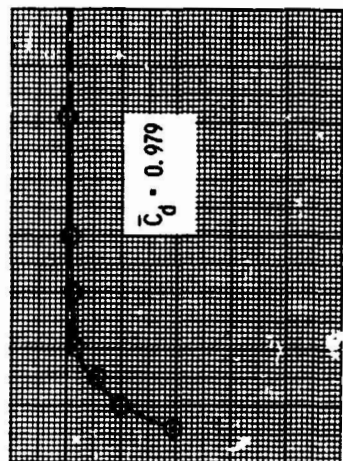
ORIGINAL PAGE IS
OF POOR QUALITY

$K_{R,1}$ to $K_{R,5} = 1.0$
 $(T_{t,j})_{nom} = 530^{\circ}R$
MCV = 22

$A_{choke} = 3.853 \text{ in}^2$

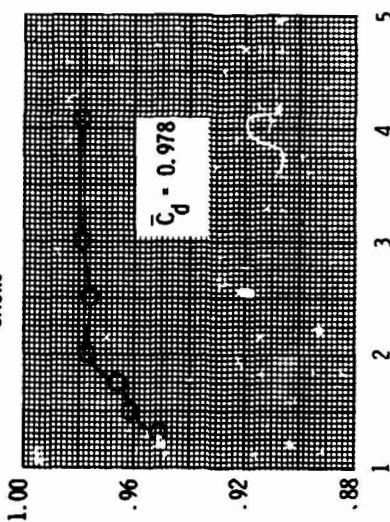


$A_{choke} = 5.779 \text{ in}^2$

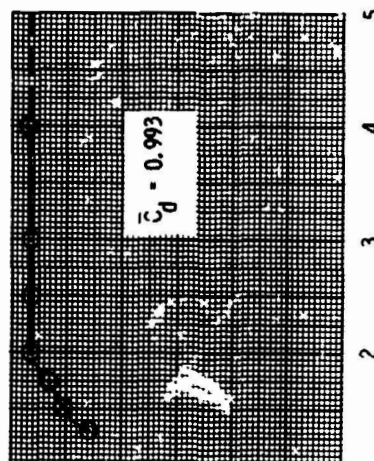


C_d

$A_{choke} = 7.549 \text{ in}^2$



$A_{choke} = 15.286 \text{ in}^2$ (screens)



NPR

(g) $A_t = 11.352 \text{ in}^2$.

Figure 11.- Concluded.

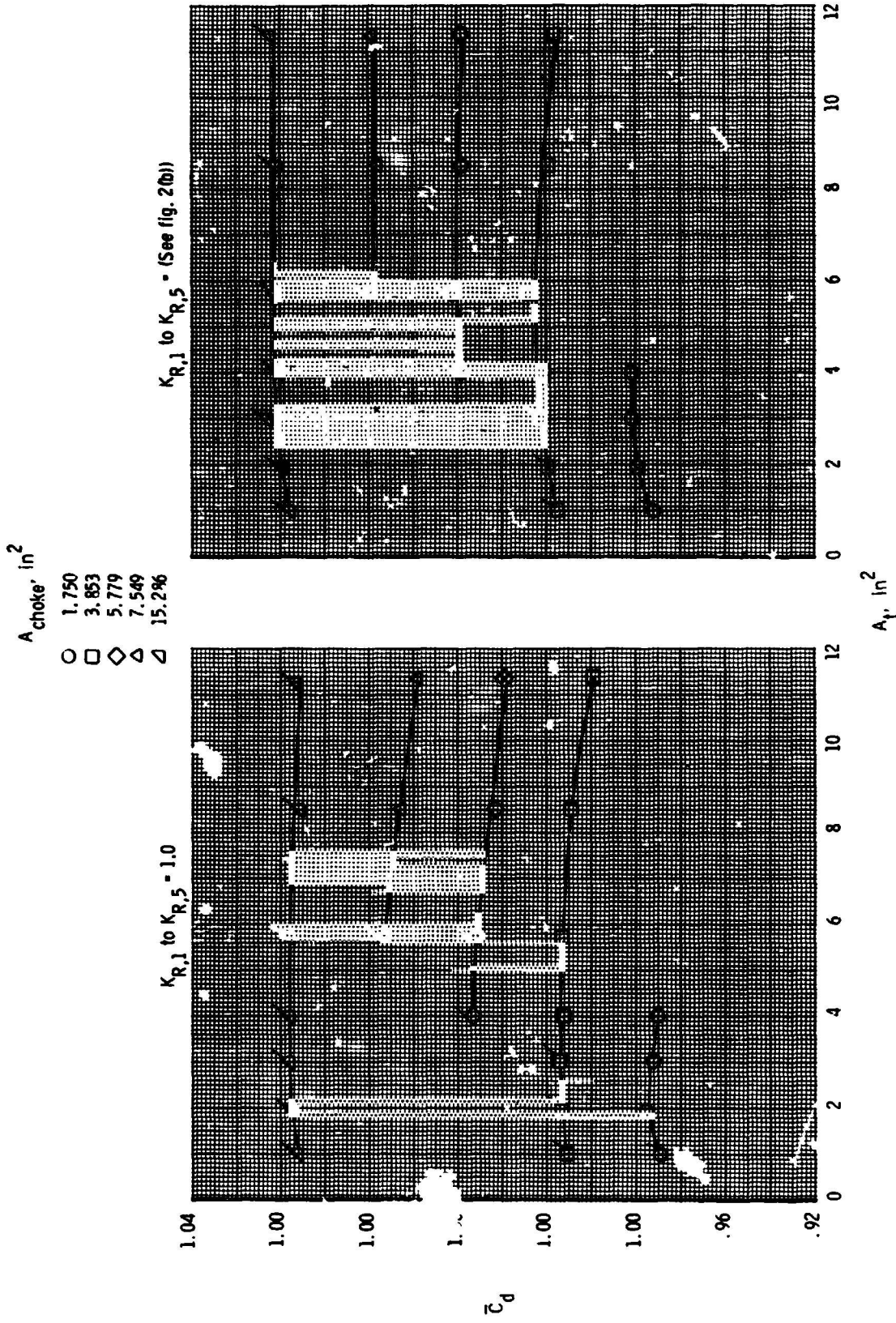


Figure 12.- Effect of nozzle-throat area on discharge coefficient. Flagged symbols indicate $A_{choke} > A_t$.



ORIGINAL PAGE IS
OF POOR QUALITY

A_{choke} , in²

- 1.750
- 3.853
- ◇ 5.779
- △ 7.549
- ▽ 15.286

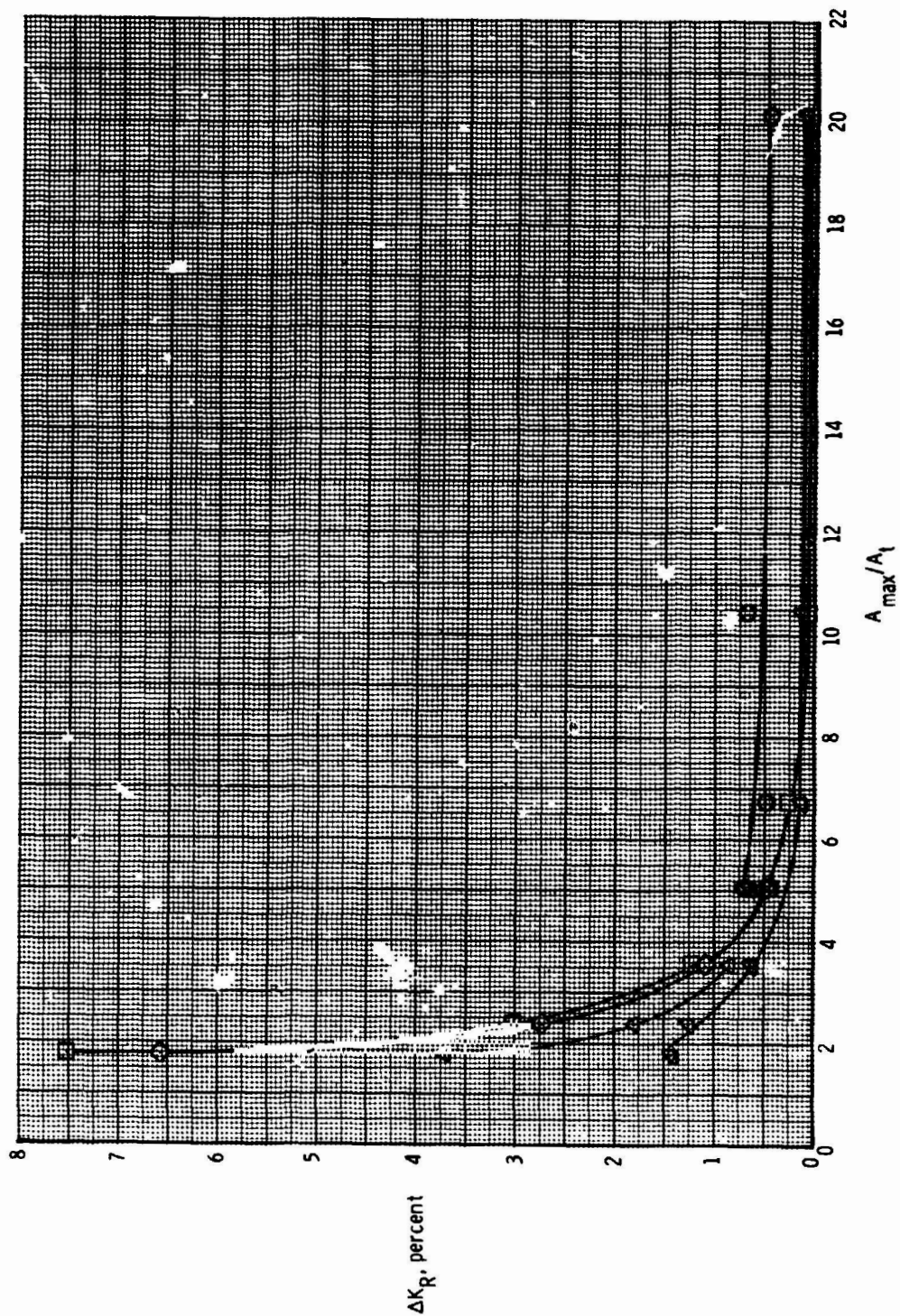


Figure 13.- Effect of contraction ratio and choke-plate open area on total-pressure distortion parameter.



- A_t , in²
- 0.999
 - 1.933
 - ◇ 3.072
 - △ 3.992
 - ▴ 5.711
 - ▾ 8.501
 - 11.352

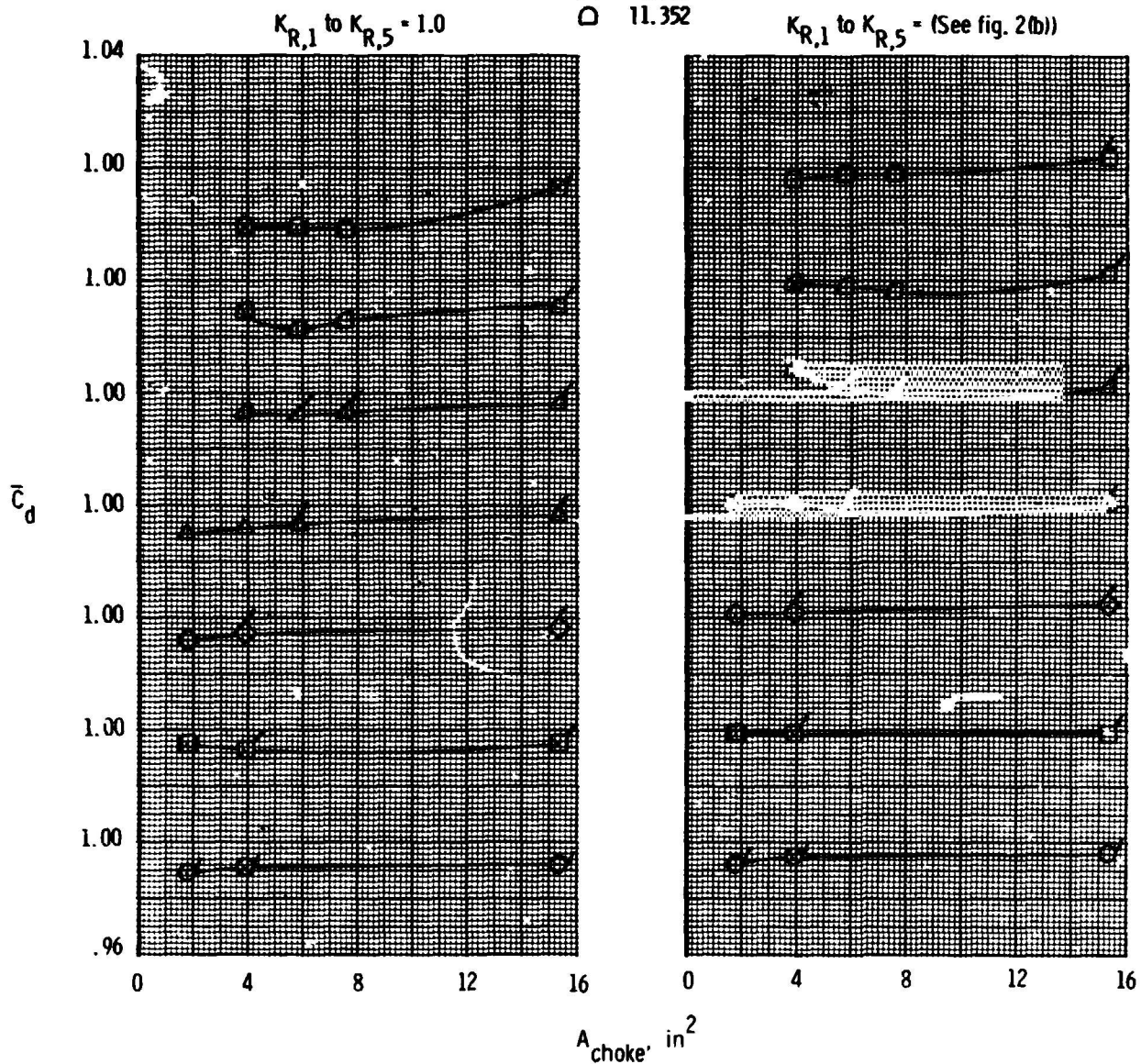


Figure 14.- Effect of choke-plate open area on discharge coefficient.
Flagged symbols indicate $A_{choke} > A_t$.



ORIGINAL PAGES
OF POOR QUALITY

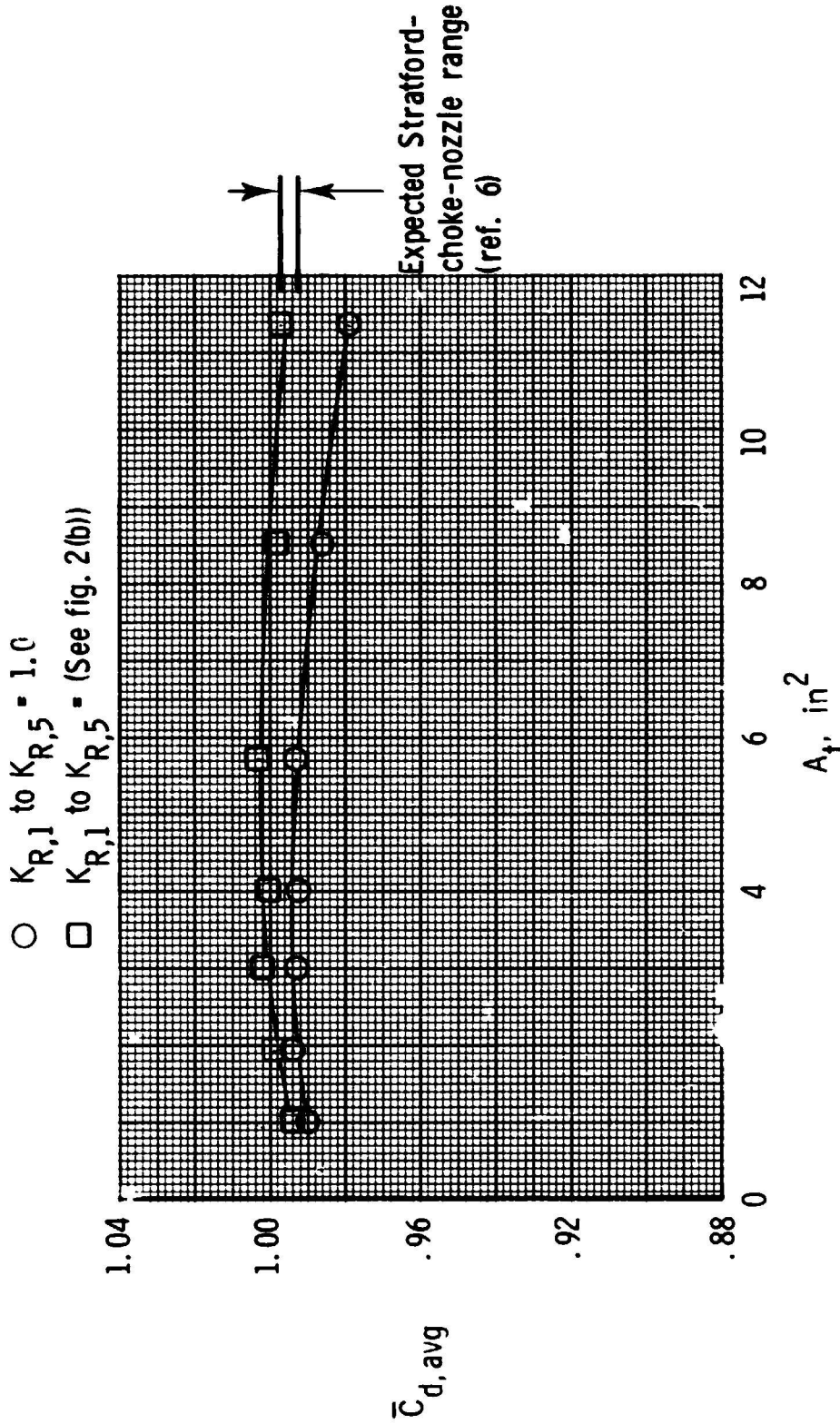


Figure 15.- Variation of average of \bar{C}_d for all A_{choke} except screens with nozzle-throat area for choked-nozzle flow operation. Choke-plate flow straightener installed; $\text{NPR} > 1.89$.

| | | | | | |
|--|--|-----------------------------|---|---|--|
| 1. Report No. NASA TM-86405 | | 2. Government Accession No. | | 3. Recipient's Catalog No. | |
| 4. Title and Subtitle Operating Characteristics of the Multiple Critical Venturi System and Secondary Calibration Nozzles Used for Weight-Flow Measurements in the Langley 16-Foot Transonic Tunnel | | | | 5. Report Date September 1985 | |
| | | | | 6. Performing Organization Code 505-40-90-01 | |
| 7. Author(s) Bobby L. Berrier, Laurence D. Leavitt, and Linda S. Bangert | | | | 8. Performing Organization Report No. L-15960 | |
| 9. Performing Organization Name and Address NASA Langley Research Center Hampton, VA 23665-5225 | | | | 10. Work Unit No. | |
| | | | | 11. Contract or Grant No. | |
| 12. Sponsoring Agency Name and Address National Aeronautics and Space Administration Washington, DC 20546-0001 | | | | 13. Type of Report and Period Covered Technical Memorandum | |
| | | | | 14. Sponsoring Agency Code | |
| 15. Supplementary Notes | | | | | |
| 16. Abstract An investigation has been conducted in the Langley 16-Foot Transonic Tunnel to determine the weight-flow measurement characteristics of a multiple critical venturi system and the nozzle discharge coefficient characteristics of a series of convergent calibration nozzles. The effects on model discharge coefficient of nozzle-throat area, model choke-plate open area, nozzle pressure ratio, jet total temperature, and number and combination of operating venturis were investigated. Tests were conducted at static conditions (tunnel wind off) at nozzle pressure ratios from 1.3 to 7.0. | | | | | |
| 17. Key Words (Suggested by Author(s)) Venturi Measurements Weight flow Mass flow Stratford nozzles | | | 18. Distribution Statement Unclassified - Unlimited Subject Category 02 | | |
| 19. Security Classif. (of this report) Unclassified | 20. Security Classif. (of this page) Unclassified | 21. No. of Pages 72 | 22. Price A04 | | |